MINERALOGY AND GEOCHEMISTRY OF SOILS OF ULTRAMAFIC ORIGIN FROM THE GREAT DYKE, ZIMBABWE AND GILLESPIE COUNTY, TEXAS

A Dissertation

by

COURAGE BANGIRA

Submitted to the Office of Graduate Studies of
Texas A&M University
in partial fulfillment of the requirements for the degree of

DOCTOR OF PHILOSOPHY

December 2010

Major Subject: Soil Science

Mineralogy and Geochemistry of Soils of Ultramafic Origin from the Great Dyke,

Zimbabwe and Gillespie County, Texas

MINERALOGY AND GEOCHEMISTRY OF SOILS OF ULTRAMAFIC ORIGIN FROM THE GREAT DYKE, ZIMBABWE AND GILLESPIE COUNTY, TEXAS

A Dissertation

by

COURAGE BANGIRA

Submitted to the Office of Graduate Studies of
Texas A&M University
in partial fulfillment of the requirements for the degree of

DOCTOR OF PHILOSOPHY

Approved by:

Chair of Committee,	Richard. H. Loeppert
Committee Members,	Charles T. Hallmark
	Youjun Deng
	Alan E. Pepper
Head of Department,	David D. Baltensperger

December 2010

Major Subject: Soil Science

ABSTRACT

Mineralogy and Geochemistry of Soils of Ultramafic Origin from the Great Dyke, Zimbabwe and Gillespie County, Texas.

(December 2010)

Courage Bangira, B.S., University of Zimbabwe; M.S., Gent University, Belgium

Chair of Advisory Committee: Dr. Richard H. Loeppert

Although soils developed from ultramafic parent materials have significance to agriculture, ecology and health, their bio-geochemistry is poorly understood. The mineralogical and bio-geochemistry of soils formed from the ultramafic parent materials of the Great Dyke, Zimbabwe and Gillespie County, Texas was investigated. The objectives were to determine the mineralogical and bio-geochemical properties of the soils in order to assess the potential impact and challenges to agriculture, and environmental quality. Soil samples were taken from the crest, shoulder, footslope and the toeslope. Chemical analyses were performed by nuclear and spectroscopic techniques. Mineral characterization was conducted by x-ray diffraction (XRD) and spectroscopic techniques. Microbial whole-community structure was determined by the fatty acid methyl esters (FAME) technique. The results indicate wide chemical and mineralogical compositions among the studied sites. The soils contain relatively high concentrations of heavy metals (some sites contain Cr(VI)), but low levels of K and Ca. The highest concentrations of trace metal were associated with chromite, Fe oxides and serpentinite. The concentrations of Mg were higher than those of Ca and varied between Zimbabwe and Texas soils largely due to the parent materials.

Unique to these soils is the occurrence of talc, serpentine, chlorite, Fe-rich smectite, amphiboles, pyroxenes, Fe and Cr oxides in relatively large amounts. These soils also lack micas and have neglible amounts of kaolinite and feldspars. Palygorskite and serpentine occurred in specific soil horizons and at specific landscape positions.

FAME profiles indicate that the soil microbial community structure is predominantly bacteria and fungi (including arbuscular mycorrhiza fungi) at each landscape position across the transect. Biomarkers for actinomycetes were undetectable. The proportions of Gram-positive bacteria were higher than those of the Gram-negative bacteria.

Very low levels of nutrients (Ca and K), higher Mg/Ca molar ratios, and the relatively high concentrations of heavy metals in these soils impact agricultural productivity. High concentrations of heavy metals, the presence of the Cr(VI) as well as its great potential to form in these soils might impact microbial activity and environmental quality. The occurrence of fibrous minerals (e.g serpentine and amphiboles) in these soils will likely impact human health.

ACKNOWLEDGEMENTS

I would like to thank my committee chair, Dr. Loeppert, and my committee members, Dr. Hallmark, Dr. Deng and Dr. Pepper, for their guidance and support throughout the course of this research.

I am grateful to the Fulbright Scholarship and Tom Slick Fellowship, which provided financial support for part of this study.

I would also like to thank Dr. W. James for assistance with neutron activation analysis; Dr. J.B. Dixon for the transmission electron microscopy analysis; Dr. J.W. Stucki for Mossbauer spectroscopy analysis; Dr. T. Gentry for assistance with microbial characterization and Ms D. Prochaska for some soil analyses.

My appreciation goes to the staff and faculty in the Department of Soil Science and Agricultural Engineering, University of Zimbabwe for their assistance with sampling and sample shipment logistics. Many thanks go to Dr. M. Wuta, Mr. E. Nyakudya, Ms D. Chinamo, Mr. E. Chikwari and Mr. P. Mubvumba for their help with sampling and shipping logistics.

Thanks also go to my friends and colleagues and the department faculty and staff for making my time at Texas A&M University a great experience.
I would also like to thank my family for their encouragement and to my wife and children for patience and love.

TABLE OF CONTENTS

CHAPTER Page

CHAPTER Page

CHAPTER Page

LIST OF FIGURES

FIGURE Page

FIGURE Page

FIGURE Page

FIGURE Page

LIST OF TABLES

CHAPTER I

INTRODUCTION

Ultramafic rocks occur widely in various parts of the globe. Large areas with ultramafic rocks are found in the Klamath Mountains (United States of America), New Foundland (Canada), The Alps (Italy and Switzerland), Japan, central Brazil, New Caledonia, western Australia, The Bushveld Complex (South Africa) and The Great Dyke (Zimbabwe). The common characteristic of the rocks in these areas is that they all have high concentrations of Fe- and Mg- containing minerals. For example, serpentine, talc and olivine often constitute the major minerals. Furthermore, the minerals may also contain high concentrations of trace metals (e.g., Cr, Pt, Ni, Co). Consequently, these areas have served as resources for industrial minerals (e.g., asbestos) and as sources of industrial metals (e.g., Cr, Pt, Ni).

Ultramafic rocks weather easily to form soil that can have unique properties and diverse bio-geochemical and mineralogical compositions; and which have important implications to agriculture, ecology, human health and overall environmental quality (Brooks, 1987). Because serpentine often constitute the major minerals in these environments, these soils have often been called “serpentine” soils. When used for crop production, ultramafic soils have very low productivity, and complete crop failure is often observed (Proctor, 1999). The best known ecological impacts of ultramafic soils are the distinct, stunted and sparse vegetation with poorer plant species diversity than that of non-ultramafic soils (Roberts and Proctor, 1992). The majority of the plants found in these areas are endemic species capable of adapting to these soil conditions. Although soil properties are thought to be the main factor in such vegetation anomalies, the actual soil characteristics leading to vegetation discrimination and poor plant growth are poorly understood. Little is known about the impact of these soils on biota. In some

---

This dissertation follows the style of Soil Science Society of America Journal.

countries (e.g., USA) the manufacture and use of asbestos minerals have been banned because of human health concerns. Consequently, the production of these minerals worldwide has been dramatically reduced or ceased. In the Gillespie County, Texas, for example, the production of asbestos and talc has been stopped. The high costs of production of some metals (e.g., Cr) and the depressed prices on the international market have also led to the cessation of mining in these areas. Vast acreages of land have now been planned for agricultural development, as well as management of the mine spoil to reduce environmental pollution. The utilization of these lands for agriculture introduces unique challenges to effective re-vegetation and sustainable land management to ensure environmental quality, food security and safety and human health.

BACKGROUND AND LITERATURE REVIEW

Previous studies have shown that soils derived from ultramafic rocks have more total and extractable Mg than Ca and often contain high total levels of Co, Cr, Fe, Mn and Ni (Roberts, 1980; Becquer et al., 2003; Oze et al., 2004; Chardot et al., 2007; Traore et al., 2008; Caillaud et al., 2009). The Mg/Ca molar ratios and heavy metal concentrations vary considerably and are impacted by the parent rock, climatic conditions and landscape position. Total Cr concentrations as high as 3.9 % in Zimbabwe (Soane and Saunder, 1959) and 7.4 % Ni in Brazil (Garnier et al., 2009) have been reported in the soil. Heavy metals, e.g., Cr, Cu and Ni, are toxic to plants, animals and microflora in high concentrations and can potentially enter the food chain by way of contaminated soil, water and agricultural products.#Previous research suggests that microflora in ultramafic soils tend to lack diversity, have lower microbial density and activity in comparison with that of non-serpentine soils (Amir and Pineau, 1998a; DeGrood et al., 2005; Oline, 2006). The low microbial diversity and density in soils can impact nutrient cycling and overall environmental quality. Microbes isolated from the rhizosphere of ultramafic soils were predominantly actinomycetes (Amir and Pineau, 1998a; DeGrood et al., 2005), and have shown tolerance to heavy metal toxicity (Mengoni et al., 2001; Pal et al., 2005; Amir et al., 2008). The characteristically high Mg/Ca ratios (>1) of ultramafic soils can detrimentally impact plant-nutrient balance and overall plant

nutrition (Brooks, 1987). Highly soluble Cr(VI), a known carcinogen and mutagen, can occur in ultramafic soils, with the potential to pollute surface- and ground-water resources (Cooper, 2002; Becquer et al., 2003).

The occurrence of specific minerals in ultramafic soils, as well as the concentration, bonding and bioavailability of heavy metal constituents is strongly impacted by geologic- and soil-weathering processes. Numerous studies on soils developed from ultramafic rocks have been conducted in the temperate and subtropical regions (Rabenhorst et al., 1982; Istok and Harward, 1982; Graham and Buol, 1990; Lee, 2003; Alexander et al., 2007). These researchers observed large amounts of serpentine, talc, chlorite, Fe oxides and smectite in the clay fractions of the soils. Magnesium-rich montmorillonites have been observed to be predominant in basin positions (Senkayi, 1977). Minerals commonly found in most agricultural soils (e.g., kaolinite, quartz) were absent or occurred in smaller amounts. The smectite was rich in Fe but contained little Al. In spite of the common minerals observed in these soils, wide variations in the kinds and relative abundances of minerals in soils derived from ultramafic rocks were observed at each study site. The occurrences of specific minerals were influenced by parent rock, drainage and landscape position (Istok and Harward, 1982; Alexander et al., 2007).

Although the Great Dyke continues to attract much scientific interest because of its significant economic value as a geologic source of chromites and platinum group elements and the uniqueness of this metal-rich ecosystem, little is known about the mineralogy and geochemistry of the soils. The microflora composition in these soils remains largely unknown. Nyamapfene and Yin, (1986) have reported the mineralogical composition of a soil profile associated with dunite in Zimbabwe. These researchers observed kaolinite to be the predominant layer-silicate mineral, with minor quantities of vermiculite-mica, smectite and talc. Due to the large aerial extent (> 4,000 km^2), spatial variations of the parent material and climatic differences along the Great Dyke, more thorough investigations are needed to identify the mineralogical and biogeochemical

constraints to plant establishment, as well as unique habitats for endemic plants, and to determine the potential impacts to human health and the overall environment.

Changing land use

The Great Dyke and Gillespie County are known for their rich mineral resources as well as their unique ecosystems for plants. The abolition of manufacture and use of asbestos and the depressed prices of Cr have led to a changing land use. Increasingly, more land is being diverted for agriculture to meet the food and fiber requirements of an expanding population. The cessation of mining operations and the increased utilization of the Great Dyke and associated areas with ultramafic soils for agriculture introduce unique challenges to effective re-vegetation and sustainable land management, as well as the need for strategies to ensure environmental quality, food security and safety, and human health.

OBJECTIVES

The objectives of the current study are:

(i) To determine the total elemental compositions of soils derived from ultramafic rocks across transects in the northern and southern regions of the Great Dyke, Zimbabwe and in Gillespie County, Texas, USA.

(ii) To determine the distribution of chemical elements (Cr, Ni, Fe and Mn) among the silicate minerals and in Fe- and Mn-oxides.

(iii) To determine the mineralogical compositions of soils derived from ultramafic rocks across the transect in the northern and southern region of the Great Dyke, and in Gillespie County.

(iv) To determine the microbial community structure in surface soils across the northern region of the Great Dyke, Zimbabwe.

CHAPTER II

MINERALOGICAL AND GEOCHEMICAL COMPOSITION OF SOIL OF ULTRAMAFIC ORIGIN FROM THE NORTHERN GREAT DYKE, ZIMBABWE

INTRODUCTION

The Great Dyke of Zimbabwe (Fig. 2.1) is one of the world's largest intrusions of layered ultramafic-serpentine rocks and is the world's second largest reserve of Cr and Pt (Wilson, 1982). It stretches north-south for about 540 km through virtually the entire length of Zimbabwe. The rock strata consist of repetitive cyclic units from the top to the bottom. The upper strata are composed principally of dunite, harzburgite and pyroxenite rocks, and the lower strata contain serpentine, chromite and sulfide minerals (Worst, 1960; Wilson et al., 1989; Wilson and Prendergast, 2001). The Great Dyke has served as a valuable geologic source of heavy metals for industry. However, due to the increasing population of Zimbabwe, high production costs and depressed Cr price on the world market, vast acreages of mineland and mine spoil associated with the Great Dyke have been targeted for settlement and crop production to meet the increasing demands for food and fiber. Serpentine, amphibole, pyroxenite and sulfide minerals in the Great Dyke contribute significant concentrations of Ni, Co, Cr, Cu, Fe and Mn to the pedosphere. The increased utilization of the Great Dyke for agriculture introduces difficult challenges to effective re-vegetation and land management, as well as the need for strategies to ensure environmental quality, food security and human health.

Agricultural, health and environmental challenges of ultramafic soils

Heavy metals, e.g., Cr, Cu and Ni, which occur in most ultramafic soils in varying concentrations (Roberts, 1980; Proctor et al., 1980; Noble and Hughes, 1991), are toxic to plants and animals in high concentrations and can potentially enter the food chain by way of contaminated soil, water and agricultural products. The characteristically high Mg/Ca ratios (>1) of serpentine soils can detrimentally impact plant-nutrient balance and overall plant nutrition (Brooks, 1987). Highly soluble Cr(VI), a known carcinogen and

mutagen, can occur in serpentine soils, with the potential to pollute surface- and ground-water resources (Cooper, 2002; Becquer et al., 2003; Oze et al., 2004).

Fig. 2.1. Location map of the Great Dyke, Zimbabwe

The occurrence of specific minerals in ultramafic soils, as well as the concentration, bonding and bioavailability of heavy metal constituents is strongly impacted by geologic and soil weathering processes. The persistence of ultramafic-serpentine minerals and the formation of secondary soil minerals are highly dependent on regional and local environmental conditions (Istok and Harward, 1982). In a chrono-sequence of a serpentinized-ultramafic derived soil in the Klamath Mountains, USA, (Alexander et al., 2007), observed the complete elimination of olivine from the oldest soil and a significant reduction of serpentine concentration in both the sand and clay particle-size separates, with a corresponding accumulation of Fe oxide. Elsewhere, similar results, where the concentrations of serpentine and smectite were observed to decrease in old soils, have been reported in different climatic regions (Rabenhorst et al., 1982; Bonifacio et al., 1997; Hseu, 2007).

Although the Great Dyke of Zimbabwe continues to attract much scientific interest because of its significant economic value as a geologic source of chromites and platinum group elements and the uniqueness of this metal-rich ecosystem, little is known about the mineralogy of the soils formed from these rocks. Nyamapfene and Yin, (1986) have reported the mineralogical composition of a soil profile associated with dunite in Zimbabwe. These researchers observed kaolinite to be the predominant layer-silicate mineral, with minor quantities of vermiculite-mica, smectite and talc. Due to the large spatial variation of the parent material across the Great Dyke, more thorough investigations are needed to identify the mineralogical and geochemical causes of poor plant establishment in certain locations of the Great Dyke and determine the potential impacts to human health and the environment.

The objectives of the current study were to (i) determine the mineralogical and elemental compositions of soils derived from ultramafic-serpentinized rocks across a transect in the northern region of the Great Dyke of Zimbabwe, and (ii) assess the relationships between geomorphic position, soil mineralogy and chemical composition, and the implications to agriculture and environmental quality.

MATERIALS AND METHODS

Study site

The study site (Fig. 2.2, left) is located on the northern part of the Great Dyke of Zimbabwe at Mpinga (17 31'45.35"S and 30 36'12.82"E). The mean annual rainfall is 850 mm, and the average annual maximum temperature is 25.5°C. The uni-modal rainy season is between November and April (Department of Meteorological Services, 1978). The study site is part of the Darwendale sub-chamber whose geology has been described in detail by several authors (Worst, 1960; Wilson et al., 1989). It consists of predominantly pyroxenite and inclusions of plagioclase oikocrysts as outcrops on higher landscape positions (i.e., the crest). Lower lying narrow bands (~50 m width) of serpentinite and chromitite are often sandwiched between the pyroxenite or dunite layers on either side of the longitudinal axis. At the footslope, there is a narrow strip of dolerite rocks (Worst, 1960). The fault line (usually along a river) marks the boundary between the Great Dyke and granitic rocks on both sides of the Great Dyke.

Sampling protocol

The sample sites were located along a northwest to southeast transect at four locations based on geomorphic position: crest (1500 m altitude), footslope (1470 m), pediplain (1460 m) and toeslope (1420 m) (Fig. 2.2). Composite soil samples were collected from each sampling depth at each landscape position. Ten subsamples for each depth were taken from each location and thoroughly mixed. The sampling depths were: 0-15 and 15-30 cm on the crest, 0-15 cm on the footslope, 0-15 and 15-30 cm on the pediplain, and 0-20, 20-40, 40-60 and 60-80 cm on the toeslope. Samples were not obtained from the backslope (between points B and C of the transect line in Fig. 2.2) because this area predominantly consisted of bare rock.

Chemical analyses

Soil samples were air-dried and gently crushed to pass a 2-mm sieve prior to analyses. Soil pH was determined with a glass/calomel electrode in 1:1 soil:water (w:v) suspension. Organic C was determined by the Walkley-Black method (Nelson and Sommers, 1996) and particle-size distribution by the hydrometer method involving

sedimentation after dispersion in pH 10 Na_2CO_3 (Gee and Bauder, 1986). Cation exchange capacity (CEC) was determined at pH 8.2 after saturation of the soil cation-exchange sites with Na^+ using 1M Na acetate, washing with 95% ethanol and displacement of the exchangeable Na with 1M ammonium acetate at pH 7.0 (Holmgren et al., 1977). Extractable Ca, Mg, K, Na and Ni in soil were displaced by pH 7.0, 1 M ammonium acetate, and the concentrations were measured by atomic absorption (Ca, Mg, Ni) and flame emission (Na, K) spectrophotometry.

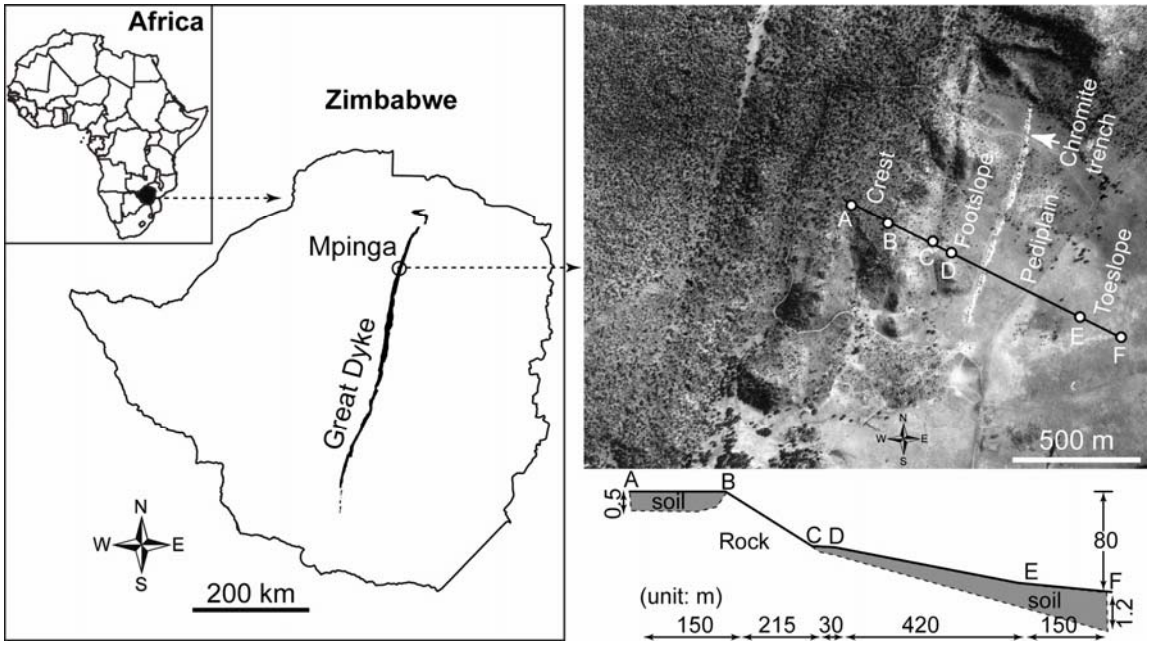

Fig. 2.2. Location of the Great Dyke (*left*), aerial photograph (*top right*) of the study area at Mpinga, Zimbabwe, and schematic illustration of the cross section between the points A, B, C, D, E and F along the transect (*bottom right*).

Chromium (VI (CrO_4^{2-}) in soil was extracted with 10 mM KH_2PO_4/K_2HPO_4 buffer solution at pH 7.2 by shaking for 1 hr (Bartlett and James, 1996). After filtration of the extract through a 0.2 μm cellulose-membrane filter, s-diphenylcarbazide solution was added to the filtrate from which the concentration of chromate was determined

colorimetrically at 540 nm using a UV-visible spectrophotometer (Beckman Coulter DU800, Brea, CA).

Total elemental analysis by neutron activation analysis

Total soil elemental composition was determined by neutron-activation analysis (NAA) (Helmke, 1996). The air-dried soil samples were ground to pass a 0.10-mm sieve, and about 55 mg of accurately weighed soil or standard-rock sample, each in triplicate, were placed into plastic vials, which were then heat-sealed. The standard reference materials included NIST SRM-1633a coal fly ash, NIST SRM-688 basalt (National Institute for Standards and Technology, Washington, DC) and USGS standard rock AGV-1 (United States Geological Survey, Lakewood, CO). Samples were irradiated at the research nuclear reactor at Texas A&M University, College Station, TX, at a nominal neutron flux of 1×10^{13} $cm^{-2}s^{-1}$. Both short-time (30 s) and long-time (14 hr) radiations were performed for NAA. The short-radiated samples were counted for 500 s for the short-lived isotopes after a 20-min delay, and the long-radiated samples were counted for 2000 s for the intermediate-lived isotopes after a 7-day decay and for 3-hr for the long-lived isotopes after a 28-day decay. The counting system consisted of an Ortec (Ortec, Oak Ridge, TN) high purity Ge detector with a relative counting efficiency of 50% and a resolution of 1.74 keV (Full Width at Half Maximum). The spectra were acquired on a Canberra Genie-PC system (Canberra Industries, Meriden, CT) and transferred electronically to the VMS-based alpha processor at the campus laboratory. Spectra were processed using the Genie gamma evaluation software (Canberra Industries, Meriden, CT) and compared to calibrated standard data using Canberra's NAA software. The accuracy of the data was within 5-10%.

Selective dissolution of mineral phases

To check the association of heavy metals with total Fe oxides, poorly crystalline Fe oxides and Mn oxides, the ground (< 0.1 mm) soil samples were extracted with dithionite-citrate (DC) (Holmgren, 1967), pH 3 ammonium oxalate (AO) in the dark (Loeppert and Inskeep, 1996), and hydroxylamine hydrochloride (HH) (Gambrell,

1996*)*, respectively. The concentrations of Fe, Cr, Mn, Ni, and Co in the extracts were determined with ICP-OES (Spectro, Mahwah, NJ).

Mineral analyses

To facilitate mineral identification and characterization, the soils were fractionated based on size, color, and magnetism. Sand (53–2000 μm), silt (2–53 μm), and clay (< 2 μm) fractions were separated by sieving and sedimentation (Gee and Bauder, 1986). Magnetic minerals in the silt fractions were collected by a hand magnet, in which the silt:water (1:15 w/v) suspension was repeatedly sonicated to disperse the particles and a magnetic stir bar wrapped in a plastic bag was dipped into the suspension to attract the magnetic minerals. The magnetic minerals were transferred to a beaker by removing the magnet from the bag. Magnetic separation was repeated until no magnetic minerals could be attracted by the hand magnet. To check the mineralogy and chemical compositions of some unique minerals such as enstatite, maghemite/magnetite, and serpentine found in the soils, we hand-picked some mineral specimens based on color, magnetism, and shape from the sand fractions of the crest subsoil and pediplain topsoil under an optical microscope. The following categories were operationally defined: black (10YR 2/1) and non-magnetic; black and magnetic; dark reddish brown (7.5YR 3/4) and magnetic; dark reddish brown and non-magnetic; light gray (5Y 7/1) and non-magnetic; light green and non magnetic; dark green and non-magnetic. Chromite specimens were concentrated by dissolving silicate minerals in the crest sample by HF/aqua-regia. Mineral compositions were analyzed by X-ray diffraction (XRD), Fourier transform infrared (FTIR) spectroscopy, and scanning electron microscopy (SEM). The XRD analysis was performed on a Bruker D8 Advance (Bruker, Madison, WI) X-ray diffractometer with a CuKα source operated at 35 kV and 45 mA. A SOL-X (Bruker, Madison, WI) energy dispersive detector was used to eliminate Fe fluorescence from the samples. Ground bulk, sand, and silt samples were mounted as powder specimens for XRD analysis. Oriented K^+- or Mg^{2+}-saturated clays were air dried from suspension on 25.4×1.6 mm round glass discs (Lakeside Brand, Hugh Courtright & Co., Monee, IL). The Mg^{2+}-saturated clay films were misted with 20% (v/v) glycerol/water solution and

allowed to equilibrate in a closed petri dish for 4 hr. The K^+-saturated clays were heated to 330°C and then to 550°C for 1 hr, and following each heat treatment were cooled to about 100°C and then immediately scanned by XRD. All XRD patterns were recorded with a dwell time of 2s and a 0.05 °2θ step.

The FTIR spectroscopy was used to verify the identity of clay minerals. Clay specimens were mixed with KBr (0.3% w:w) and pressed to pellets at a pressure of 20,000 psi for 5 min under vacuum suction and then oven dried at 140°C for 24 hr prior to spectrum collection using a Spectrum 100 FTIR spectrometer (Perkin Elmer, Waltham, MA). The spectra were recorded in transmission mode in the range of 4000-400 cm^{-1} at 4 cm^{-1} resolution.

The SEM analyses were performed using a FEI- QUANTA 600 FE-SEM (FEI, Hillsboro, OR) microscope. The sand and silt specimens were mounted by pressing the particles on conductive C tabs (Ted Pella, Redding, CA). Clay particles were mounted by drying a diluted clay suspension on the C tab. All samples were coated under vacuum with about a 40-nm thickness of graphite C. Images and energy dispersive X-ray spectra were acquired at an accelerating voltage of 20 kV and a working distance of 10 mm.

RESULTS AND DISCUSSION

Soil physical and chemical properties

With decreasing elevation from the crest to the toeslope, the following trends in pH, extractable cation concentrations, and clay content were observed (Table 2.1). Soil reaction changed from strongly acidic (pH 5.1-5.4) to alkaline (pH 7.5-7.9) accompanied by increasing per cent base saturation; the percentage of extractable Ca, Mg, K, and Na increased from about 70% to nearly 100%. The exchangeable cation composition was

Table 2.1. Selected physical and chemical properties of soil at Mpinga site.

Depth (cm)	Color (moist)	pH	O.C.†	Clay	Silt	Sand	Exchangeable bases Ca	Mg	K	Na	Ni	CEC	Mg/Ca	Great Group
			--- Weight % ---				--- cmol(+) kg-1 ---							
							Crest							
0-15	2.5 YR 3/3	5.1	2.4	27	27	46	0.8	7.5	0.2	0.1	0.37	11.5	9.4	Haplustolls
15-30	2.5 YR 3/3	5.4	1.9	22	23	55	0.7	5.7	0.1	0.1	0.40	10.3	8.1	
							Footslope							
0-15	2.5 YR 3/3	5.2	2.7	22	17	61	1.5	7.5	0.1	0.1	0.44	12.0	5.0	Haplustolls
							Pediplain							
0-15	2.5 YR 3/3	6.2	2.9	28	22	50	0.6	7.6	0.1	0.1	0.74	12.5	12.7	Haplustolls
15-30	2.5 YR 3/3	6.4	2.1	21	20	59	0.6	7.7	0.1	0.1	0.93	11.4	12.8	
							Toeslope							
0-20	2.5 Y 3/1	7.5	4.8	61	22	17	3.9	74.3	0.2	0.1	0.22	72.8	19.1	Haplusterts
20-40	2.5 Y 4/2	7.7	2.7	58	23	20	4.1	71.9	0.1	0.1	0.18	77.7	17.5	
40-60	2.5 Y 4/2	7.8	0.6	59	18	23	2.1	54.4	0.1	0.1	0.19	57.9	25.9	
60-80	2.5 Y 4/2	7.9	0.5	64	16	21	2.2	57.1	0.1	0.1	0.20	62.4	26.0	

†O.C.- Organic carbon.

dominated by Mg^{2+}; the percentage of ammonium-acetate extractable Mg among the base cations increased from about 87 to 96 % and the Mg/Ca ratio increased from about 9 to 26, from crest to toeslope. Clay and organic-C concentrations increased from about 25 to 60 % and 2 to 5 % (w/w), respectively; soil CEC was greatest at the toeslope. These trends suggest transport of fine soil particles and dissolved chemical species from the upper slope (crest and footslope) to the toeslope either along the slope surface or in small subsurface channels. One of the unique properties of the soils is the high concentration of ammonium-acetate extractable Ni, with concentrations ranging from about 0.2 cmol(+)kg^{-1} (117 ppm) at the toeslope to about 1 cmol(+)kg^{-1} (587 ppm) at the pediplain.

Total elemental composition

The soils had relatively high-concentrations of Fe, Mg, and the heavy metal elements Cr, Ni, and Co but relatively low concentrations of Ca, Na, and K (Table 2.2). Except for the toeslope soils, most samples contained > 30% (w/w) total Fe (as Fe_2O_3) with the highest concentrations occurring in the pediplain soils. Similarly, Cr and Ni were in highest concentration in the pediplain soils, which contained about 7% Cr_2O_3 and 0.5% NiO by weight. The concentrations of total Fe and Cr in the toeslope soils were only about one-third of those in the pediplain soils. As will be shown by the mineralogy data (mineralogy section), the high concentrations of Fe, Cr, and Ni in the pediplain soils were mainly due to the chromite rich parent materials. The occurrence of chromite is especially evident in the abandoned chromite trenches as shown in Fig. 2.2. The high Ni concentrations in the pediplain soils are attributable to the high concentrations of serpentine.

Table 2.2. Total elemental concentrations (% w/w) in soil at Mpinga site.

Depth (cm)	Fe_2O_3	Al_2O_3	Cr_2O_3	MgO‡	CaO‡	Na_2O	MnO	NiO	ZnO	CoO
					Crest:					
0-15	30.9	5.5	3.5	8.4	0.04	0.11	0.42	0.28	0.02	0.05
15-30	31.8	5.9	3.9	9.1	0.06	0.11	0.43	0.29	0.02	0.05
					Footslope:					
0-15	30.6	5.8	3.7	7.9	0.16	0.10	0.47	0.21	0.02	0.05
					Pediplain:					
0-15	33.7	5.3	6.4	7.7	0.09	0.12	0.39	0.44	0.03	0.06
15-30	34.8	5.8	6.4	5.6	0.07	0.16	0.46	0.48	0.04	0.06
					Toeslope:					
0-20	14.9	7.0	2.1	8.2	0.09	0.17	0.34	0.24	0.03	0.04
20-40	12.8	7.1	1.9	7.8	0.08	0.18	0.26	0.24	0.03	0.04
40-60	11.8	7.2	1.1	9.1	0.08	0.21	0.27	0.24	0.03	0.03
60-80	10.9	7.5	1.1	9.1	0.08	0.26	0.23	0.22	0.03	0.03

‡Determined by atomic absorption spectrophotometer in aqua-regia/HF.

Heavy metals extracted by DC, AO, and HH

Fe

Dithionite-citrate (DC) and acidified ammonium oxalate (AO) (in the dark) extractions have been utilized extensively to obtain quantitative estimates of total and poorly crystalline Fe-oxide concentrations, respectively, in soil (Holmgren, 1967). Both of these extractants might also result in partial dissolution of Fe-rich silicate phases, e.g., serpentine and Fe-rich smectite. In the current study, more than 40% of the total soil Fe

was extracted by DC from each of the samples, but with considerably higher proportions from the toeslope soil (Table 2.3). These results suggest a higher proportion of the total Fe as Fe oxide in the toeslope soil. Moreover, there was a trend of increasing proportion of DC-extractable Fe with depth in the toeslope soil, as it reached nearly 90% of total Fe in the lowest horizon. Contrary to the extraction results, the less distinct goethite peaks in XRD patterns of toeslope samples compared to samples from the upper transect positions (discussed in mineralogy of the clay fraction section) suggest a lower concentration of crystalline Fe oxide at the toeslope. These anomalous results are attributable to two factors: (i) the probable partial dissolution of Fe-rich smectite that is predominant in the toeslope soils (discussed in mineralogy of the clay fraction section) and (ii) the likely poorer crystallinity and greater relative ease of dissolution of Fe oxides from the toeslope (as discussed below). AO extracted 2% or less of the total soil Fe from the upper landscape positions of the transect compared to 8-12% of the total Fe from the toeslope soils (Table 2.3). The apparent higher proportion of poorly crystalline Fe oxide at the toeslope position is attributable to the relatively high concentration (~60% of the total clay fraction) of easily weatherable Fe rich silicate minerals, the alternating redox conditions at the toeslope position that are conducive to the formation of Fe oxide, and the relatively high organic matter and dissolved Si concentrations that provide kinetic inhibitions to the formation and crystal growth of well crystalline Fe oxides (Kodama and Schnitzer, 1977; Cornell and Schwertmann, 1979; Vempati and Loeppert, 1989). These results together imply that a greater proportion of poorly crystalline Fe oxide and a greater overall reactivity of Fe oxide at the toeslope position. Further research will be needed to verify the mineralogy of the soil Fe oxide phases.

Table 2.3. Percentages of total Fe, Mn, Cr, and Ni dissolved by hydroxylamine hydrochloride (HH), ammonium oxalate (AO), and dithionite-citrate (DC) methods.

Depth (cm)	Fe			Mn			Cr			Ni		
	HH	AO	DC	HH	AO	DC	HH	AO	DC	HH	AO	DC
						Crest:						
0-15	0.1	1.2	40.5	40.3	34.7	8.3	<0.01	0.2	7.8	11.3	12.1	39.3
15-30	0.1	1.2	40.4	37.8	31.1	5.8	<0.01	0.2	6.7	8.8	8.6	41.0
						Footslope:						
0-15	0.2	1.3	49.8	36.2	31.9	9.1	<0.01	0.2	9.1	18.4	20.3	78.3
						Pediplain:						
0-15	0.2	2.1	51.5	30.6	31.0	25.3	<0.01	0.1	2.2	16.2	21.9	61.5
15-30	0.2	1.7	42.6	24.7	25.0	22.6	<0.01	0.1	2.2	15.5	21.2	62.1
						Toeslope:						
0-20	0.8	12.6	54.2	40.2	36.3	41.2	0.03	0.3	6.6	23.9	47.5	62.7
20-40	0.6	9.9	68.7	56.3	54.3	56.0	0.04	0.3	7.7	31.6	49.7	89.0
40-60	0.7	8.3	78.4	56.6	53.1	57.5	0.07	0.5	16.9	32.0	50.0	98.9
60-80	0.7	8.7	89.4	66.6	57.9	68.9	0.08	0.6	17.2	36.2	60.8	~ 100

Mn

Hydroxylamine hydrochloride has been used to selectively and quantitatively dissolve the easily-reducible Mn oxides and hydroxides (Chao, 1972). It is possible that acidic HH might dissolve poorly crystalline Fe oxides too. HH extracted more than 25% of the total Mn, suggesting that a greater proportion (~40%) of the total Mn was in silicate or other mineral phases (e.g., spinels) that are resistant to dissolution by HH. When all the three extractions are compared, AO-extractable Mn proportions were similar to the HH-

extractable Mn proportions in all the soils, implying that irrespective of the dissolution mechanism of Mn oxides by HH or AO an acidic pH (<3) solution is necessary for quantitative dissolution of the Mn oxides. The Fe oxides (e.g.,ferrihydrite) and crystalline Mn oxides have been reported to dissolve in acidified AO (Chao and Theobald, 1983). In crest soil, the proportion of the DC-extractable Mn was only one-fifth of that of the HH-extractable Mn, but the proportions of Mn extracted by DC in toeslope soil were nearly equal to that extracted by HH. These trends are attributed to the inverse proportions of hematite and goethite (and/or ferrihydrite) in crest and toeslope soil as shown by the XRD patterns (discussed in mineralogy of the clay fraction section). Goethite and poorly crystalline Fe oxides, which are predominant in the toeslope soil, tend to incorporate more Mn (up to 30 mole % in goethite) in their structures compared to hematite (Ebinger and Schulze, 1989). In toeslope soil, periodic wetting and drying cycles create alternate redox conditions that result in redox-sensitive coprecipitation of Mn and Fe.

Cr

Only a small proportion of the total soil Cr was extracted from each of the soils by HH (< 0.1% of total Cr) or AO (< 1%), suggesting that only trace amounts of Cr were associated with Mn oxides or poorly crystalline Fe oxides. The apparent lack of association of Cr with Mn oxides, in spite of the relatively high concentrations of both species, is attributable to the oxidation reactions of Cr(III) to Cr(VI) by Mn oxides (Bartlett and James, 1979; Fandeur et al., 2009) and prevention of incorporation of Cr(III) by Cr oxide crystal lattice. In most soils, except the pediplain soil, more than 7% of the total Cr was extracted by DC, and the variation of Cr percentage followed a similar trend with DC- extractable Fe, suggesting a strong association/incorporation of Cr by the crystalline iron oxides.

Ni

Much higher proportions of Ni than of Cr were extracted by each of the three extractants, indicating the strong association of Ni with both Mn oxides and Fe oxides. Previous studies have shown that Ni can co-precipitate with Fe oxides or form surface

adsorption complexes with Fe oxides (Singh and Gilkes, 1992; Trolard et al., 1995; Singh et al., 2002). The similarity between the AO- and HH-extractable Ni concentrations indicate desorption of Ni from the surfaces of Fe and Mn oxides and the dissolution of Ni-rich mineral phases during the acid extractions. In acidic conditions, the surfaces of the Fe oxides become positively charged due to protonation of surface sites with the subsequent repulsion of the surface adsorbed Ni^{2+}. More than 10% of the total Ni was therefore associated with Mn oxides and/or surface-adsorbed Fe oxides. This percentage increased from the crest to the toeslope, indicating that goethite and the poorly crystalline Fe oxides were the principal sites for Ni retention. Similarly, an increasing trend of DC-extractable Ni from 40% in crest soil to about 100% in toeslope soil was observed, implying that Ni was not incorporated with the layer silicates.

Occurrence of Cr (VI) in soils

Due to the high concentration of total Cr in the soils and concerns about its toxicity, the toxic species Cr (VI)) was quantified in all soils. The concentrations of Cr (VI) were generally below the detection limit; however, samples from the crest surface soil and subsoil contained 0.31 and 1.5 mg Cr (VI) kg^{-1}, respectively. Although these concentrations account for only 0.005% or less of the total Cr in these soils, they are the most mobile and toxic forms of Cr to living organisms in the natural systems. The presence of Cr (VI) and the increased concentration with depth is likely impacted by the relatively high concentration of easily weatherable Cr-rich enstatite (Fig. 2.2), the occurrence of Mn(III,IV) oxides that can result in the oxidation of Cr(III) to Cr(VI) (Bartlett and James, 1979; Kim et al., 2002; Fandeur et al., 2009), and the lower organic matter concentrations in the subsoil.

Mineral compositions of soils and parent rocks

Primary minerals common to each of the soils were enstatite, talc, quartz, and chromite (discussed in spatial variation of soil mineral phases section). Talc and quartz were found in all soil particle-size fractions. Likewise, smectite, vermiculite/chlorite, kaolinite, and Fe oxides were secondary minerals that occurred in each of the soils

irrespective of geomorphic position. Minerals such as serpentine and magnetite/maghemite were only found at specific landscape positions, therefore suggesting the influence of parent material and drainage conditions.

Mineralogy of the clay fraction

The XRD, FTIR, and electron microscopic analyses indicated that the clay fractions of the soils contained talc, serpentine, smectite, vermiculite, kaolinite, and Fe oxides (including goethite and hematite).

Talc

Talc is evident by its 0.94 nm d(001) and higher order diffraction peaks on the XRD patterns. Those XRD peaks were unaltered in ion exchange, solvation, and heat treatments (Figs. 2.3 and 2.4). Further evidence of talc was its characteristic infrared bands at 3677, 3661, 669, and 467 cm^{-1} (Fig. 2.5). The occurrence of the absorption band at 3661 cm^{-1} suggested substitution of Fe, Ni, or both for Mg in the octahedral sheet of talc (Wilkins and Ito, 1967; Farmer, 1974), which has been ascribed to OH-stretching vibration at the MgMgFe(Ni)-OH site. Nearly pure talc aggregates were also separated from the silt and sand fractions by hand (Fig. 2.6, image A). The infrared band of the sand-sized talc aggregate at 3661 cm^{-1} was relatively more intense than that of the clay fractions. Moreover, there is an additional band at 3644 cm^{-1} that has been attributed to the OH-stretching vibration of the MgFe(Ni)Fe(Ni)-OH (Wilkins and Ito, 1967). Energy dispersive spectroscopic analysis indicated that Fe but not Ni was the substituting cation in the structures (Fig. 2.7, spectrum a). The SEM-EDS analyses suggest that most silicate minerals were coated by Fe oxides (Fig. 2.7, spectra b and c) and that minor amounts of Cr and Ni were associated with either the iron oxides or the silicate phases. Trace amounts of Al and Cr were also detected in the talc aggregates and in dithionite-citrate treated clay by the SEM-EDS and TEM-SAED analyses (Fig. 2.8).

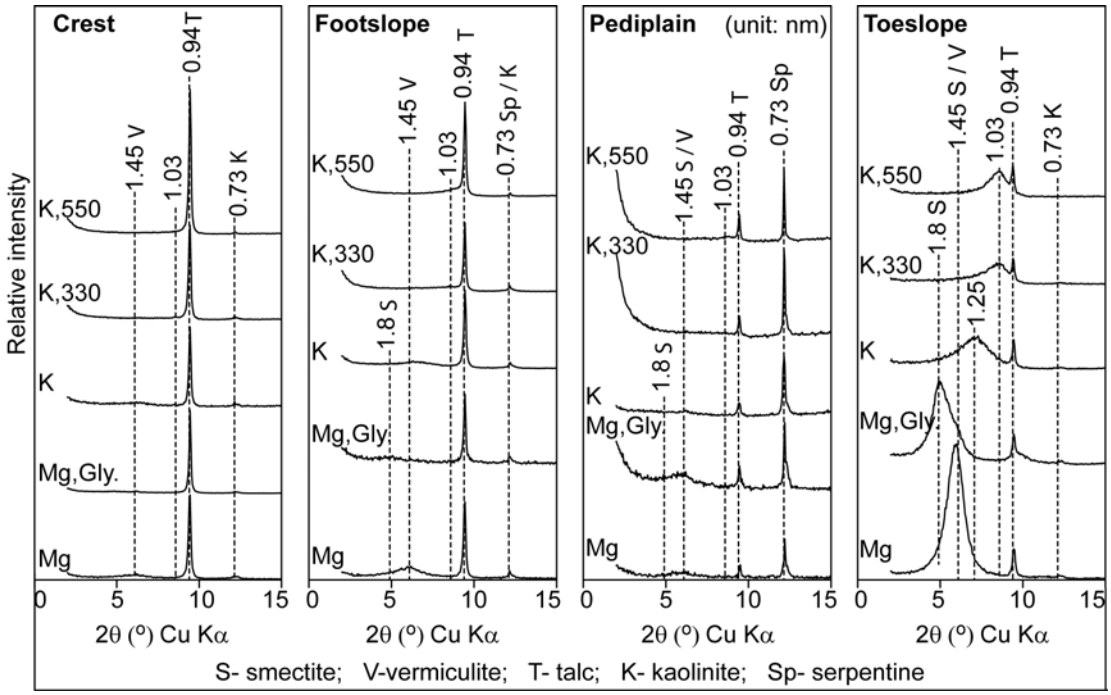

Fig. 2.3. Representative X-ray diffraction patterns of the subsoil clay fractions from each landscape position after ion exchange, glycerol solvation, and heat treatment.

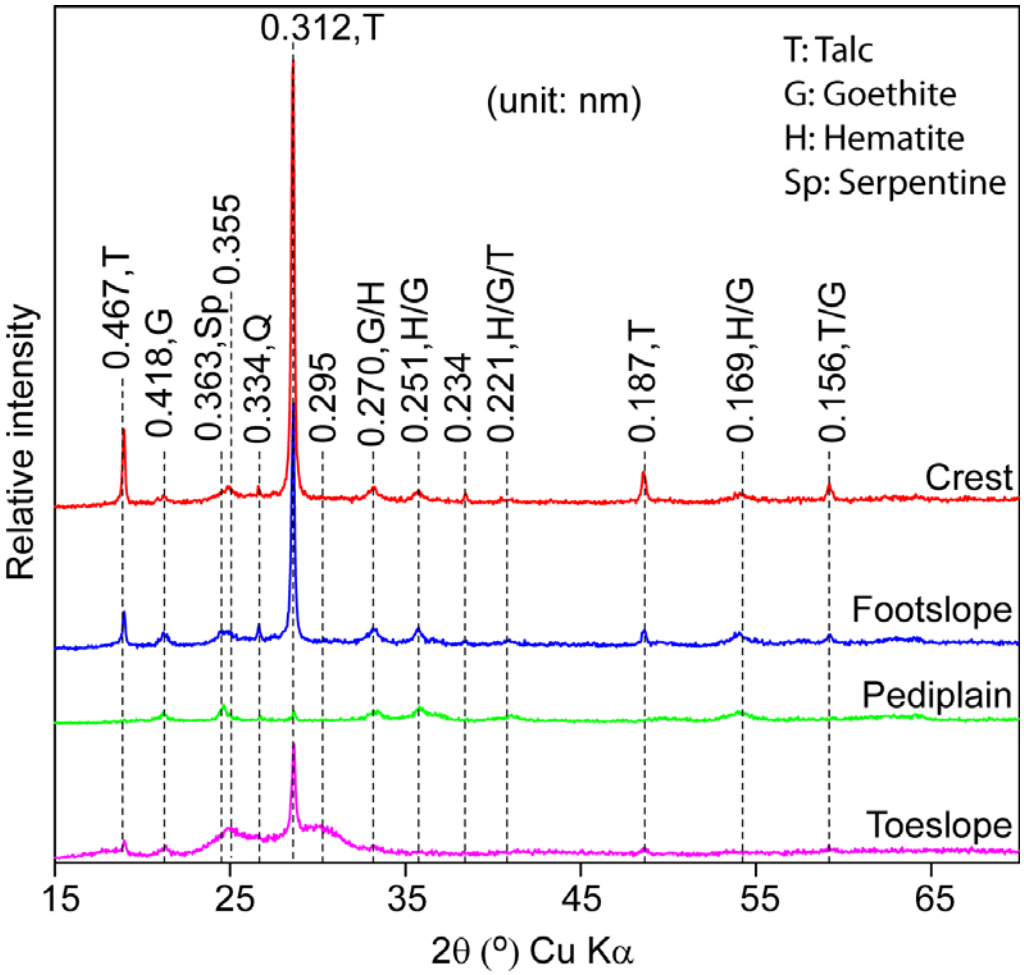

Fig. 2.4. X-ray diffraction patterns at room temperature of Mg-saturated clay fractions in subsoil from four landscape positions.

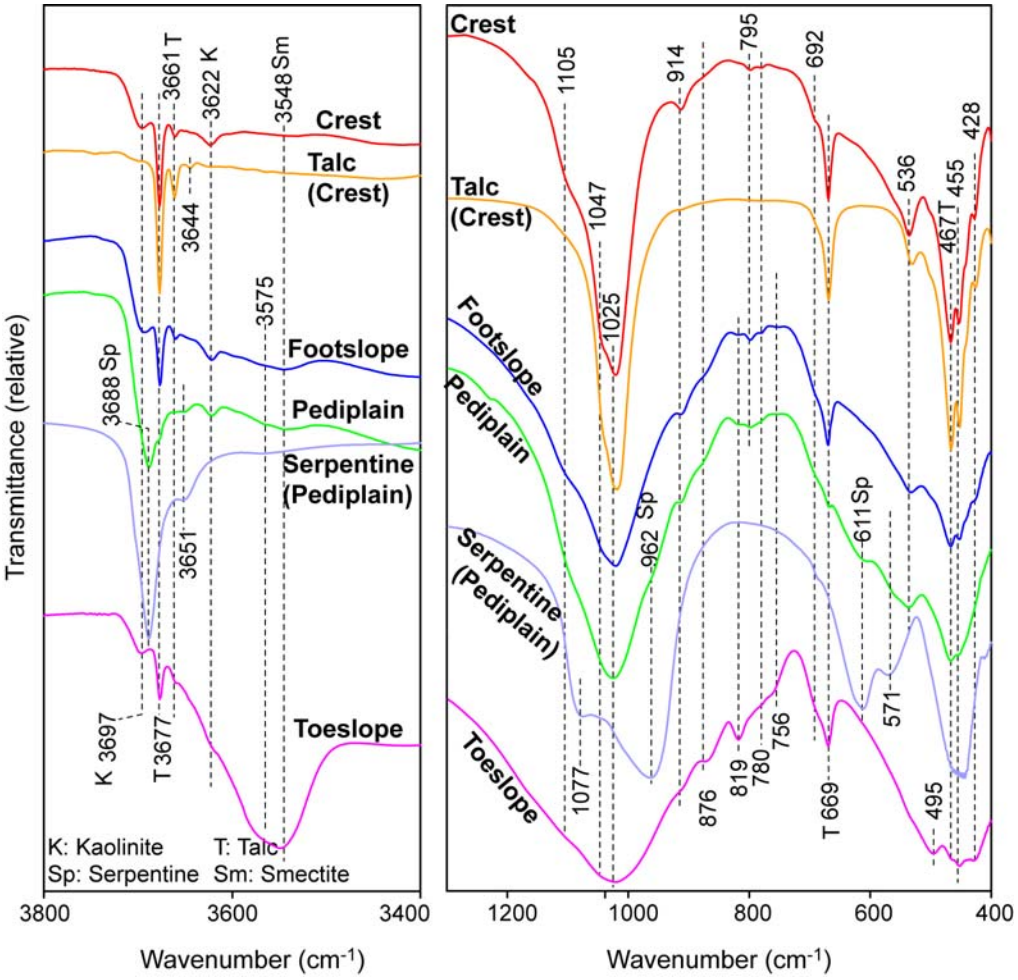

Fig. 2.5. Fourier transform infrared spectra of the clay fractions and of hand-picked talc and serpentine specimens from the crest and pediplain subsoils, respectively.

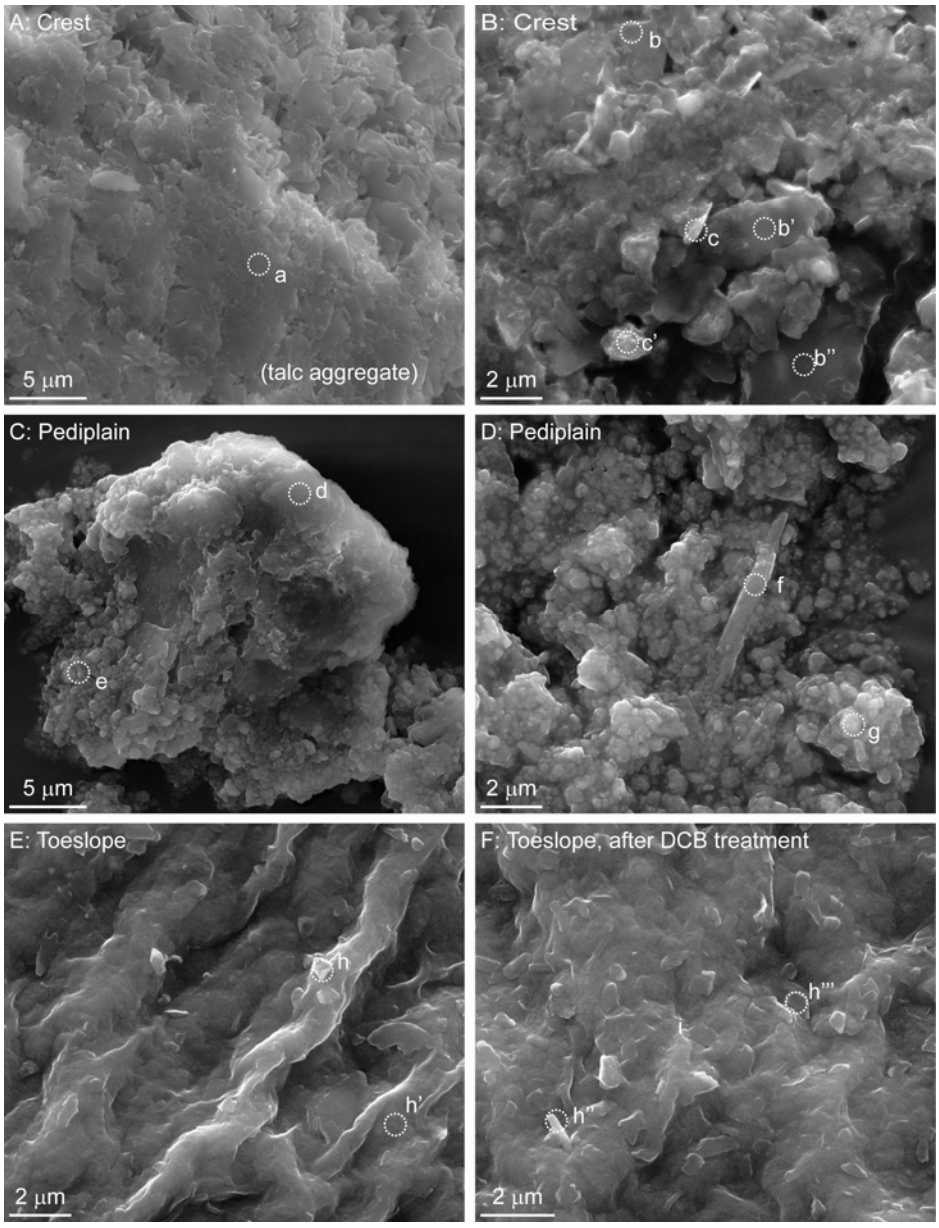

Fig. 2.6. The SEM images of silicate clay minerals in subsoils from the various landscape positions.

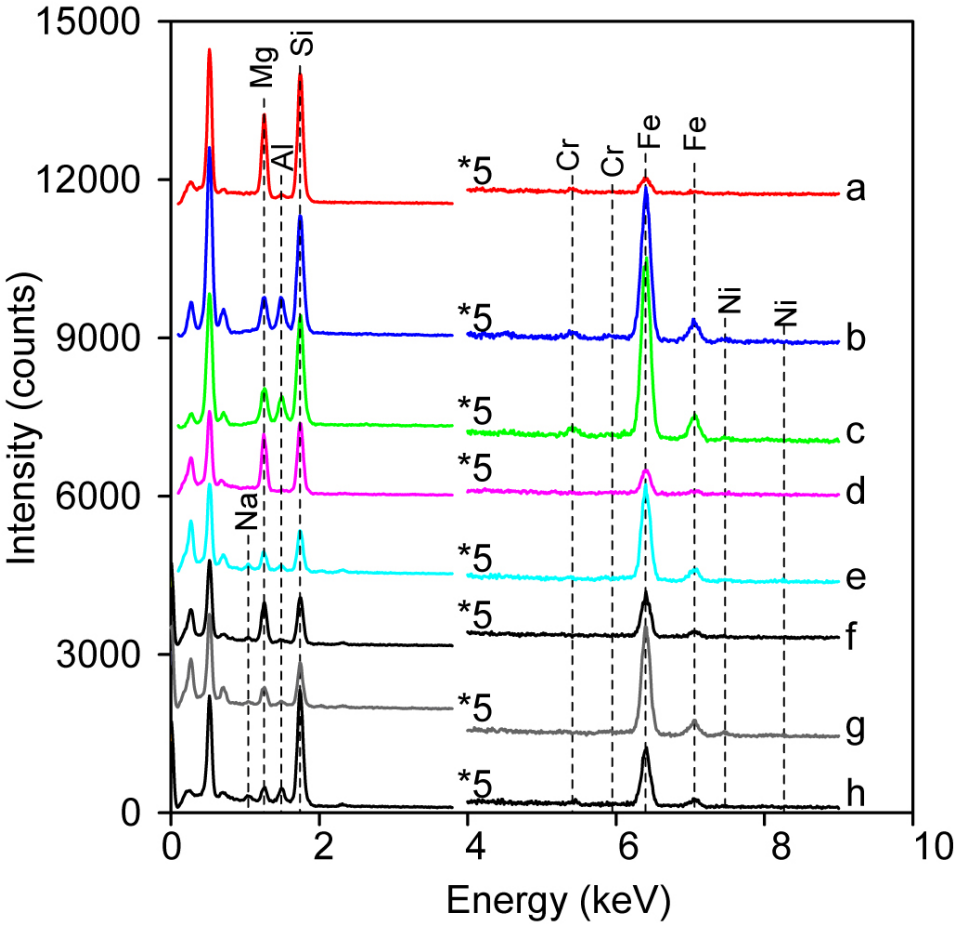

Fig. 2.7. EDS spectra of selected particles in the SEM images shown in Fig. 2.6. Similar letters at specific locations represent identical composition.

Serpentine

Serpentine had characteristic XRD peaks at 0.73 and 0.363 nm that were not affected by the ion exchange reactions or heat treatment (Figs. 2.3 and 2.4). The 3688, 962, 611, and 571 cm^{-1} infrared bands are also diagnostic for serpentine (Fig. 2.5, pediplain). Both platy and short fabric serpentine particles have been observed in the pediplain soils (Fig. 2.6, image C and D) by SEM. Transmission electron microscopy (TEM) analyses of the dithionite-citrate treated clay further confirmed the platy and curled morphology of serpentine. The SEM-EDS and TEM-SAED analyses of the clay sized-particles

indicated that the serpentine minerals are rich in Mg but also contain minor amounts of Fe and Ni (Fig. 2.7, spectra d and f). The selected area electron diffraction (SAED) of the serpentine clay particles shows linear and irregular patterns (Fig. 2.8, image C) suggesting curled and planar morphology, respectively. No Al or Cr was detected in the serpentine specimens (Fig. 2.8).

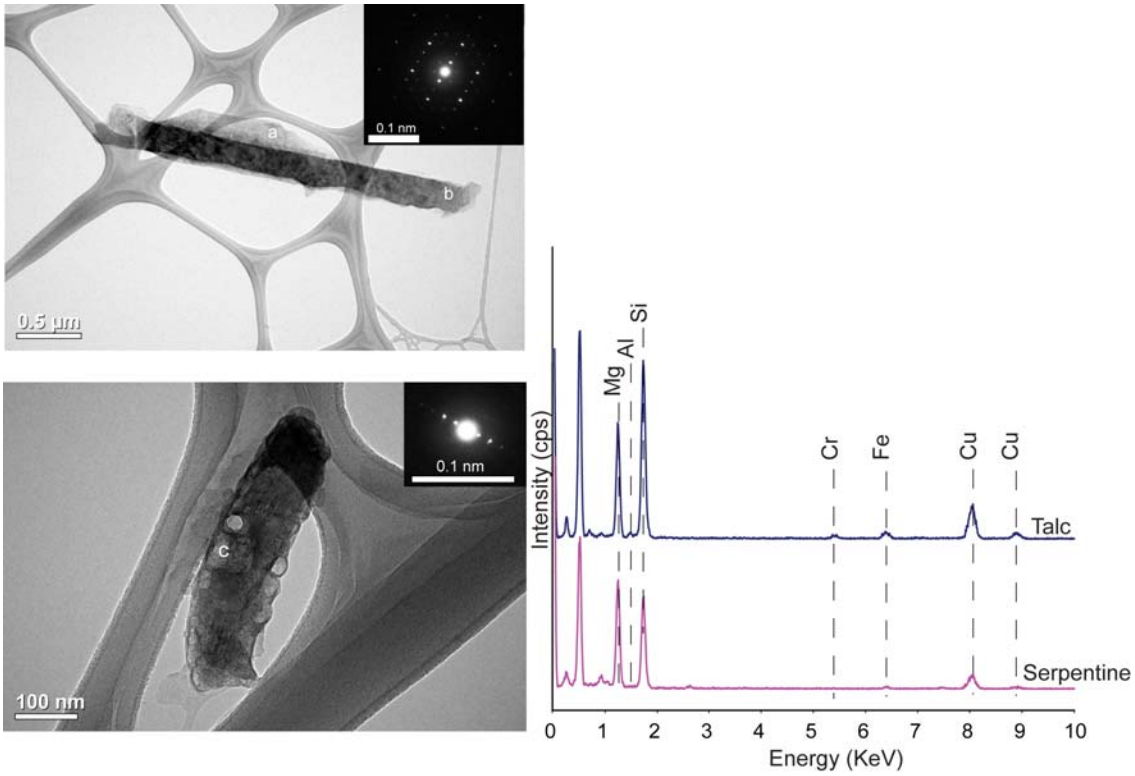

Fig. 2.8. Transmission electron images of talc (*top left*) and serpentine (*bottom left*) treated with dithionite-citrate and the selected area diffraction patterns (*right*). Talc and serpentine were taken from the crest and pediplain subsoils. Talc particles were lath shaped with sharp edges. Serpentine had a curled morphology and subjected to beam damage (oval spots). The selected electron diffraction patterns and elemental compositions of the particles were determined from positions marked a, b and c. The EDS showing Cu are from the sample holder.

Iron-rich smectite

Smectite was identified by the appearance of a 1.8 nm peak or the weakened intensity of the 1.45 nm peak in the XRD patterns after the glycerol solvation treatment (Fig. 2.3). The intense infrared bands at 3575, 3548, 876, 819, and 495 cm^{-1} (Fig. 2.5, toeslope) are characteristic infrared bands for Fe-rich smectites such as nontronite. The substitution of Fe for Al in the octahedral sheet causes shifts of the stretching (3400-3600 cm^{-1}) and bending (700-920) vibrations of the OH groups to lower frequencies (Farmer, 1974). The 819 cm^{-1} band originates from the OH-bending vibrations at the Fe(III)Fe(III)-OH site, and its strong intensity suggests abundant Fe in the octahedral sheet of the smectite. The 495 cm^{-1} band is the Fe-O-Si bending and deformation vibration (Bishop et al., 2002a). EDS analysis of the clays from the toeslope position after the DCB treatment (Fig. 2.7, spectrum h) indicated abundant Fe and a small amount of Cr in the smectite structure. Smectites that contain structural Cr are not common in soils, although their occurrence has been reported in the Nevada, USA (Foord et al., 1987). In Zimbabwe, (Anderson, 1975) reported the occurrence of Cr-rich nontronite in the Mzongwe River bank, Mafungabusi, which, is located several miles west of the Great Dyke.

Vermiculite and kaolinite

The presence of minor amounts of vermiculite in the clay samples was shown by the weak 1.45 nm XRD peak for the glycerol-treated samples but the absence of this peak with the 550°C heated samples (Fig. 2.3).The occurrence of vermiculite in addition to smectite in the soils was the likely reason for the relatively high soil-CEC values (Table 2.1). Kaolinite was identified by its infrared absorption bands at 3697, 3622, and 914 cm^{-1} (Fig. 2.5). The absorption bands in the OH stretching region (3697 and 3622 cm^{-1}) were weak and broad, and the other two characteristic absorption bands of kaolinite at 3670 and 3650 cm^{-1} were too weak to be observed, suggesting a poorly crystalline and defective structure. These bands were evident in most clay samples, except those from the pediplain. The EDS analyses suggest that most silicate minerals were coated by Fe oxides (Fig. 2.6, spectra b and c), and that minor amounts of Cr and Ni were associated with either the Fe oxides or the silicate phases.

Iron oxides

Crystalline goethite and hematite in the clay fractions were identified by XRD (Fig. 2.4). Overall, the Fe oxide XRD peaks were weak and relatively broad, suggesting small crystallite sizes.

Mineralogy of sand and silt fractions

Enstatite

Enstatite was found in the sand fractions of all soils but not in the silt or clay fractions, suggesting rapid weathering of the mineral once the particle size becomes smaller. The sharp angular edges and corners of the enstatite sand particles (Fig. 2.9, images A and B) indicate that the enstatite was not transported for a long distance from its sources. Abundant longitudinal dissolution pits, grooves, and corrugated terraces were observed on the surfaces of the particles (Fig. 2.9, images A1 and B2). These features were consistent with the dissolution of pyroxenes and amphiboles that occurs along crystallographic planes of weakness parallel to the c-axis (Berner and Schott, 1982; Proust et al., 2006). Many irregularly-shaped and sub-μm sized Ni- and Cu-rich particles were observed on surfaces of the enstatite (Fig. 2.9, image A1). Some of the particles contained Ti, Mn, Fe, and Al (Fig. 2.10, spectra c and d), but much less Mg or Si compared to the enstatite. We interpret these particles as the oxide phases of Ni, Fe, and Ti with incorporated Mn, Cu, and Al. They existed as either protrusions on the edges of the dissolution pits or coatings on the surfaces. Fine Mg- and Fe-rich silicate plates, with minor amounts of Cr in their structures (Fig. 2.9, image B2; Fig. 2.10, spectrum e), were also found on the surfaces of enstatite. The chemical compositions of the enstatite particles were close to the ideal formula, $MgSiO_3$, with minor amounts of Fe, Ca, and Cr in the structures as indicated by the X-ray energy dispersive spectra of the particles (Fig. 2.10, spectra a and b). This composition was in agreement with that of the bronzitite reported in the Darwindale sub-chamber P1 layer pyroxenes (Wilson, 1992).

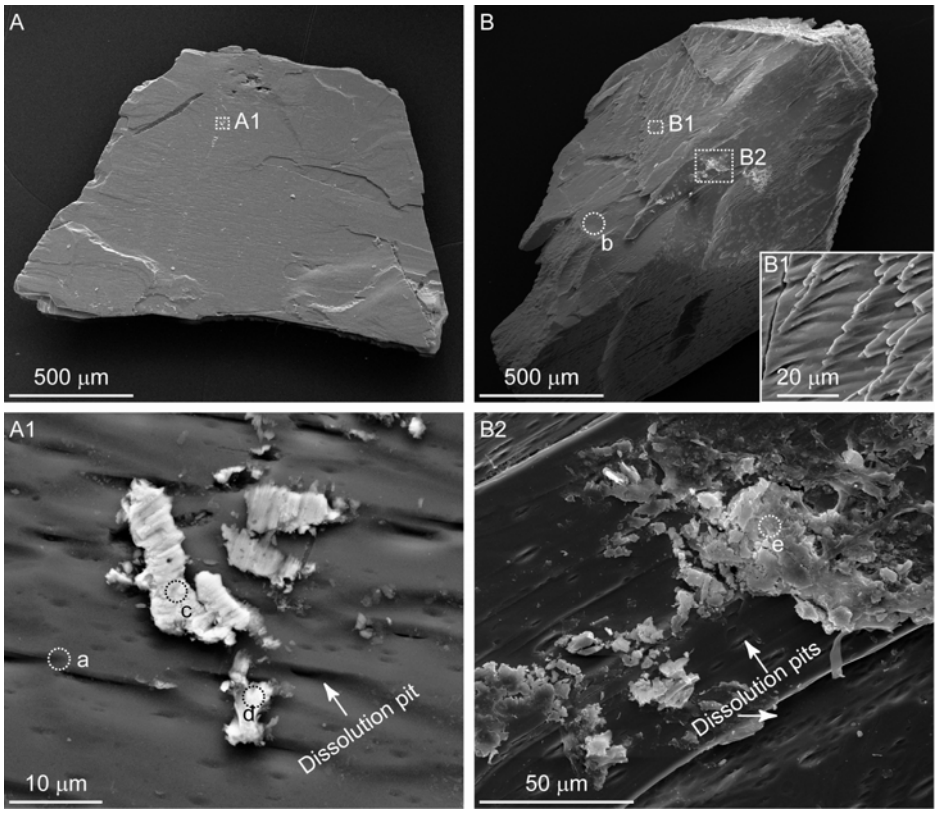

Fig. 2.9. Hand-picked enstatite sand particles (A and B) from the crest subsoil and their respective Ni-, Ti-, Cu-, Mn-, and Fe-rich weathering products (A1 and B1). The energy dispersive spectra of the marked areas (a-e) are shown in Fig. 2.10.

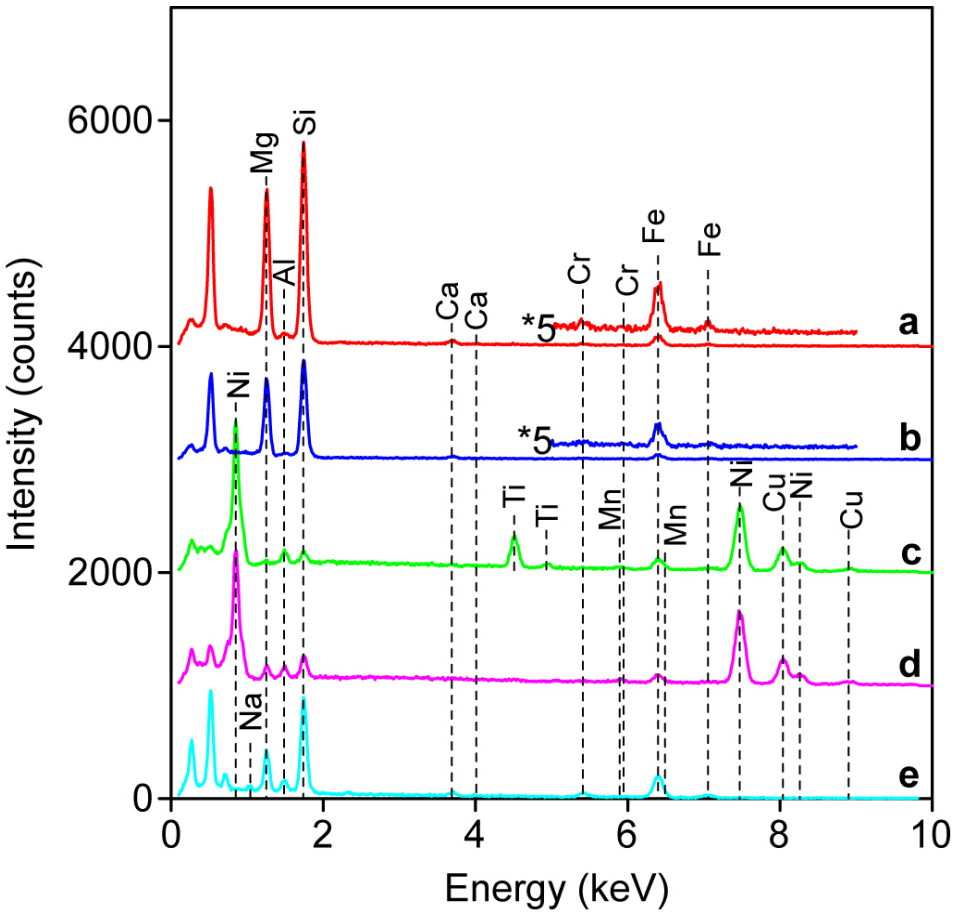

Fig. 2.10. Energy dispersive spectra of marked areas (a-e) on enstatite particles and their weathering products shown in Fig. 2.9.

Chlorite and serpentine

X-ray diffraction patterns showed sharp peaks of low intensity at 0.145 nm that were assigned to chlorite (data not shown). These peaks were only detected in the silt fraction of the pediplain soil. Smaller amounts of serpentine were found in surface soils at the toeslope, but it was absent in subsoils. It is likely that serpentine was transported from the upper landscape positions of the transect.

Quartz

Quartz occurred in the sand and silt particle-size fractions at all geomorphic positions across the transect, although in lower abundance at the pediplain. Trace amounts of quartz were also identified in the clay fractions of the crest, footslope and pediplain soils (Fig. 2.4). Feldspars, which are abundant minerals in the sand and silt fractions in common agricultural soils were noticeably absent in soils at all the landscape positions.

Chromite

Chromite was identified in the sand and silt fractions of all samples but not in the clay fractions. Many chromite particles exhibited euhedral octahedron morphologies (Fig. 2.11) and smooth flat surfaces, indicating the high degree of crystallinity of these minerals. The individual chromite particles demonstrated different relative resistance to the aqua regia - HF treatment, a common procedure used to digest of soil and sediment samples (Hossner, 1996). Some particles showed abundant etched cavities following the reaction (e.g., Fig. 2.11, image B), whereas other particles were largely unaffected by the treatment (Fig. 2.11, image C). The chromite particles also exhibited different degrees of magnetism at room temperature. Some chromite particles were easily attracted by a hand magnet (Fig. 2.11 image D), but those that survived aqua regia-HF treatment could not be readily attracted to a hand magnet (Fig. 2.11, images A-C). The differences in magnetic behavior of the chromites could be attributed to differences in Al, Mg substitution and Fe^{2+}/Fe^{3+} content in the chromite structure. The chromite particles had chemical compositions of Cr, Fe, Mg, Al and O. The different intensities of Mg and Al peaks in their EDS spectra indicated various degrees of substitution of Mg for Fe^{2+} and of Al for Cr (Fig. 2.12, a-d).

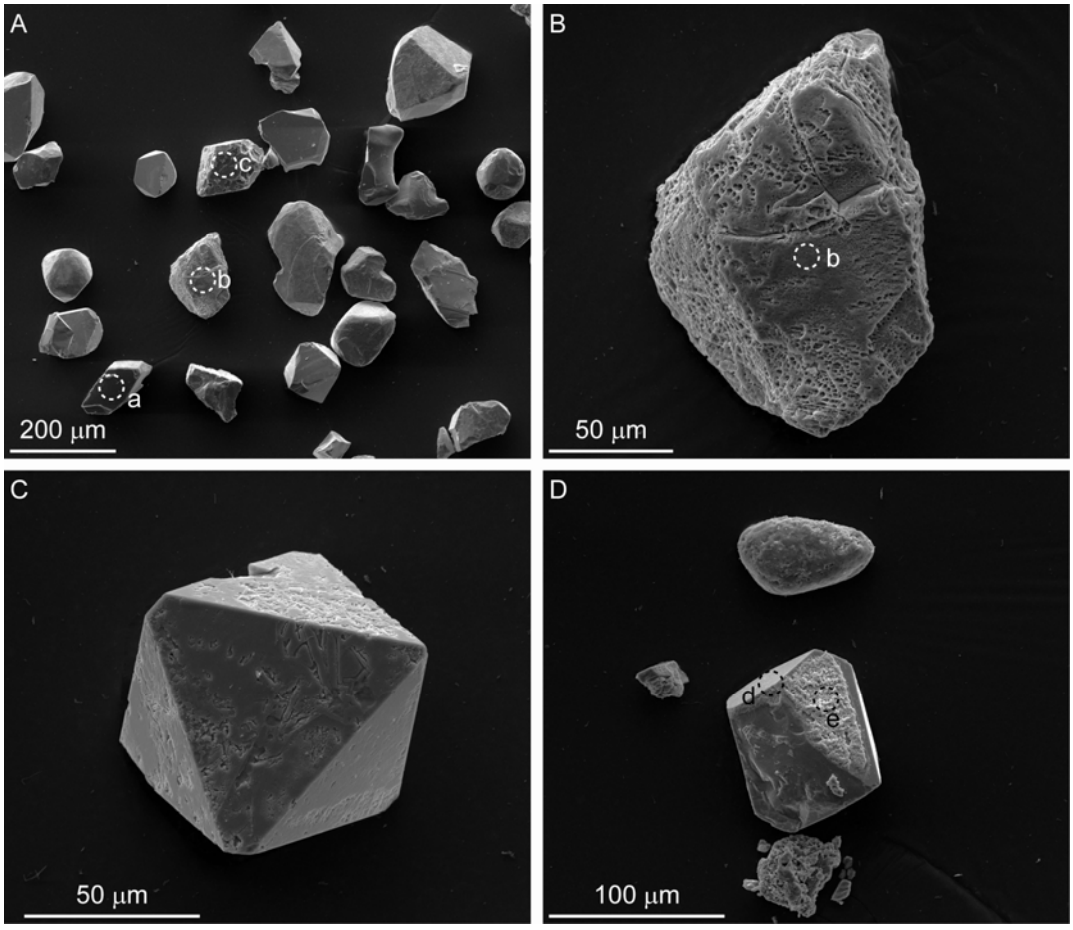

Fig. 2.11. Chromite particles from the sand-size fraction of the pediplain subsoil after aqua regia/ HF treatment (A-C) and chromite in the magnetic sand fraction of the crest subsoil (D). The energy dispersive spectra of the marked areas (a-f) are shown in Fig. 2.12.

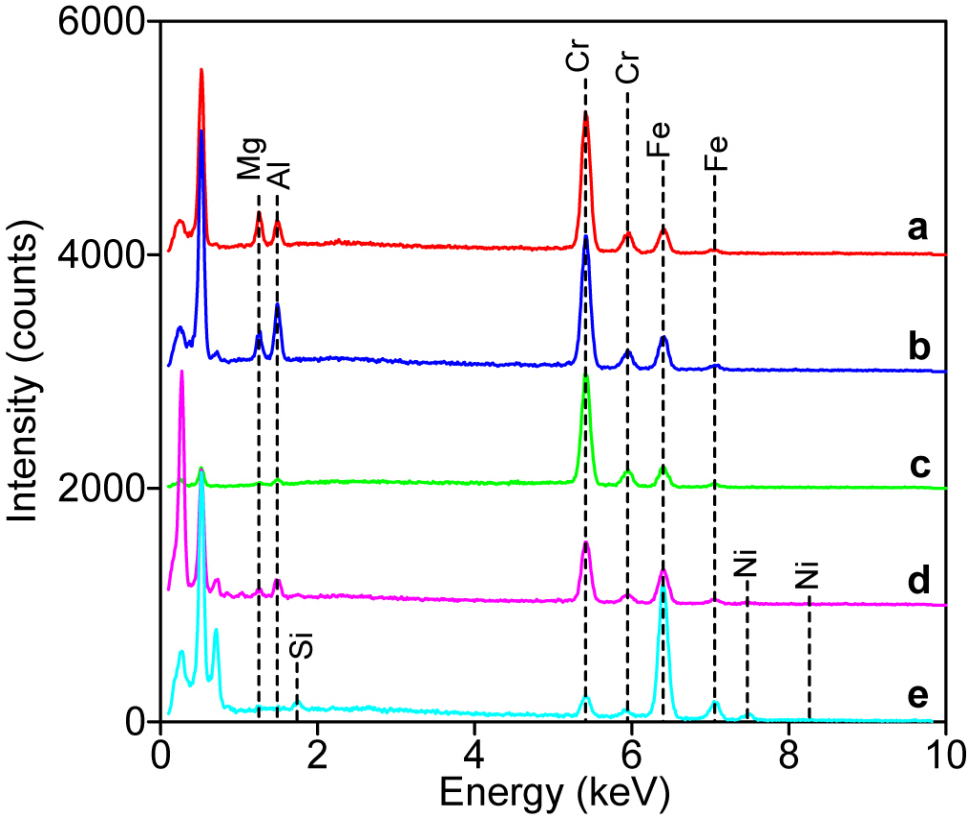

Fig. 2.12. Energy dispersive spectra for marked areas (a-e) on chromite particles shown in Fig. 2.11.

Fe and Mn oxides

Mineralogy of the magnetic particles indicated a predominance of magnetite/maghemite. The SEM images and the associated EDS spectra of the hand-picked, and magnetically separated sand particles (Figs. 2.13 and 2.14) indicated that both the coarse oxide particles and their fine coatings contained substantial amounts of Fe, Cr, Ni, and Mn. The coatings (e.g., Fig. 2.13) on the magnetic particles were Fe oxides with associated Cr and Ni (Fig. 2.14, spectra d and e) . Nickel was also found in the large particles (e.g., Fig. 2.14, spectrum c and d). Magnetite/maghemite occurred mostly in the silt fraction and in highest concentration at the crest (47%, w/w of silt) and pediplain (44%) and in

relatively lower concentration at the footslope (33%). Magnetite, which is black in color and of lithologic origin, has been reported to transform to reddish brown maghemite as a result of fire in the presence of organic C (Schwertmann and Taylor, 1989; Ketterings et al., 2000). The prevalence of fires in our study area could explain the relatively high ratios of magnetite/maghemite in the silt fraction. Although sand and silt fractions from the crest to the pediplain soil were largely magnetic, those from the toeslope were not.

Smooth Mn-rich coatings were evident on the black non-magnetic (mostly kaolinite and Fe oxides) particles (Fig. 2.13, image B). The EDS spectrum (Fig. 2.14, spectrum f) suggested that the Mn oxides contained more Ni than Fe. No Cr was detected in the Mn-coated particles because of the strongly oxidizing properties of the Mn oxides. Manganese oxides are the only known naturally occurring oxides capable of oxidizing Cr(III) to Cr(VI) in soils (Bartlett and James, 1979).

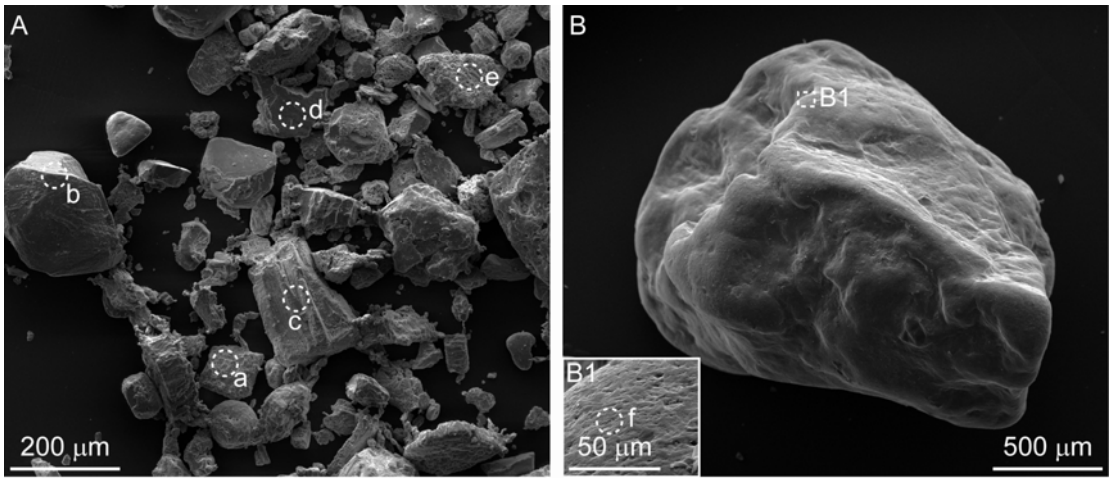

Fig. 2.13. Magnetic sand particles containing abundant iron oxides and chromite (*left*); a hand-picked black non-magnetic sand particle (*right*). The particles were taken from crest and pediplain subsoil. The energy dispersive spectra of marked areas (a-f) are shown in Fig. 2.14.

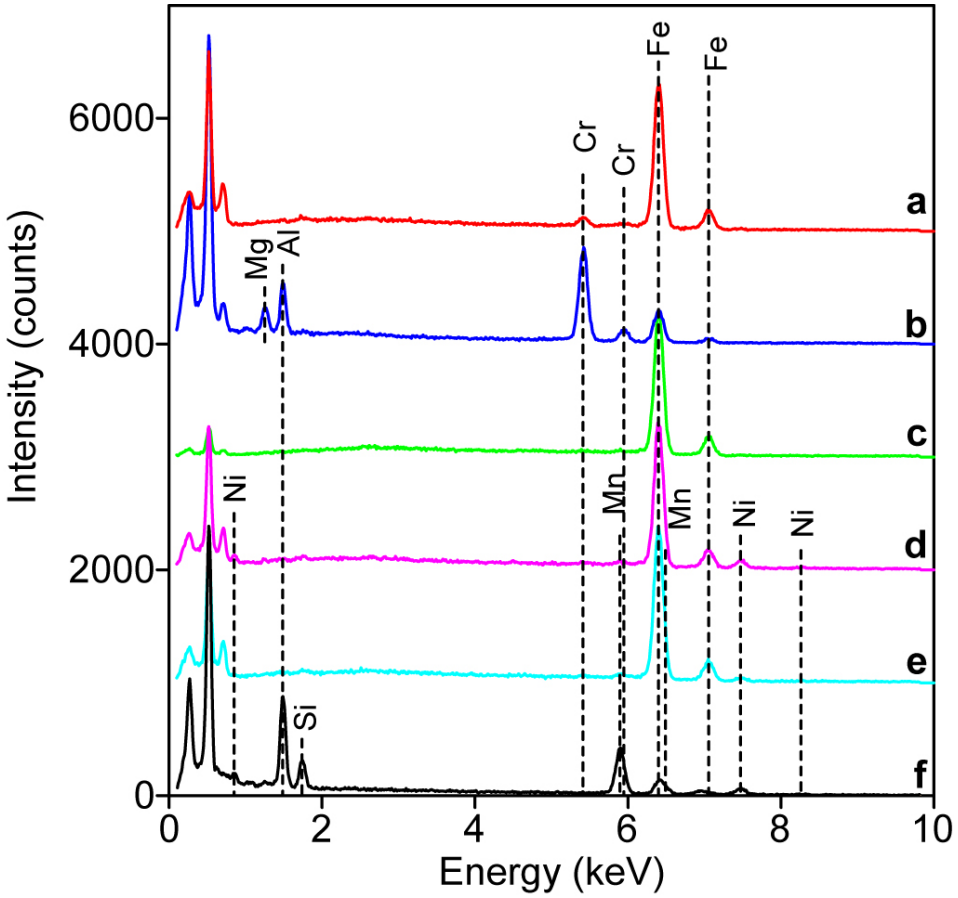

Fig. 2.14. Energy dispersive spectra of marked areas (a-f) on iron oxides and chromite particles shown in Fig. 2.13.

Spatial variation of soil minerals

In spite of the common occurrence of clay minerals at landscape positions across the transect, the relative abundances varied considerably with geomorphic position, but comparatively little vertically within each profile (Table 2.4). The X-ray diffraction patterns show greater concentrations of Fe oxides in upper and well drained landscape

positions but were generally least abundant in toeslope soil. However, DC- extractable Fe suggests that greater amounts of Fe oxides are present at the toeslope position. The AO- extractable Fe further indicates considerable amounts (8-12% w/w) of poorly crystalline Fe oxides at the toeslope position. The high values of poorly crystalline Fe oxides would be expected to be predominant at the toeslope because of increased weathering. Talc and enstatite were predominant in clay and sand particle size fractions, respectively, in crest and footslope soils. The footslope receives and accumulates soil and rock fragments from the crest through erosion by water, hence its mineralogical similarity with the crest soil. Serpentine was most abundant in the pediplain soils and occurred in all soil particle size fractions, suggesting lithologic origins. The XRD patterns in combination with SEM and FTIR absorption bands of clay minerals in the OH-stretching region (Fig. 2.5) indicated Fe-rich smectite was predominant in the toeslope, where it may have formed directly from solution originating from increased weathering under the prevailing higher moisture conditions and accompanying alternate wetting and drying cycles. At all landscape positions, kaolinite was either absent or it was the least abundant, which reflected the very low concentrations of Al in the parent rocks.

Table 2.4. Relative abundance (based on XRD relative peak intensity) of minerals in soil across the Mpinga transect.

Landscape Position	Particle Size fraction	Chromite	Enstatite	Fe oxides	Quartz	Serpentine	Talc	Smectite	Chlorite/ Vermiculite	Kaolinite
Crest	Clay	a*	a	ooooo	o	a	ooooo	oo	oo	o
	Silt	o	o	ooooo	oo	a	ooo	a	a	a
	Sand	ooo	oooo	ooooo	oooo	a	ooo	a	a	a
Footslope	Clay	a	a	ooooo	a	o	ooooo	oo	o	a
	Silt	ooo	o	ooooo	ooooo	o	oo	a	o	a
	Sand	o	oooo	ooooo	ooooo	a	ooo	a	a	a
Pediplain	Clay	a	a	ooooo	o	ooooo	oo	oo	o	a
	Silt	oooo	o	ooooo	o	ooooo	oo	a	a	a
	Sand	ooo	oo	oo	ooo	ooooo	oooo	a	a	a
Toeslope	Clay	a	a	oo	o	a	ooo	ooooo	oo	o
	Silt	oo	oo	a	ooooo	a	oooo	a	oo	a
	Sand	o	ooo	a	ooooo	a	o	a	a	a

*a- absent/neglible; o- least abundant; ooo- abundant; ooooo- most abundant.

Comparison with other ultramafic soils

Although there are general similarities in mineralogical compositions of the soils derived from ultramafic parent materials from Zimbabwe with soils of similar parent rocks reported elsewhere, wide differences in elemental compositions, relative distribution in the various soil particle-size fractions and abundances are apparent. In the current study, feldspars and mica were absent and talc persistently occurred at all landscape positions. In previous studies of ultramafic-derived soils, low levels of illite, mica and feldspars have been reported (Bonifacio et al., 1997; Alexander et al., 2007; McGahan et al., 2008). Unlike ultramafic soils in other places with minor/trace amounts of chromite, enstatite and serpentine, our study has shown the predominance of these minerals in soil. Consequently, Zimbabwean soils contain very high concentrations of Cr and very low levels of K. In addition, high concentrations of Cr(VI) occurrences in crest soil corroborate earlier findings in Zimbabwean ultramafic soils (Cooper, 2002) and New Caledonia (Fandeur et al., 2009). In these studies, chromite is regarded as the main source for Cr in soil that is eventually oxidized, however, our results suggest that pyroxenes are the major Cr-releasing minerals in the Zimbabwean soil. Chromite examined in Zimbabwean soils lacked Ni, in contrast to the one studied in Brazil (Garnier et al., 2009). Even though talc is considered unstable in soil, earlier findings have attributed the preservation of talc in well drained positions to the protective Fe oxide coatings (Harris et al., 1984; Nyamapfene and Yin, 1986). The implications are that talc might not exist under alternate dry and wet conditions normally found at the toeslope. Due to the likely high Mg and Si activities in solution resulting from the weathering of serpentine and other minerals, it can be predicted that talc would remain relatively stable under the current soil conditions.

In temperate and other tropical regions, serpentine, chlorite and vermiculite have been observed to be dominant in the clay fraction of soils derived from ultramafic rocks (Rabenhorst et al., 1982; Istok and Harward, 1982; Graham and Buol, 1990; Bulmer and Lavkulich, 1994; Lee et al., 2003; Gaudin et al., 2004; Gaudin et al., 2005; Traore et al.,

2008). Our findings of talc, vermiculite and smectite in crest soil are similar to earlier reports on soils developed from dunite on the Great Dyke (Nyamapfene and Yin, 1986).

IMPLICATIONS

Agriculture

The current study has shown high total concentrations of trace metal tens of times higher than in most common agricultural soils distributed in the various soil mineral phases. High concentrations of trace metals (e.g., Ni, Cr(VI)) can be toxic to some plants, animals and microorganisms, and can impact overall environmental quality (Robertson and Meakin, 1980; Brookes et al., 1986; Mertens et al., 2006). The chemical species of Ni are of major concern because a larger proportion of the total Ni is surface –adsorbed but weakly bonded, and potentially mobile and relatively bioavalaible (Manceau et al., 1992; Trivedi et al., 2001). Furthermore, Cr(VI) is readily desorbed, very soluble and readily bioavailable (Fendorf et al., 1997). These soils have very low concentrations of K and Ca, which is a result of the lack of major K- and Ca-containing minerals such as mica and feldspars. The predominance of easily weatherable minerals, which have higher Mg relative to Ca, in turn, disrupts the Ca:Mg balance of greater than unity commonly found in agricultural soils. Most plants do not grow under these conditions and only endemic plants capable of adapting to such soil conditions can do so. Low levels of K and Ca, which are essential plant nutrients, limit the potential of these soils for agricultural development without appropriate management strategies. The deficiency of K in these soils is exacerbated by the presence of vermiculite and high-charge smectite, which have high capacity to irreversibly retain K^+ and NH_4^+ (Barshad and Kishik, 1970; Shen et al., 1997). High concentrations of Fe oxides will potentially impact plant available P in these soils. The maintenance of adequate soil nutrients and moisture is therefore important in sustainable management of the soils for agricultural production. However, there are further concerns of heavy metal uptake by plants when grown in these soils, which could eventually lead to heavy metal uptake by humans and animals by way of food ingestion.

Environment and health

The abundant presence of serpentine minerals and high concentrations of highly toxic, carcinogenic and mutagenic Cr(VI) in these soils potentially creates a serious human health hazard. The concurrent presence of high amounts of the easily weatherable Cr - silicate minerals (e.g., enstatite) and high concentrations of Mn oxides provide ideal conditions for the formation of Cr(VI). Serpentine minerals and Cr (VI) have been implicated in various human cancers (Mossman and Gee, 1989; Manning et al., 2002). There are concerns to human health when high concentrations of other metals (e.g., Ni, Cu) are ingested via the food chain. Appropriate management strategies (e.g., liming) that reduce trace metal bioavailability and mobility in soil are needed.

CHAPTER III

MICROBIAL COMMUNITY STRUCTURE OF SOME SOILS ACROSS THE TRANSECT OF THE GREAT DYKE, ZIMBABWE

INTRODUCTION

Soil micro-organisms are an important part of the ecosystem. In soil environments, bacteria, fungi, actinomycetes and protozoa are particularly of agricultural and ecological interest because of their function in nutrient and C cycling (Haselwandter et al., 1990; Sprent and Parsons, 2000; Högberg and Högberg, 2002) and soil formation (Sterflinger, 2000; Burford et al., 2003). These functional roles are accomplished by a diverse group of microbes. The diversity of microbes in soil and their function in the environment have often been used as indicators of ecosystem health and environmental quality (Gregorich et al., 1997). The survival and function of microbes in the soil environment is largely influenced by pH, drainage, moisture, organic carbon content and chemical properties of the soil. High concentrations of heavy metals in soil have been implicated in reducing microbial activity and numbers (Baath et al., 1998); however, some microbes are capable of adapting to these extreme environmental conditions.

The Great Dyke, Zimbabwe, is one of the largest areas with soils derived from ultramafic (or serpentine) parent materials. Ultramafic soils usually contain high concentrations of Fe, Mg, Cr, Ni, and V and low levels of K and Ca (Brooks, 1987; Proctor, 1999). The impact of the ultramafic soil properties on plants and agriculture has been extensively documented (Brooks and Yang, 1984; Roberts and Proctor, 1992). However, studies on the impacts of these soils on microbial activity and function, and the overall microbial community structure are limited. Previous studies have shown that serpentine soils tend to have lower microbial biomass and lower microbial diversity than non-serpentine sites (Amir and Pineau, 1998b; DeGrood et al., 2005; Oline, 2006). Bacteria isolated from ultramafic soil showed tolerance to heavy metals (Mengoni et al., 2001; Pal et al., 2005; Amir et al., 2008). In spite of being one of the largest known areas

with ultramafic parent materials and a unique ecosystem for plants, the microbial community structure of the Great Dyke remains largely unknown. The objectives of the current study was to determine the microbial community structure at diverse locations across a transect of ultramafic-derived soils of the Great Dyke, Zimbabwe. The current study is vital to a better understanding of the environmental challenges, as well as addressing the potential management and remediation strategies of these fragile ecosystems.

METHODS AND MATERIALS

Field sampling

Sampling was conducted on separate landscape positions of the Mpinga transect (Fig. 3.1). A total of 20 sub-samples each were taken from the 0-15cm depth at the crest, footslope, pediplain and toeslope landscape positions. The subsamples from each landscape position were thoroughly mixed to form a composite sample that was air-dried before analyses.

Fatty acid methyl ester (FAME) analysis

The microbial community structure of the whole soil was determined by the fatty acid methyl ester (FAME) profiles (Kennedy, 1994). Fatty acids are important constituents of the cell membranes of microbes, and the fatty acids of a given soil sample can be considered as a fingerprint of the microbial community (Kennedy, 1994). In the following procedure, all glassware was baked in an oven at 150^{o}C for 24 hr before use. About 3.0 g of sieved (< 2 mm) and air-dry soil samples were placed onto the aluminum foil and transferred into glass centrifuge tubes. Lipids were extracted by adding 15 mL of 0.2 M KOH to each tube to lyse the bacteria. The tube was agitated on a vortex shaker for 20 seconds and then placed in a water bath at 37^{o}C. The tubes were further shaken for every 10 minutes for 10 seconds for 1 hr. The pH of the aqueous (0.2 M KOH) suspension was adjusted to neutral (~pH 7) by adding 3 mL of glacial acetic acid to the tubes. Fatty acids were extracted by adding 10 mL of hexane to the tubes and agitating the mixture on a vortex shaker for 20 s. The tubes were centrifuged at 1000 x g for 20

minutes at 4°C. About 2/3 of the immiscible hexane layer was removed by pipette and placed in oven-baked 9 mL tubes. The solution was slowly evaporated to dryness under N_2 gas and transferred into small labeled vials. The vials were quickly tightly closed to retain N_2 and stored at -20°C. Analysis of fatty acids was conducted by gas chromatography (Agilent, Wilmington, DE). Chromatogram peak identification was performed using the Sherlock Eukary program (MIDI, Inc., Newark, DE).

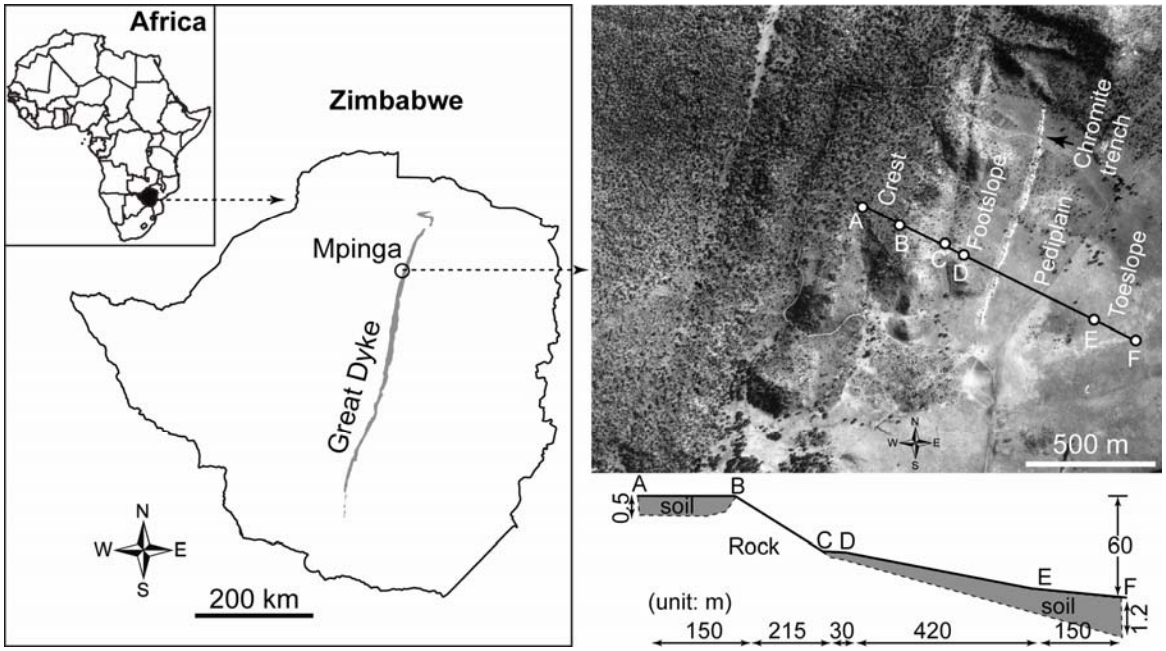

Fig. 3.1. Location of the Great Dyke (*left*), aerial photograph (*top right*) of the study area in Mpinga, Zimbabwe, and schematic illustration of the cross section between the points A, B, C, D, E and F along the transect (*bottom right*).

The standard IUPAC-IUB was used to name the fatty acids methyl esters. For example, in 16:1ω5c, the numbers before and after the colon refer to the number of C atoms and number of double bonds, respectively; ω refers to the position of the first double bond, followed by the number of C atoms at the aliphatic end. The letters "c" and "t" refer to

the *cis* and *trans* configurations, respectively. A total of 64 fatty acids were identified but only 39 compounds with known signatures, and with relative abundances >0.2 % were considered for further analysis. The percentages of the selected FAMEs were normalized to 100% and used for calculations of the relative abundances of each group of microbes. Ratios of the Gram-negative and Gram-positive bacteria were calculated from the total known bacteria biomarkers. The proportion of fungi:bacteria at each landscape position was calculated by using FAMEs biomarkers for fungi and bacteria (Bossio et al., 1998; Zelles, 1999). Species richness, eveness and Shannon diversity indices were calculated for each landscape position using PC-ORD5 software (MjM, Gleneden Beach, OR). The correlation of FAMEs with soil properties was examined by the multivariate and principal component analyses (PC-ORD5, MjM, Gleneden Beach, OR).

RESULTS AND DISCUSSION

Selected soil properties

The soil properties shown in Appendix B have been used in the statistical analyses.

Distribution of FAME across the transect

A greater proportion of the individual FAMEs were biomarkers for Gram-positive bacteria (16:0) and fungi (18:1ω9c and 16:1ω5c) (Fig. 3.2). Biomarkers for protozoa (20:4ω6c) were detected in the footslope and pediplain soils but their relative abundance were less than 2% (Fig. 3.2). The biomarker 16:1ω5c is specific to arbuscular mycorrhizal fungi (AMF) (Olsson et al., 1997). The relative abundance of biomarkers for fungi was similar at the crest and footslope positions but increased almost 2-fold at the toeslope position. Under conditions of nutrient deficiency and metal toxicity, mycorrhizal fungi form symbiotic associations with plants in order to increase nutrient availability as well as to protect the plants from the toxic metals (Hopkins, 1987; Meharg, 2003). Due to very low nutrient availability and high concentrations of trace metal in these soils, plant species adapted to ultramafic soil environments might form symbiotic associations with mycorrhizae fungi. The biomarkers for fungi were most

abundant in the footslope soil (20%) and least abundant in the toeslope soil (12%), suggesting ideal fungal growth in relatively well drained landscape positions and relatively high organic C. It is also possible that fungal growth was influenced by the *Acacia sp.* that was predominant at this site. Another striking observation is the relatively greater abundance of the 18:1ω9c and 19:0 cyclo c11-12 biomarkers in the toeslope soils. The latter FAME is the biomarker for methanotrophs, and is usually common in oxygen-depleted environments and high Mg^{2+} concentrations (Harwood and Russel, 1984). The toeslope generally experiences fluctuating drainage conditions during the rainy season with the potential to produce methane. It could be expected that the methanotrophic bacteria would be predominant when conditions become reducing. Furthermore, the toeslope soil contains the highest concentration of exchangeable Mg (Appendix B).

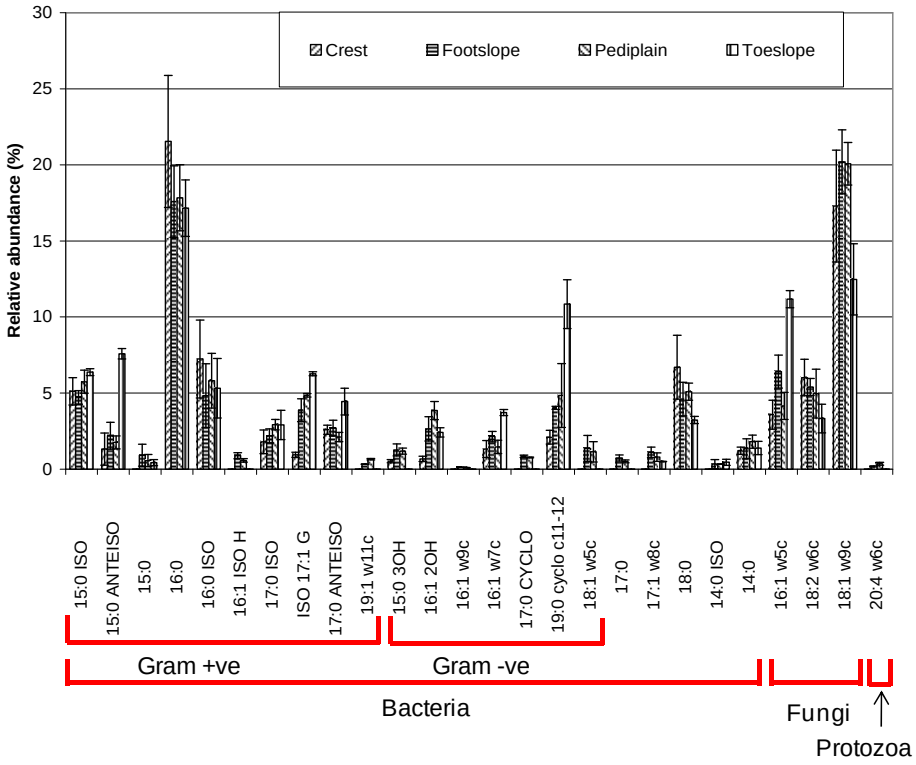

Fig. 3.2. Relative abundance (mean) and distribution of FAME in soil across the transect at Mpinga. Error bars are the standard deviations, *s*, *n*=3.

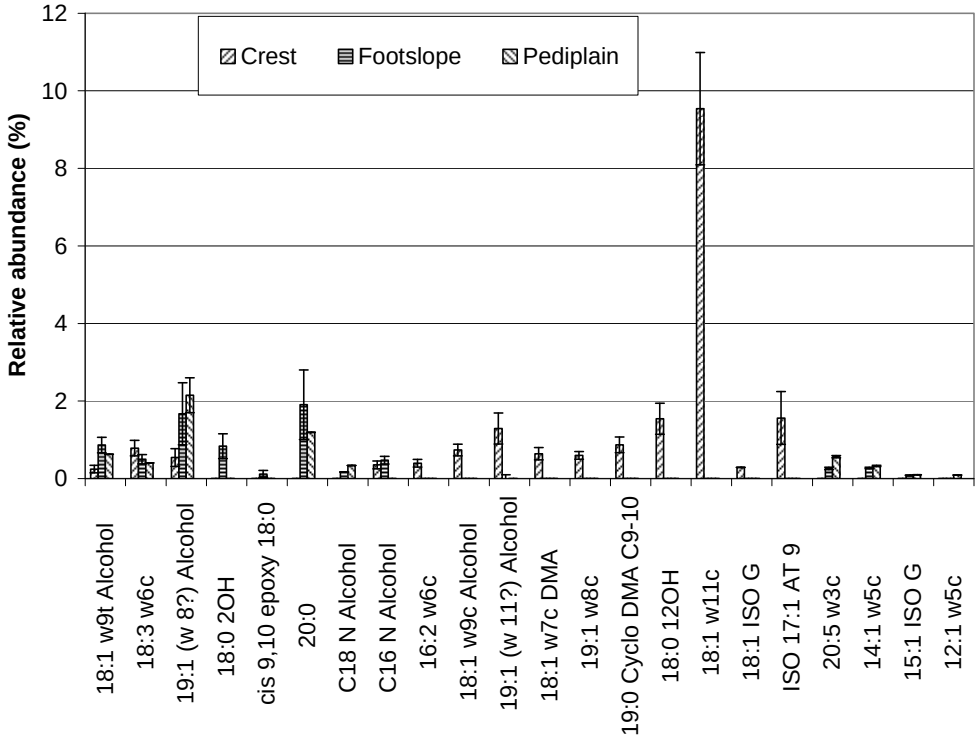

Fig. 3.2. continued

Other FAMEs were found in soil of the Great Dyke, but in some cases, their signatures are unknown. The highest proportion of FAMEs with 18-19 C was in crest soil. The presence of the FAMEs in crest could be impacted by the toxic Cr(VI) species, which was detected only at this site.

Spatial distribution of bacteria and fungi

Each of the landscape positions was dominated by bacteria. The relative abundance of Gram-positive bacteria was about twice as high as that of the Gram-negative bacteria in soils at each of the landscape positions, suggesting resilience in soils with high concentrations of trace metals and deficient in the major nutrients (Fig. 3.3). In New Caledonian ultramafic soils, Gram-positive bacteria were more abundant than Gram-

negative bacteria (Amir and Pineau, 1998a). Ultramafic soils from the Saddle Hills, India, had almost equal proportions of Gram-positive and Gram-negative bacteria (Pal et al., 2005). Although, soil properties can influence the microbial community structure, vegetation type and land use also impact the microbial community structure of soils (Grayston et al., 2004; Innes et al., 2004; Batten et al., 2006). The predominance of Gram-positive bacteria in these soils could also be due to the dominance of grasses (e.g., *Andropogon gayanus, Cymbopogon sp.*) that might select for these bacteria in the rhizosphere. Of the common microbial populations in soil, the least abundant FAMEs included those for the protozoa (<1 %) and actinomycetes (0%). Our results differ from earlier reports of microbial populations in which actinomycetes were found to be more prevalent in serpentine than in non-serpentine soils (DeGrood et al., 2005). In New Caledonia, very high proportions of actinomycetes have been observed in soils derived from serpentine when cultured on soil agar plates (Amir and Pineau, 1998b). These differences might be impacted by the locally predominant vegetation and the relative concentrations of the various metals in soil.

Shannon diversity indices decreased in the order footslope (3.01)> pediplain (2.92)> toeslope (2.64) > crest (2.48). These results suggest that greater diversity of microbes is generally associated with favorable soil conditions for plants.

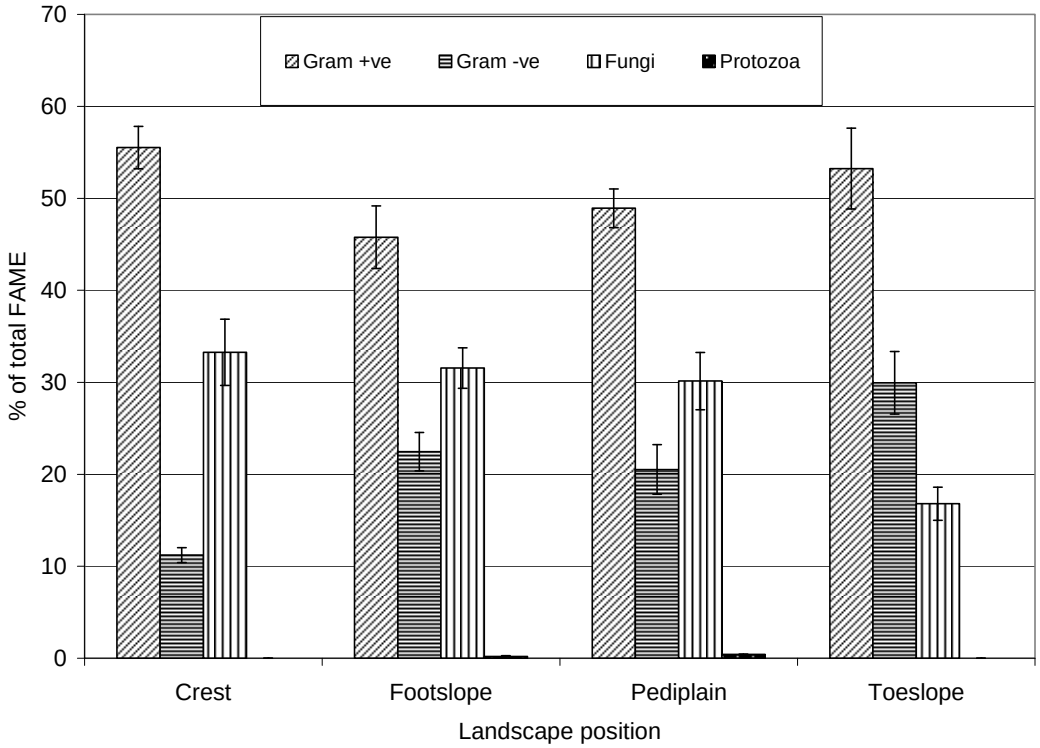

Fig. 3.3. Relative abundance and distribution of FAMEs known biomarkers in soil across the transect at Mpinga. Error bars are the standard deviations, *s* and *n* =3.

FAME multivariate analysis

The principal component analysis shows that the sites are separated by the clay content, Ca, pH and organic C (Fig. 3.4). The FAMEs 16:0, 16:0 ISO and 18:0 showed correlation with Fe, Mn, Zn and Mg. Although total Cr and Ni were included in the analysis, no significant difference was observed at each landscape position. Principal component (PC1) explained 47.69% of the variation and PC2, 32.96%. The most significant attributes were organic C, pH, exchangeable Ca, exchangeable Mg, total Fe, Mn and Zn. The dithionite citrate extractable metals (Fe, Mn) also showed similar results (not shown here).

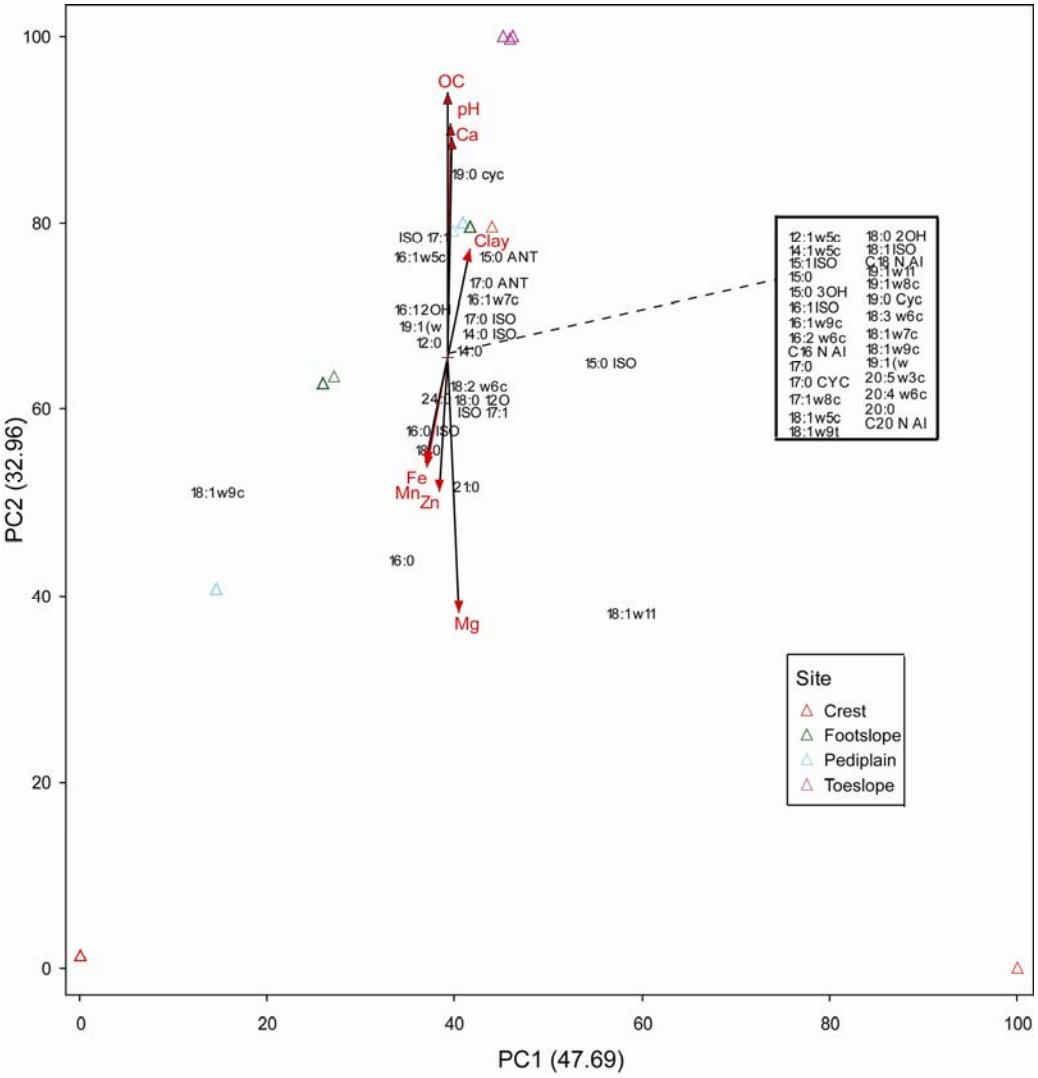

Fig. 3.4. Principal component analysis of the whole soil microbial community structure at different landscape positions at Mpinga. FAMEs connected by the dotted line were clustered around the centroid of the axis. The box is used for clarity only.

SUMMARY

The soil microbial community structure at Mpinga transect is predominantly bacteria and fungi. Biomarkers for actinomycetes were not detected. Although these soils contain high concentrations of Cr and Ni, the landscape positions were largely discriminated on the basis of Mg, pH, organic C, Fe, Mn and Zn concentrations. The presence of high amounts of arbuscular mycorrhiza fungi suggests low nutrient availability to the plants.

CHAPTER IV

SOIL CHEMICAL AND MINERALOGICAL COMPOSITIONS ACROSS AN ULTRAMAFIC TRANSECT IN SOUTHERN GREAT DYKE, ZIMBABWE

INTRODUCTION

Ultramafic geo-environments are known for their rich resources of industrial minerals and as unique ecosystems for plants. Of the best known areas with ultramafic minerals worldwide, the Great Dyke of Zimbabwe is probably the largest. The Great Dyke (Fig.4. 1) spans about 550 km long in the north-south direction and varies from 3 to 12 km (Worst, 1960; Wilson, 1982). The geology of the Great Dyke consists of sections of layered intrusions of mafic and ultramafic rocks much of which has been mined for Cr, Ni and base metals (Wilson et al., 2000). Although Pt and Pd are currently mined in some parts of the Great Dyke, depressed Cr prices on the international market have recently led to the changing land use in which vast amounts of land are now planned for restoration of degraded lands and agricultural development.

Mineral weathering in ultramafic geo-environments not only contributes significant concentrations of heavy metals (e.g., Cr, Ni, Co, Cu and Mn) to the pedosphere, but also impacts overall environmental quality through mineral species and mineral transformations within the ecosystem. In areas with similar geology, mineral weathering is largely influenced by climate and topography factors (Istok and Harward, 1982). Previous research on soil minerals derived from ultramafic rocks has shown the predominant presence of serpentine, smectite, talc, chlorite and vermiculite in the clay fractions (Bulmer and Lavkulich, 1994; Lee et al., 2003; Alexander et al., 2007). The relative abundances of the minerals are related to landscape position (Rabenhorst et al., 1982; Istok and Harward, 1982). At well-drained landscape positions Fe-rich smectites (e.g., nontronite), vermiculite and Fe oxides have been observed to form in soil impacted by ultramafic minerals. In humid tropical climates, intense weathering of serpentinized ultramafic rocks has produced Fe- and Mn-oxyhydroxides, smectites, talc and

interstratified chlorite-vermiculite (Hseu, 2007; van Cromphaut et al., 2008; Yongue-Fouateu et al., 2009) that often scavenge most trace metals. These researchers have found relatively high concentrations of trace metals (e.g., Ni, Cr, Co) and variable Mg/Ca molar ratios but with generally higher concentrations of Mg than Ca. In sub-tropical climatic conditions, limited studies of the soil chemical compositions and mineral formation from ultramafic rocks have been conducted.

In spite of the Great Dyke's large areal extent (>4,000 km^2) and the different parent rock compositions along its length, limited soil chemical and mineralogical studies have been conducted. Nyamapfene and Yin (1986) have studied the mineralogical composition of soil derived from dunite on the northern region of the Great Dyke and observed kaolinite to be the predominant clay mineral; with minor occurrences of talc, smectite, vermiculite-mica and goethite. Previous studies of soil derived from ultramafic rocks in Zimbabwe have shown high concentrations of total trace metal (e.g., Ni and Cr) and higher concentrations of extractable Mg compared to Ca (Soane and Saunder, 1959; Proctor et al., 1980).

The Great Dyke has served as a valuable geologic source of minerals (e.g., asbestos) and ores (e.g., chromite) for industry. However, due to environmental and health concerns and regulation in the use and manufacture of asbestos and the falling prices and high production costs of chromium, vast acreages of mine land have been planned for settlement and crop production to meet the demand for food and fiber for the expanding population. The current study site (Fig. 4.1) represents one of the areas that has been targeted for irrigated agriculture (Munjonji et al., 2006). Notwithstanding the abundant water supply, very low crop yields and sometimes total crop failures have been reported in these areas (Manyevere, A., personal communication). The increased ultilization of the Great Dyke for agriculture introduces the complex challenges of effective re-vegetation and land management, as well as the need to ensure environmental quality, food security and safety, and human health. In order to effectively and sustainably manage these fragile lands, a thorough understanding of the mineralogy and

geochemistry is needed. The objectives of the current were to determine the chemical and mineralogical compositions of the soils formed on ultramafic parent materials across a transect in the southern region of the Great Dyke, and assess the potential impact and challenges to agriculture and environmental quality.

MATERIALS AND METHODS

Study site

The study area, Bannockburn, is located on the Great Dyke in the southern-most part of Zimbabwe (Fig. 4.1). It is at an altitude ranging from about 1000 to 1200 m and lies in Zimbabwe's agro-ecological region IV that is characterized by mean annual rainfall and temperature of 500 mm and 30^{o}C respectively (Department of Meteorological Services, 1981). The rainy period occurs from approximately November to April but is relatively unpredictable. Natural vegetation consists of scattered bushes of *Combretum hereroense*, *Combretum imberbe*, *Combretum apiculatum* and *Acacia nilotica.*

The study site lies in the southern most Wedza sub-chamber of the Great Dyke that is about 80 km long and up to 6 km wide (Wilson and Prendergast, 1989). The Wedza sub-chamber consists of an ultramafic sequence of rocks comprised of dunites, harzburgites, olivine pyroxenites and pyroxenites overlying the mafic sequence of gabbros and norites (Wilson and Prendergast, 1989). Varying amounts of plagioclase, interstitial quartz, potassium feldspar and biotite are contained within the pyroxenites (Prendergast, 1990). The mafic sequence at this site forms the highest elevations (mountains) along the longitudinal axis of the Great Dyke. The western region of the study site is composed of mafic rocks (e.g., gabbro and norite); the margins of the mafic rocks are composed of websterite and bronzitite, which, in turn, are bounded by other ultramafic rocks containing chromite. The ultramafic rocks form an abrupt boundary with granitic rocks on the eastern and western sides of the longitudinal axis of the Great Dyke. A detailed study of the geology of a nearby area (~3 km south of the study site on the Great Dyke) has been conducted (Prendergast, 1990).

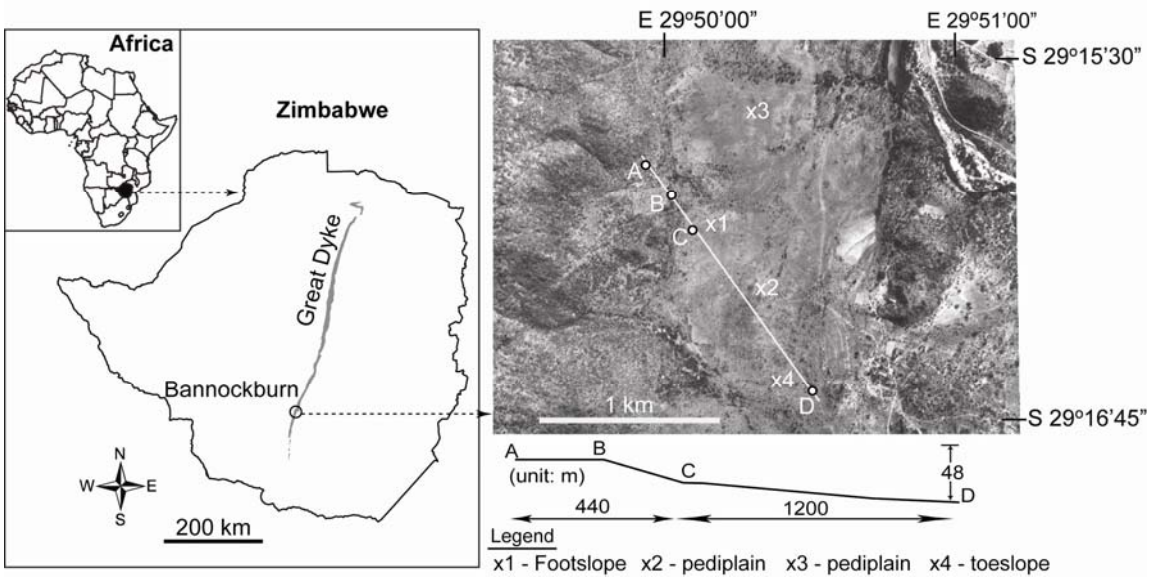

Fig. 4.1. Location map (*left*) and a scanned aerial photograph (*right*) of the study site. A sketch diagram showing the cross-section between the points A, B, C and D is shown below the aerial photograph. Points X1 to X4 indicate the location of the soil pedons across transect.

Field sampling

Sampling was conducted in the field following a detailed soil survey (Munjonji et al., 2006). Soil samples were taken from A and B horizons of representative soil pedons that were located at the footslope, pediplain and toeslope.

Laboratory analyses

The chemical and physical analyses summarized in this subsection were performed on air-dried soils that were gently crushed and passed through a 2-mm sieve. Soil pH was determined in a 1:5 soil:solution (w:v) 0.01 M $CaCl_2$ suspension using a calomel/glass electrode. Cation-exchange capacity was determined at pH 8.2 after saturation of the soil cation exchange sites with Na^+ using 1 M Na acetate, washing with 95% ethanol and displacement of the exchangeable Na^+ with 1 M ammonium acetate at pH 7.0. Also to obtain information on extractable cation balance, Ca, Mg, K, Na and Ni in soil were

extracted with pH 7.0 1 M ammonium acetate, and the concentrations were measured by atomic absorption (Ca, Mg, Ni) and flame emission spectrophotometry (Na, K).

Chromium (VI) (CrO_4^{2-}) in soil was extracted with 10 mM KH_2PO_4/K_2HPO_4 buffer solution at pH 7.2 by shaking for 1 hr (Bartlett and James, 1996). After filtration of the extract through a 0.2 μm cellulose-membrane filter, s-diphenylcarbazide solution was added to the filtrate from which the concentration of chromate was determined colorimetrically at 540 nm using a UV-visible spectrophotometer (Beckman Coulter DU800, Brea, CA).

Total elemental composition was determined by neutron activation analysis (NAA) (Helmke, 1996). The air-dried soil samples were ground to pass through a 0.10-mm sieve, and approximately 55 mg of accurately weighed soil or standard rock sample, each in triplicate, were placed into plastic vials, which were then heat-sealed. The standard reference materials included NIST SRM-1633a coal fly ash, NIST SRM-688 basalt (National Institute for Standards and Technology, Washington, DC) and USGS standard rock AGV-1 (United States Geological Survey, Lakewood, CO). Samples were irradiated at the research nuclear reactor at Texas A&M University, College Station, TX, at a nominal neutron flux of 1×10^{13} $cm^{-2}s^{-1}$. Both short-time (30 s) and long-time (14 hr) radiations were performed for NAA. The short-time radiated samples were counted for 500 s for the short-lived isotopes after a 20-min delay, and the long-time radiated samples were counted for 2000 s for the intermediate-lived isotopes after a 7-day decay and for 3-hr for the long-lived isotopes after a 28-day decay. The counting system consisted of an Ortec (Ortec, Oak Ridge, TN) high purity Ge detector with a relative counting efficiency of 50% (compared to that of a 5 inch by 5 inch sodium iodide detector at 25 cm above the source) and a resolution of 1.74 keV (FWHM). The spectra were acquired on a Canberra Genie-PC system (Canberra Industries, Meriden, CT) and transferred electronically to the VMS-based alpha processor at the campus laboratory. Spectra were processed using the Genie gamma-evaluation software (Canberra Industries, Meriden, CT) and compared to calibrated standard data using Canberra's

NAA software (Canberra Industries, Meriden, Inc., CT). The accuracy of the data was within 5-10%.

The association of heavy metals with Fe oxides and Mn oxides in soil samples was determined by extraction with dithionite-citrate (DC) (Holmgren, 1967), ammonium oxalate (AO), pH 3, 0.3 M, in the dark) (Loeppert and Inskeep, 1996), and hydroxylamine hydrochloride (Gambrell, 1996), on ground (< 0.1 mm) soil samples, respectively. The concentrations of Fe, Cr, Mn, Ni, and Co in the extract were determined by atomic absorption spectrometry (Perkin Elmer, Waltham, MA).

Mineralogical characterization

Mineral characterization was performed on fractionated clay after pretreatment of the bulk soil with 30% H_2O_2/CH_3COONa and 1M HCl (Kunze and Dixon, 1986) and then dispersion with pH 10 Na_2CO_3 and centrifugation. X-ray diffractograms were obtained using the Bruker D8 (Bruker, Madison, WI) x-ray generator operated at 35 kV and 45 mA with a CuKα source. A SOL-X detector (Bruker, Madison, WI) was used to eliminate Fe fluorescence from the samples. Separate clay samples were prepared by saturating with 1 M KCl and 0.5 M $MgCl_2$ and then removing excess salt by washing with de-ionized water (DW), centrifugation and decantation of the supernatant. Oriented specimens of K^+- and Mg^{2+}-saturated clays were prepared by pipetting aqueous clay suspensions onto round glass slides (Lakeside Brand, Hugh Courtright & Co, Monee, IL), and subsequent air-drying. Samples were scanned from 2 to 65^o 2θ at a scan rate of 0.05^o 2θ for each 2 s step to obtain x-ray diffraction patterns. Air-dried K^+-saturated clays were heated to 330^{o}C and then to 550^{o}C for 1 hr. After cooling in the oven to about 100^{o}C, samples were immediately scanned from 2 to 15^o 2θ after each heating step. The set of Mg^{2+}-saturated clay samples were sprayed with 20 % (v/v) glycerol mist and allowed to equilibrate in closed petri dishes for 4 hr before being scanned to obtain x-ray diffraction patterns.

The Fourier transform infrared (FT-IR) spectroscopy technique was used to confirm the identity of several clay minerals. Clay specimens in KBr (0.3 % w:w) and a blank (KBr only) were pressed at a pressure of 20,000 psi for 5 min under suction to obtain pellets. The pellets were oven dried at 140^{o}C for 24 hr prior to analysis. A Spectrum 100 FT-IR spectrometer (Perkin Elmer, Waltham, MA) was used to record spectra of the pellet samples in transmission mode, with the IR beam passing perpendicularly through the specimen, in the range of 4000-400 cm^{-1} at 4 cm^{-1} resolution. Prior to obtaining the spectra of the samples, a pressed KBr blank was scanned 32 times. The samples were scanned with the same instrument parameters before averaging and subtracting the KBr background signal. The display and analysis of the spectra were performed using Spectra^{TM} software.

For scanning electron microscopic (SEM) and field emission microscopic (FEM) analyses, fractionated clay particles were diluted in de-ionized water and then deposited using a pipette onto double-stick tape mounted on the electron microscope stub (Ted Pella, Redding, CA). After air-drying for 48 hrs, a graphite-C coating of about 40 nm was applied under vacuum before making observations with a FEI-QUANTA-600FE-SEM (FEI, Hillsboro, OR) scanning-electron and field-emission microscope equipped with secondary and backscattered electron detectors. Images and energy dispersive spectra (EDS) of soil samples were acquired at an accelerating voltage of 20 kV and a working distance of 10 mm. Chemical elements were identified from the soil particle EDS spectra using Inca® software.

Clay particle morphology was determined using a Jeol 2010 transmission electron microscope (TEM) (JEOL USA, Peabody, MA) operated at 200 kV and 100 μA. Dispersed clay suspensions were diluted in deionized water and then deposited onto the Cu-coated disc using a disposable glass pipette. The disc was heat-dried using a bench lamp for 30 min. The dried sample was again gently dipped into de-ionized water and held for 30 s to remove excess salts. Further preparation of the sample was performed as described above.

Sand and silt powder specimens were front-end loaded onto sample holders (2 inches diameter) and XRD patterns were obtained by scanning from 2 to 65^{o} 2θ at a scan rate of 0.05^{o} 2θ for each 2 s step. The morphology and composition of the silt particles were determined by SEM as described in the preceding paragraph.

RESULTS AND DISCUSSION

Soil physical and chemical properties

The soil was generally slightly acidic at the footslope position but tended towards less highly acidic to slightly alkaline at the pediplain and toeslope landscape positions, especially with increasing depth (Table 4.1). Unlike the sub-horizon (> 90-120 cm) at the footslope that was more acidic than the overlying horizons, the underlying horizons at the pediplain and toeslope positions were slightly alkaline. Clay content in the subsoil in most cases was at least twice that at the surface horizons. Cation exchange capacity (CEC) was higher in horizons with higher clay content and was greater in soil pedons at the pediplain and toeslope compared to the soil pedons at the footslope position. These trends imply higher contents of vermiculite and smectite at the pediplain and toeslope. At all landscape positions, extractable Mg concentrations were always higher than Ca concentrations in each horizon and the concentration of both elements generally increased with depth. The concentrations of extractable Ca and Mg were at least four times greater in pediplain and toeslope soils compared with the footslope soil. These trends also suggest a greater degree of weathering at the pediplain than the footslope. Extractable K concentrations were very low and were much less than the concentrations of Na.

Table 4.1. Selected soil properties of representative soil pedons at Bannockburn site. X1 to X4 are soil pedons. The number in brackets is the altitude in meters.

					----------Extractable cations----------				
Depth (cm)	pH	Clay	Silt	Sand	Ca	Mg	K	Na	CEC
		---------Weight %--------			----------cmol(+) kg^{-1}----------				
					X1 (1042 m)				
0-23	5.7	8	4	88	0.7	3.4	0.27	0.25	6.6
23-44	6.0	14	4	82	0.9	5.5	0.04	0.26	11.8
44-68	6.1	21	5	74	1.1	7.4	0.04	0.28	16.5
90-120	4.9	17	9	74	1.3	7.3	0.06	0.13	15.9
					X2 (1023 m)				
0-19	5.9	20	10	70	1.8	3.2	0.07	0.20	18.0
19-40	6.2	21	10	70	2.1	12.3	0.04	0.15	20.2
					X3 (1026 m)				
0-22	6.7	25	12	63	7.2	22.0	0.03	0.03	46.8
22-40	7.5	44	11	45	10.2	18.2	0.04	0.07	48.6
40-62	7.8	45	9	46	7.2	17.8	0.02	0.15	45.3
62-84	8.0	43	17	40	7.5	20.3	0.03	0.20	40.7
84-110	8.0	39	19	42	9.1	24.1	0.00	0.24	43.8
					X4 (1014 m)				
0-17	6.8	34	15	51	8.6	8.8	0.05	0.25	35.8
17-38	7.3	32	13	55	10.9	22.9	0.03	0.03	43.1
38-53	7.6	35	14	51	11.9	17.6	0.02	0.02	37.6

The near neutral to slightly alkaline pH values (pH 6.7 -8.0) reaction at the toeslope and pediplain landscape positions were due to the high exchangeable base concentrations. The predominance of extractable Mg relative to Ca is attributable to the predominance of

easily weatherable Mg-containing silicate minerals such as talc. Soil pedons located on the pediplain and toeslope contained higher concentrations of Mg that those from the footslope because of increased weathering (higher clay content) resulting from greater moisture and also because of transport and subsequent accumulation of clay at the toeslope.

Total elemental concentrations

Soil at the footslope landscape position contained much higher total Fe concentrations compared to the pediplain or toeslope soils (Table 4.2). In contrast, the pediplain and toeslope soils had Al and Ti concentrations considerably higher than those of the footslope soil. The concentrations of Cr were generally similar across the transect, except for the surface-most horizons at the pediplain that had almost twice as much Cr as the subsoils. This phenomenon suggests soil enrichment by Cr from the nearby chromite trenches. There was little variation in Ni concentration between soils and within soils profiles. Irrespective of landscape position, Mg concentrations were about four times higher than the concentrations of Ca. As will be discussed later (mineralogy section), the easily-weatherable soil minerals at this study site have higher Mg than Ca concentrations. Total Na concentrations generally increased from the footslope to the toeslope soil, indicating transport by water and subsequent accumulation at the lower landscape positions. Although total K concentrations in surface soils were higher than Na concentrations, extractable K concentrations were much lower than those of Na, suggesting fixation by vermiculite and high charge smectite (Barshad and Kishik, 1970). Higher concentrations of K in the surface horizons than the subsoil are attributed to sediment deposition from the adjacent mafic and granitic rocks.

Table 4.2. Total elemental concentrations in soil (by NAA) at Bannockburn site.

	Element									
Depth	Al[†]	Ca	Mg	Na	K	Fe	Cr	Mn	Ni	Ti
(cm)	Concentration (mg kg^{-1})									
0-23	14060	11330	50900	940	1280	80230	4460	1700	680	1350
23-44	17640	9770	49100	900	1070	87410	4480	1760	830	950
44-68	17280	10280	49400	890	985	87710	4560	1770	810	920
90-120	15510	10580	50700	820	960	87650	4610	1680	780	860
0-22	70860	7930	36600	1190	1460	61870	11100	1960	680	1190
22-40	74660	11260	43100	1080	1120	66840	10220	1320	650	1600
84-110	63750	22750	56200	940	780	66240	6880	860	650	1680
0-19	28440	12420	48800	1650	2020	74060	5770	1430	590	1390
19-40	33440	10710	50200	1710	1690	78110	5300	1500	650	1670
0-17	57770	11630	45300	1430	1080	57920	3520	1530	500	2360
17-38	60120	11370	46600	1250	1200	60680	4010	1400	570	1910
38-53	53790	16020	55600	1400	740	61040	4360	1950	630	1670

[†]Chemical elements whose total concentrations were below 200 mg kg^{-1} are not shown in this table.

Selective extraction

Selective dissolution techniques were used to assess the forms, potential mobility and bioavailability of trace metals of concern to agriculture, environment and human health. The hydroxylamine hydrochloride has been used to selectively and quantitatively dissolve the easily-reducible Mn oxides and hydroxides (Chao, 1972). It is possible that

acidic HH might dissolve a portion of the poorly crystalline Fe oxides as well. The dithionite-citrate (DC) and acidified ammonium oxalate (AO) (in the dark) have been used extensively to obtain quantitative estimates of total and poorly crystalline Fe-oxide concentrations, respectively, in soil (Holmgren, 1967). Both these extractants might also result in partial dissolution of Fe-rich silicate phases e.g., Fe-rich smectite. The results show that up to 25 % and 3 % of the total Fe were extracted by DC and AO respectively, (Fig. 4.2). The greatest percentage of DC extractable-Fe was at the footslope and the lowest percentage in the toeslope soil. The differences in the DC extractable-Fe are attributable to the drainage conditions at the site and the original total Fe content of the soil. The footslope position is well drained and contains higher concentrations of total Fe (~9%) and a greater percentage of Fe oxide. The latter are readily dissolved in DC. At the pediplain and toeslope positions, the drainage is moderate and the soils contained relatively lower concentrations of total Fe (6-7%). Consequently, during the wet periods the Fe oxides would have been exposed to biochemically reducing conditions that would be conducive to the formation of Fe^{2+} that is more mobile than its oxidized analog. The proportion of DC extractable-Fe decreased by 50% from the footslope to the toeslope landscape positions. However, AO extractable-Fe concentrations increased from the footslope to the toeslope position. This phenomenon might also be impacted the higher organic matter contents at the toeslope position, that might provide kinetic inhibitions to the formation of more highly crystalline Fe oxide phases (Kodama and Schnitzer, 1977; Cornell and Schwertmann, 1979). The presence of higher concentration of AO extractable Fe oxide implies alternating oxidation and reduction processes and kinetic inhibitions to the formation of highly crystalline Fe oxide phases.

A similar trend of decreasing DC-extractable Cr from the footslope to the toeslope was observed at all landscape positions, though much lower Cr proportions were extracted by each of the three extractants (Fig.4.2). The corresponding trends of DC-extractable Fe with DC –extractable Cr suggest a strong association of Cr with Fe. The HH-extractable

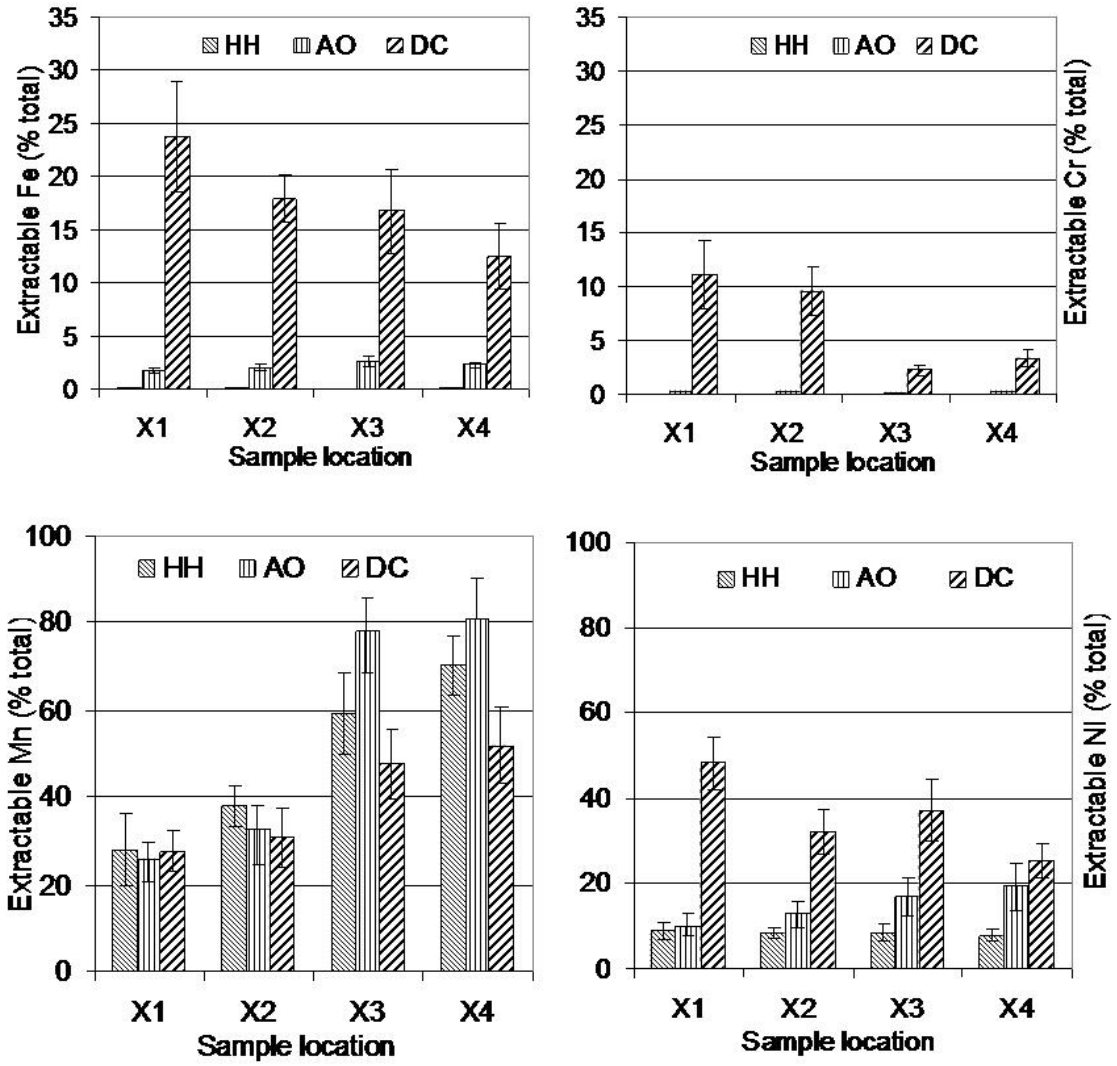

Fig. 4.2. Mean metal concentrations extracted by hydroxylamine hydrochloride (HH), ammonium oxalate (AO) and dithionite-citrate (DC). Error bars are standard deviations.

Cr was below the detection limit. These results also indicate that a greater percentage of the total Fe and Cr were bound in other mineral phases such as silicates and chromites (discussed in mineralogy section). The silicate- and chromate-bound Fe and Cr are likely unavailable to plants and living organisms in the short term.

Unlike DC-extractable Fe and Cr, Mn extractable by each of the three extractants (AO, DC, and HH) showed a trend of increasing concentration from the footslope to the toeslope. These results suggest either a greater release of Mn release from minerals at the toeslope or Mn transport and accumulation in the toeslope soil. Mn is sensitive to redox and pH conditions of the soil. Consequently, the alternating wet (reducing) and dry (oxidizing) conditions at the toeslope have resulted in a relatively high proportion of Mn oxides, which can occur as concretions and nodules (White and Dixon, 1996). Furthermore, it can be predicted that the slightly alkaline soil reaction (pH 7-8) and the more highly oxidized conditions in pediplain and toeslope soils could favor the stability of Mn (III,IV) oxides (McBride, 1994). The results further show that Mn was less highly associated with Fe oxides (extractable by DC). The results seem to imply seem to imply that a small proportion of the total Mn was associated with other phases, possibly the silicates. In footslope and shallow (~50 cm deep) pediplain soils, the proportion of HH-extractable Mn was slightly higher than that of AO-extractable Mn. However, in deeper (> 50 cm) pediplain and toeslope soils, the proportion of AO- extractable Mn was much greater than that of HH-extractable Mn. These results suggest that with increasing intensity of weathering and poor drainage conditions, Mn might also be present in poorly crystalline Fe oxide phases. Well-drained conditions resulted in the formation of crystalline Mn oxides that were preferentially dissolved by HH.

Of the total Ni concentration in soil, about 50% was extractable with DC at the footslope landscape position (Fig. 4.2). However, DC-extractable Ni proportions decreased to about 25% in the toeslope soil. Similar trends with HH-extractable Ni and AO-extractable Ni were observed across the transect. In general, a greater proportion of the total Mn and Ni occurred in the extractable forms while Cr was less readily extracted.

Clay mineralogy

Footslope

The footslope is composed of predominantly smectite, talc, Fe oxides (goethite) and kaolinite (Fig. 4.3). Smectite was identified by the expansion of its basal spacing to 1.75

nm after glycerol solvation and its collapse to 1.02 nm after heating of the K-saturated clays to 550^{o}C. Talc was confirmed by the 0.94 nm peak of the orientated clay specimen that remained unaffected after glycerol solvation or heat-treatment of the K^{+}-saturated samples. Higher order XRD peaks at 0.46 and 0.312 nm were corroborative evidence of talc. Kaolinite was identified by the basal spacing at 0.71 nm and 0.357 nm; the former peak disappeared when the K^{+}-saturated samples were heated to 550^{o}C.

In SEM micrographs, both platy and spherical particle morphologies were observed, the latter being characteristic of Fe oxides (Fig. 4.4). The elemental composition of the clay fractions consisted predominantly of Al, Cr, Mg, Fe, Na, O and Si (Fig. 4.4). Cr was associated with Fe oxides (as evident from the DC-extractions) and as a structural component of the phyllosilicate clay minerals (e.g., talc). Substitution of Cr^{3+} (r_{ion} = 0.063 nm) for Fe^{3+} (r_{ion} = 0.064 nm) in the octahedral layer of smectites and in Fe oxides has been reported (Cornell and Schwertmann, 2003) due to the similarities of ionic radii (r_{ion}). The relative abundances of Al, Fe and Mg in the clay-sized mineral structures was probed by SEM-EDS and FT-IR. Energy-dispersive spectra indicated strong peak intensities for Al, Fe and Mg (Fig. 4.4), and strong but broad FTIR absorption bands between 3500 and 3620 cm^{-1} were observed (Fig. 4.5). These bands have been attributed to the overlap of various components such as $Al^{3+}Fe^{3+}$ -OH (3585-3600 cm^{-1}); $Fe^{3+}Mg^{2+}$-OH (3575 cm^{-1}) and $Fe^{3+}Fe^{3+}$-OH (3550 cm^{-1}) (Farmer, 1974; Petit et al., 2002). The intensities of the absorption bands in the region 3500-3600 cm^{-1} increased in subsoil horizons, indicating greater Fe and Mg substitution in the mineral structures (Fig. 4.5). Bands located at ~ 3577 and 3548 cm^{-1} in the OH-stretching region of the spectrum are characteristic of Fe-rich smectite and nontronite (Bishop et

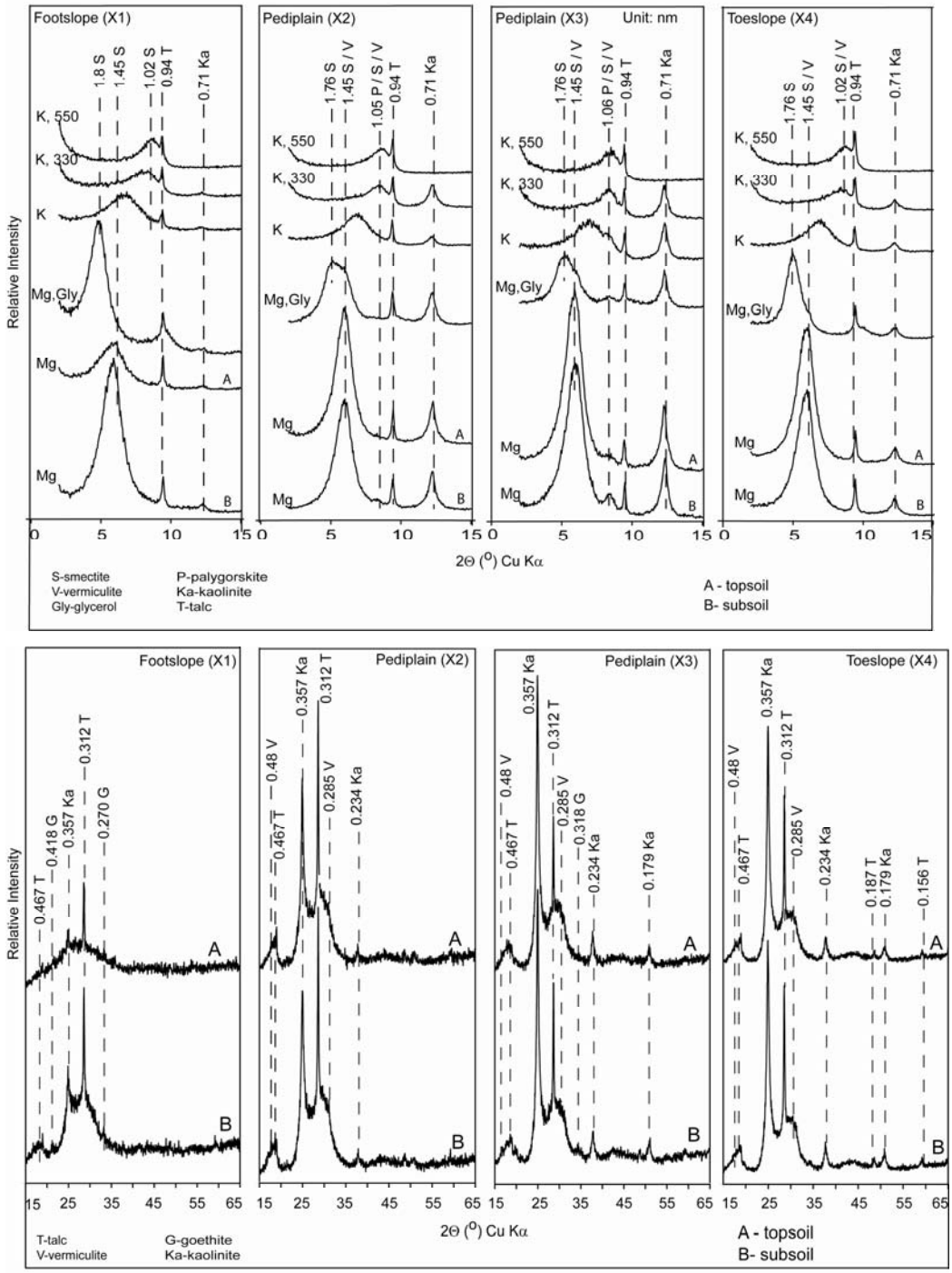

Fig. 4.3. X-ray diffraction patterns of orientated clay from the A and B horizons across the southern transect. Mg-glycerol treated samples are for the subsoil. Smectite, talc and kaolinite occurred in all the soil irrespective of landscape position.

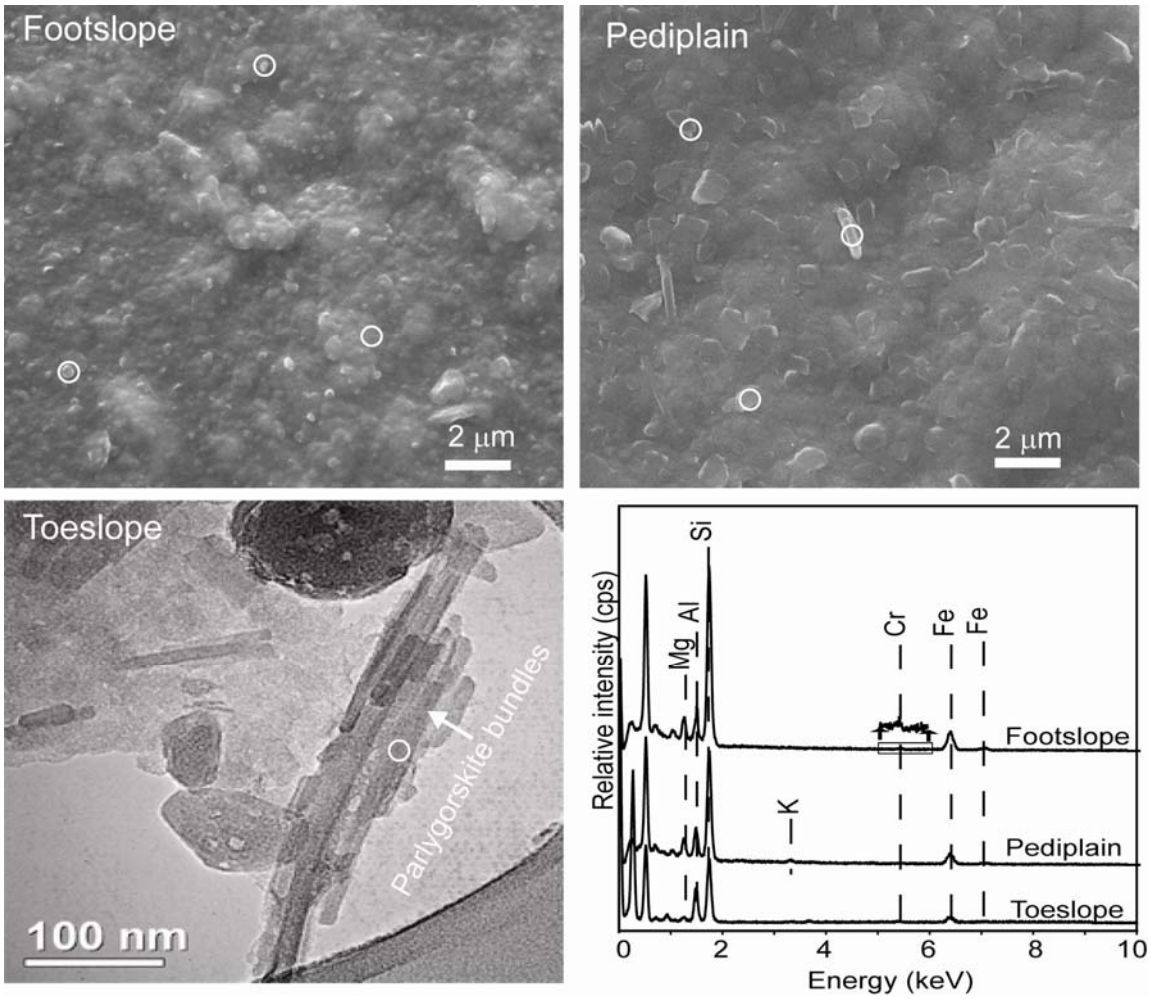

Fig. 4.4. SEM images (*top*) of clay from the footslope and pediplain. Particles in footslope soil show aggregates of Fe oxides and platy particles. Pediplain clay have both platy and lath-shaped particles. Below (*left*) show TEM images of the palygorskite in toeslope soil. The compositions of the particles in marked areas (O) are shown on the energy dispersive spectra graph (*bottom right*).

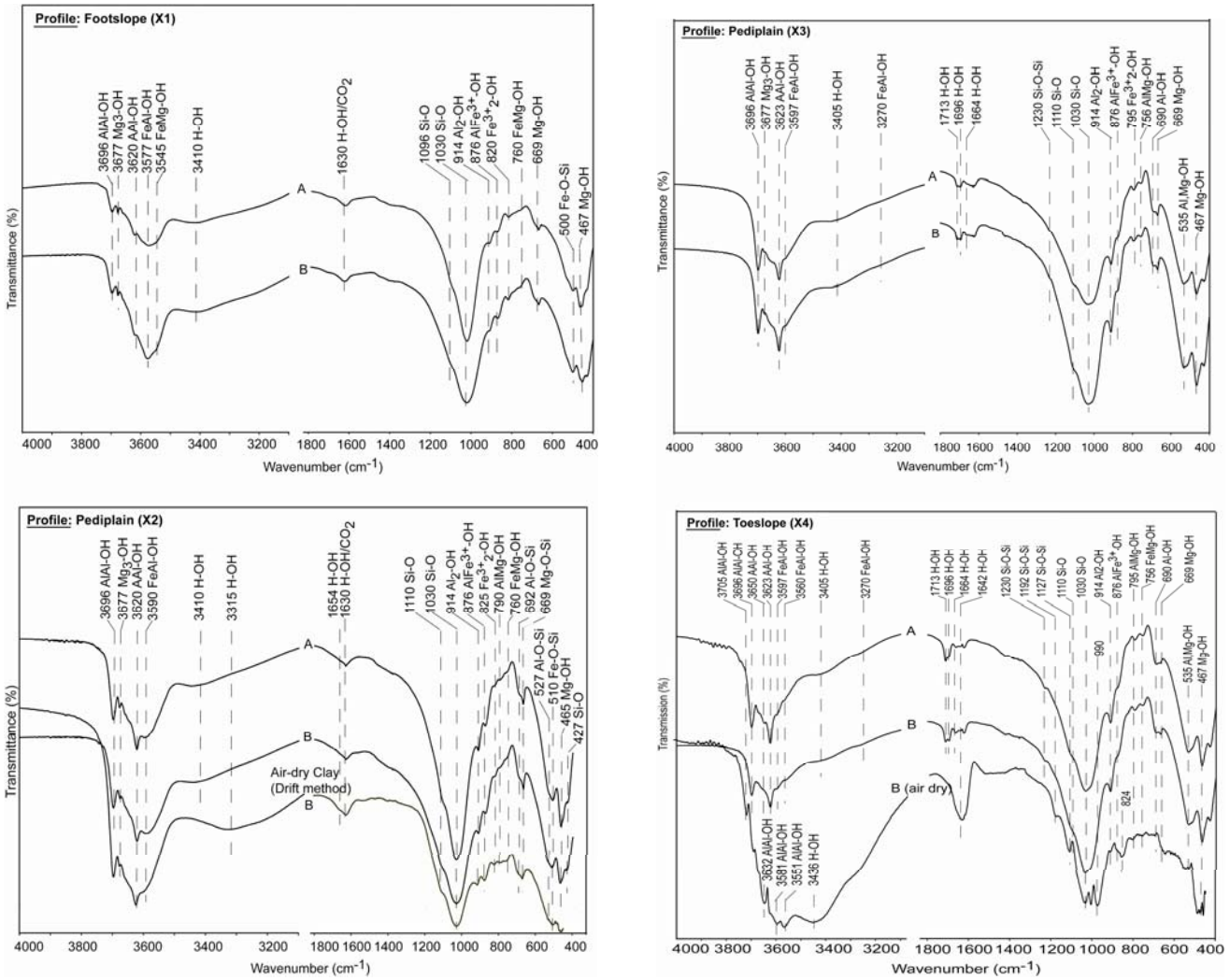

Fig. 4.5. Fourier transform infrared (FTIR) patterns for the clay samples from topsoil (A) and subsoil (B) across the transect.

al., 2002b). In the OH-bending vibrations in octahedral cations (950~590 cm^{-1}) (Farmer, 1974; Gates, 2005), the relatively higher content of Fe and its occupancy in the phyllosilicate structure is reflected by the intense absorption bands at ~876 and 820cm^{-1} due to $AlFe^{3+}$-OH and $Fe^{3+}Fe^{3+}$-OH, respectively (Fig. 4.5, X1). The octahedral occupancy of Fe in the structure of phyllosilicate is also shown by the strong absorption band at ~500 cm^{-1} due to the bending vibrations (Si-O-Fe^{3+}) of octahedrally-linked tetrahedral groups. In contrast, Al-rich smectites have strong bands at 3630, 914 and 530 cm^{-1} (Bishop et al., 2002b). Previous studies of Zimbabwean soils have indicated that the phyllosilicate are dominated by montmorillonite (Nyamapfene, 1984; Hungwe, 1988). There is limited literature on Fe-rich smectite occurrences. Absorption bands that are diagnostic for kaolinite (3696, 3670, 3620 cm^{-1}) and Fe^{2+}-substituted talc (3677, 3661, 3644 cm^{-1}) were evident in all the spectra. The weak absorption bands at 1015, 790, 692 and 535 cm^{-1} are also attributable to talc and kaolinite.

Pediplain

The pediplain soil was dominated by smectite, kaolinite, talc, vermiculite and palygorskite (Fig. 4.3). The relative abundance of smectite increased with depth in relation to the increase in clay content (Table 4.1). Vermiculite was differentiated from smectite by the non-expandable but collapsible d-spacing (1.45 nm) of orientated samples after glycerol solvation but collapsible after K^+- saturation (Fig. 4.3). Vermiculite was further identified by the 003 (0.48 nm) and 005 (0.285 nm) XRD peaks of orientated clay samples. Unlike the low-charge smectite at the footslope that expanded to 1.85 nm after glycerol *vapor* solvation, the smectite at the pediplain and footslope expanded to 1.76 nm only after solvation with glycerol *liquid*, suggesting a greater layer charge of the pediplain smectite. The higher layer charge in these clay minerals could originate from the structural reduction of Fe^{3+} to Fe^{2+} in Fe-rich smectites (Stucki, 1984) as well as vermiculite. Clay minerals with high layer charge can potentially fix K^+ and NH_4^+ in their structures (Barshad and Kishik, 1970). The fixed chemical species become unavailable for plant uptake in the short term.

Palygorskite was identifiable by the 1.06 nm basal spacing that remained unaffected by all cation-saturation treatments. The occurrence of specific clay minerals was further corroborated by FTIR (Fig. 4.5). The relative X-ray diffraction relative peak intensity and FTIR absorption bands indicated a higher concentration of kaolinite at the pediplain than the footslope landscape positions. Palygorskite forms in soil where drainage is impeded and where evapotranspiration exceeds precipitation (Singer, 2003). The actual mechanism involved in its formation is still the subject of much debate. Paquet and Millot (1973), however, stated that palygorskite is unstable and converts to smectite when rainfall exceeds 300 mm evidence for which was corroborated in west Texas (Bigham et al., 1980). Weaver and Beck (1977) have presented evidence that palygorskite forms from the reaction of smectite with excess silica derived from siliceous organisms. Recent studies have proposed that palygorskite forms by the alteration of precursor minerals like mica and smectite followed by the addition of Si and Mg (Callen, 1984; Jones and Galan, 1988; Suarez et al., 1994). In a study of caliche clay minerals in southern Turkey, Kadir and Eren (2008) have demonstrated the direct formation of palygorskite from over-saturated solutions. These authors disputed the idea that palygorskite was a detrital mineral as previously suggested by other researchers. In the current study, we show that palygorskite can remain stable even when rainfall surpasses 500 mm per annum. We suspect that the increasing concentration of palygorskite with increasing depth in pedons was due to direct precipitation from solution enriched with Si, Mg at relatively high pH (>8.0). The importance of Mg during the formation of palygorskite was demonstrated by Nyamapfene (1984), who observed that, even though the vertisols developed from basalt and mudstone have montmorillonite as the dominant mineral, significant amounts of palygorskite and chrysotile are present in the vertisols developed from pyroxenes and limburgitic materials in the same area in south-east Zimbabwe. Although palygorskite can also result from the hydrothermal alteration of ultramafic parent material, it is unlikely the case in this study because of its absence in soils with acidic characteristics within the same locality.

Although kaolinite typically forms in warm, wet and high leaching environments with high contents of feldspars that act as a source of Al and Si (Gaskin et al., 1979), its association with the ultramafic parent material that inherently lack feldspars in semi-arid conditions is unusual. The easily-weatherable minerals (e.g., amphiboles) at the current study site have relatively high concentrations of structural Al and Si (discussed in sand and silt section) that can be released to solution during weathering and cause the precipitation of kaolinite from the over-saturated solutions. In a study of amphibole weathering, (Proust et al., 2006) observed the formation of kaolinite-smectite interstratifications, saponite and montmorillonite in specific crystallographic directions.

In shallow soils (depth <50 cm), kaolinite, talc and vermiculite were predominant and there was no evidence of the presence of palygorskite. In contrast, deeper soils (>50 cm) contained much more Fe-rich smectite and palygorskite that increased with soil depth. Lack of palygorskite in shallow soils is attributable to the prohibitive acidic pH.

Although absorption bands for specific minerals could be identified, overlapping bands with Al- and Mg-containing minerals were common. For example, the absorption bands of palygorskite in the OH-stretching region coincide with those of Fe-rich smectite (3575, 3550 cm^{-1}), kaolinite (3620 cm^{-1}) and vermiculite (~3590 and 3560 cm^{-1}). Also the band positions of the former are influenced by the moisture status of the sample. FTIR spectroscopy of powdered air-dry clay samples by the diffuse reflectance infrared transform (DRIFT) method on air-dry clay powder samples showed the absorption bands at 3621, 3551, 3450, 3280, 1642, 1192, 1127, 1048, 990 cm^{-1} that are diagnostic of palygorskite (Fig 4.5, X4). In contrast, the bands at 3705, 1192, 1127 and 990 cm^{-1} previously observed in air-dry clay samples (DRIFT) disappeared and a new set of absorption bands at 1230 and 1110 cm^{-1} emerged when the clay sample was oven-dried. The concurrent disappearance and emergence of new bands was attributed to structural or coordinated water that is lost during de-hydration. Spectroscopic studies of palygorskite from different localities by several researchers have reported common absorption bands in the range of 1115-1190 cm^{-1} due to Si-O stretching vibrations and

1630-1676 cm^{-1} assigned to OH-stretching vibrations of zeolitic or coordinated water (Frost et al., 2001; Suárez and García-Romero, 2006; Wang et al., 2009). Air-dry clay powders whose XRD patterns lacked evidence of palygorskite occurrence did not show discernible peak shifts nor the formation of new ones when determined by either the pellet or drift method (Fig. 4.5, X2).

The majority of clay particles in pediplain soil were platy with angles of about 120^{o} that are characteristic of kaolinite (Fig. 4.4). A few lath- or needle-shaped particles composed of Al, Mg, Na, Fe, O and Si were probably talc or palygorskite. Transmission electron microscopy (TEM) images of the clay fraction containing palygorskite showed laths or needle-shaped morphology (Fig. 4.4, toeslope) that occurred as fibers or bundles. Fiber length ranged from ~100 nm to 300 nm and 5-10 nm in width. The chemical composition of the palygorskite particles showed much higher Al content and lower Mg and Fe contents than would be expected for the ideal palygorskite composition. These results suggest the substitution of Si by Al, as well as Mg by Al and Fe in palygorskite structure.

Toeslope

X-ray diffraction pattern indicated that the clay mineral composition at the toeslope was similar to that at the pediplain and consisted of smectite, talc, kaolinite, vermiculite and smaller amounts of palygorskite (Fig. 4.3). The FTIR (Fig. 4.5d) showed strong absorption bands at 3696 and 3623 cm^{-1} (AlAl-OH) in the OH-stretching region and the corresponding absence of $Fe^{3+}Fe^{3+}$-OH bands (3575 and 3548 cm^{-1}), indicating the predominance of Al in the mineral structures. In the OH-bending vibrations of the octahedral cations (~590-950 cm^{-1}), strong absorption bands at 914 cm^{-1} (AlAl-OH), 756 cm^{-1} (AlMg-OH), 692 cm^{-1} (Al-OH) and 535 cm^{-1} (Al,Mg-OH) complement evidence of the predominance of Al and Mg in mineral structures. Vermiculite was much more abundant at the toeslope than either the footslope or pediplain even though the amount of kaolinite was identical. The toelsope is located near the contact zone of ultramafic and

granitic rocks that could have resulted in the formation of higher amounts of vermiculite during the metamorphic processes (Fig. 4.1).

Sand and silt

The X-ray diffraction patterns indicate that pyroxenes (e.g., enstatite) were the predominant minerals in the sand fractions of all pedons across the transect (Fig. 4.6). Smaller amounts of talc, quartz and chromite were also present. In the silt fractions, quartz, enstatite, amphiboles, chlorite and talc were predominant (Fig. 4.7). Scanning electron microscopy (SEM) micrographs indicate the presence of small amounts of Ca-plagioclase and K-feldspars in the silt fractions (Fig. 4.8), even though they were not identifiable by x-ray diffraction. The feldspar could have been transported by wind and water from the adjacent mafic and granitic rocks, where they occur in relatively large proportions. The relative EDS peak heights of various elements in pyroxenes and amphiboles suggest wide compositional variations in Mg, Ca, Al, Cr, Si, Ti, V, Na and O (Fig. 4.8). The pyroxenes analyzed in this study have relatively low concentrations of Cr, Al and Ca but higher concentrations of Mg compared to the amphiboles and garnets (Fig. 4.8). Ni-containing minerals were present in relatively low concentration, as shown by the chemical composition of the soil. The SEM– and EDS indicated the presence of numerous phytoliths in the silt fraction of the footslope soil (Fig. 4.9), suggesting the rapid release of Si by weathering, and subsequent loss by leaching or plant uptake. Some mineral phases had relatively high concentrations of Cr or Ti in combination with Si, Al, Mn and Mg. These minerals were interpreted as garnets and titanite respectively. At the pediplain, smaller amounts of chromite isolated with the aid of an optical microscope and confirmed by SEM-EDS, also occurred throughout the soil pedons. Some amphiboles at the pediplain had fibrous morphology (Fig. 4.10). The fibers are ~20 μm long.

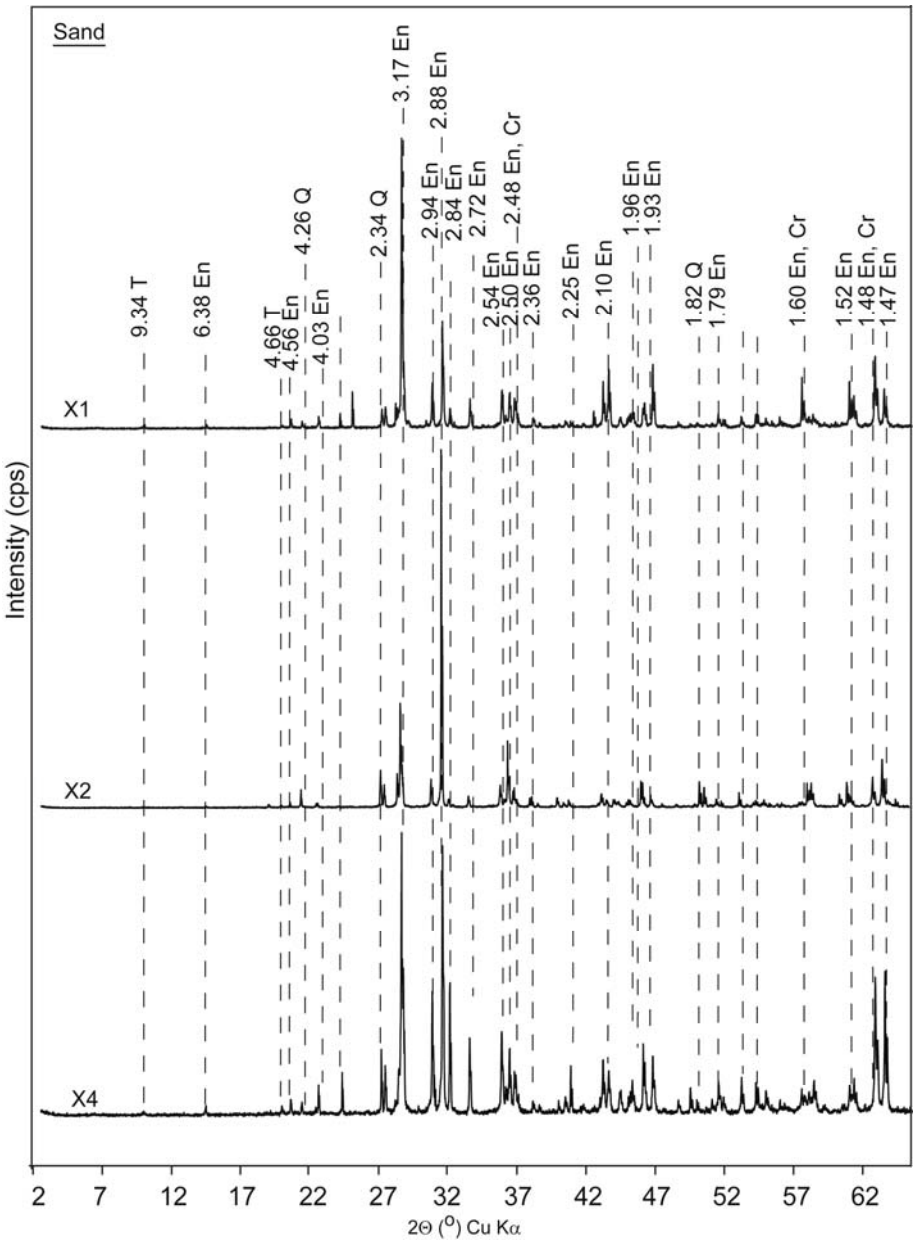

Fig. 4.6. Powder XRD patterns of the sand fraction samples taken from the footslope (X1), pediplain (X2) and toeslope (X4). The predominant minerals were enstatite (En), quartz (Q) and talc (T).

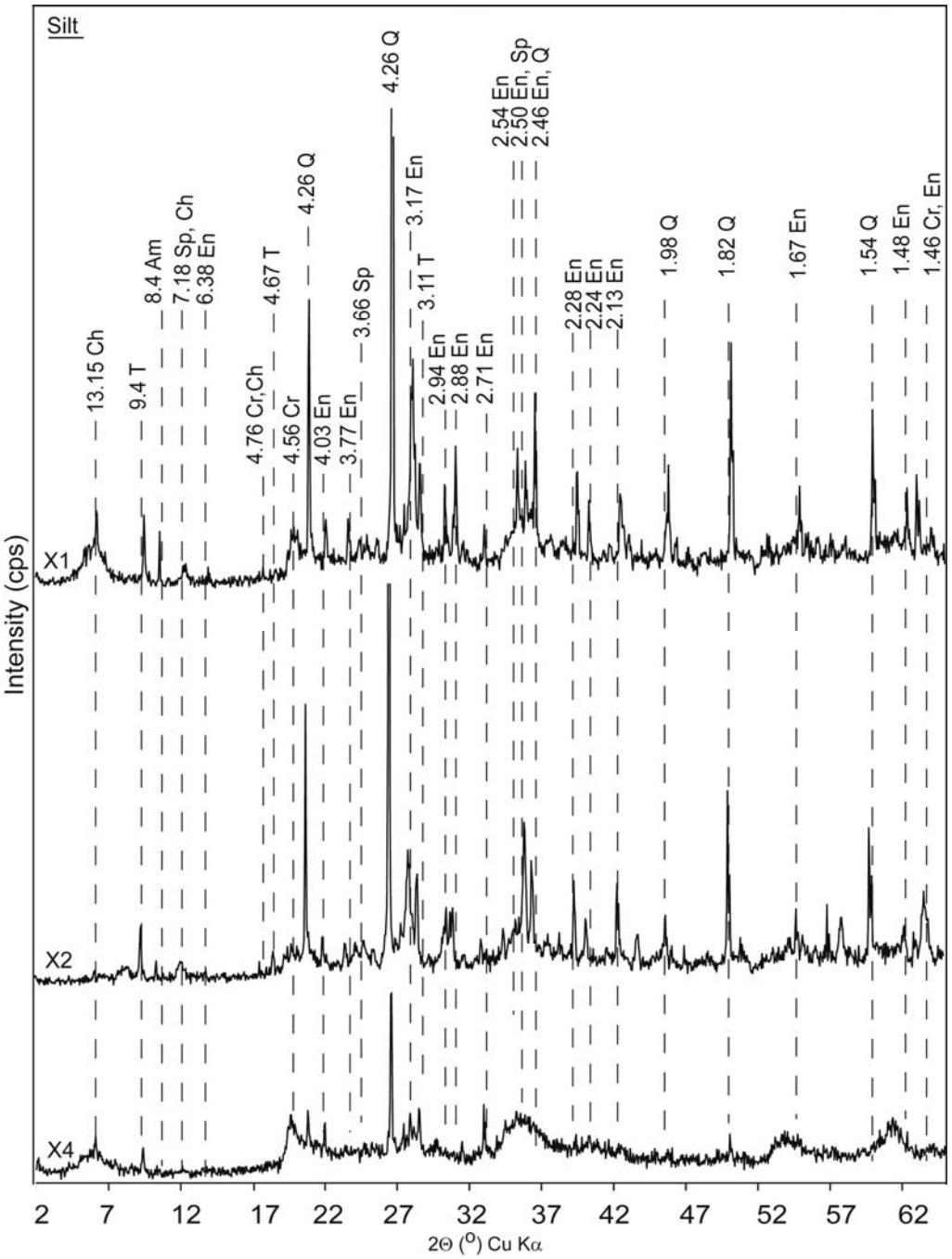

Fig. 4.7. Powder XRD patterns of the silt fraction samples taken from the footslope (X1), pediplain (X2) and toeslope (X4). The predominant minerals were enstatite(En), quartz (Q), talc (T), chlorite (Ch), amphibole (Am) and chromite (Cr).

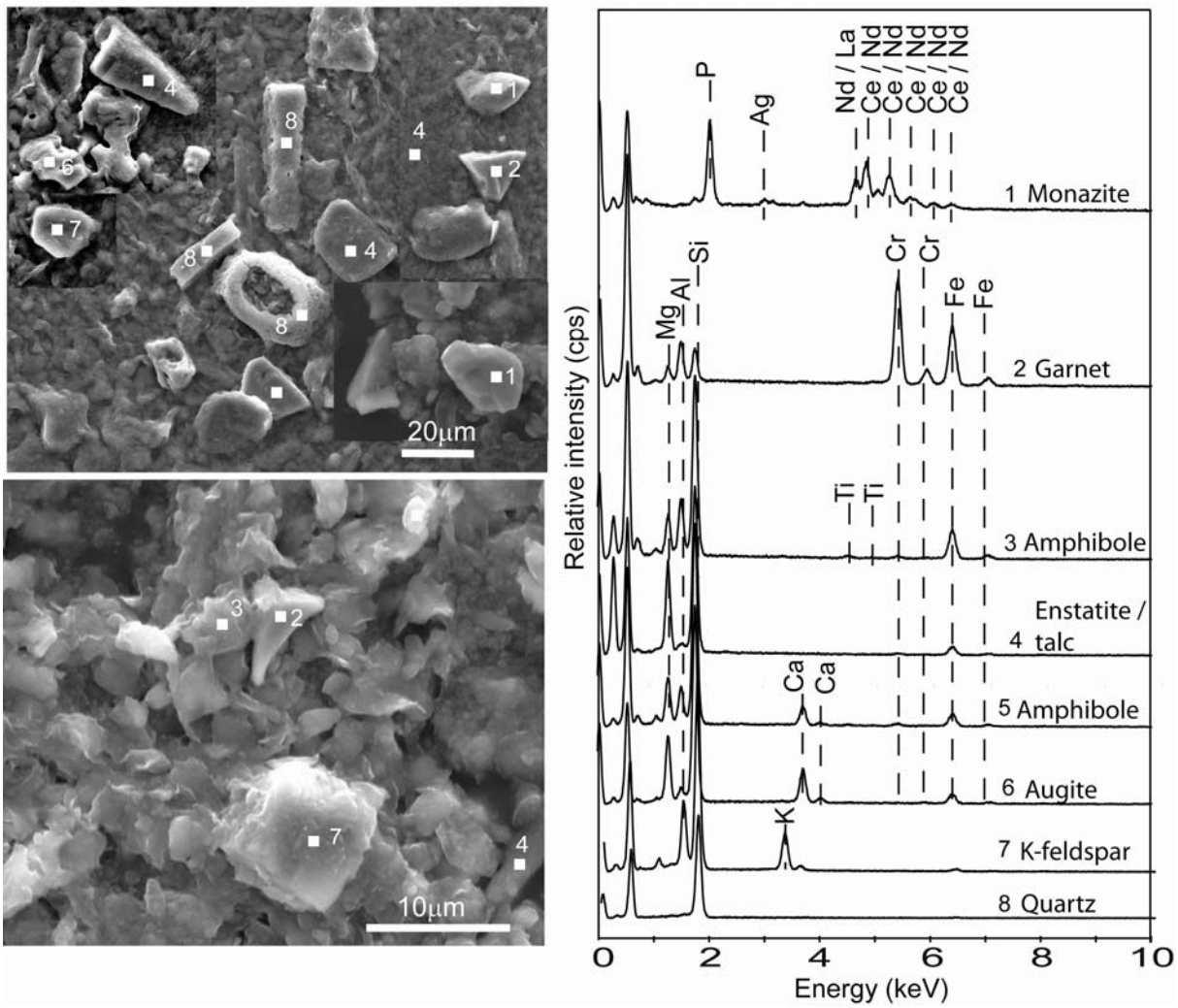

Fig. 4.8. Morphological and compositional variations of selected minerals in the silt fraction at Bannockburn. All the silts contained enstatite, talc, quartz, amphiboles and feldspars. Particles marked with the same numbers have identical chemical compositions.

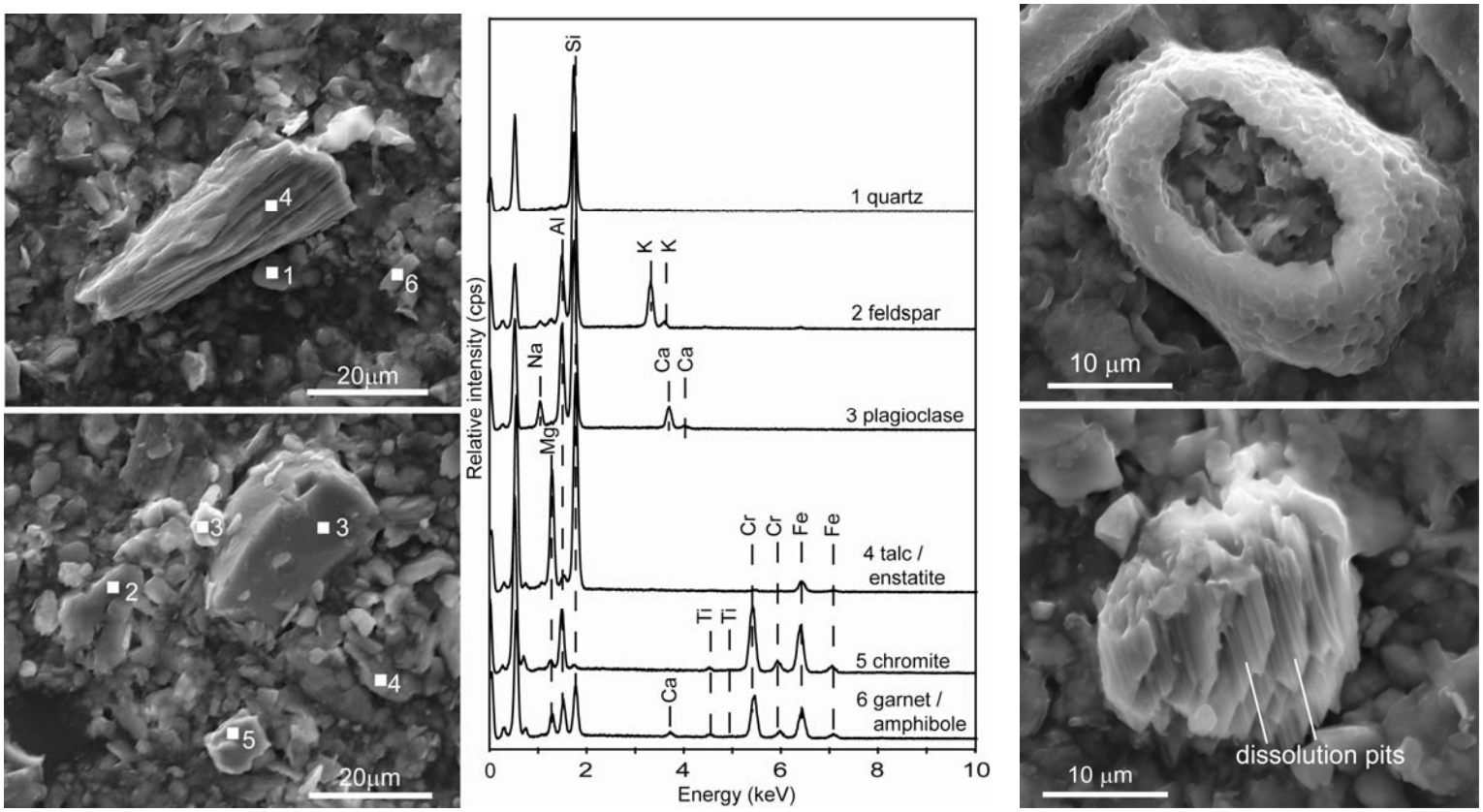

Fig. 4.9. Morphological and compositional variations of selected mineral particles in the silt fraction at Bannockburn. All the silts contained enstatite, talc, quartz, amphiboles and feldspars. Particles marked with the same numbers have identical chemical chemical compositions. Higher amounts of poorly crystalline Si minerals (phytoliths) *(top right, spectrum 1*) were found in footslope silts. The pyroxenes (*bottom right*) show longitudinal dissolution pits.

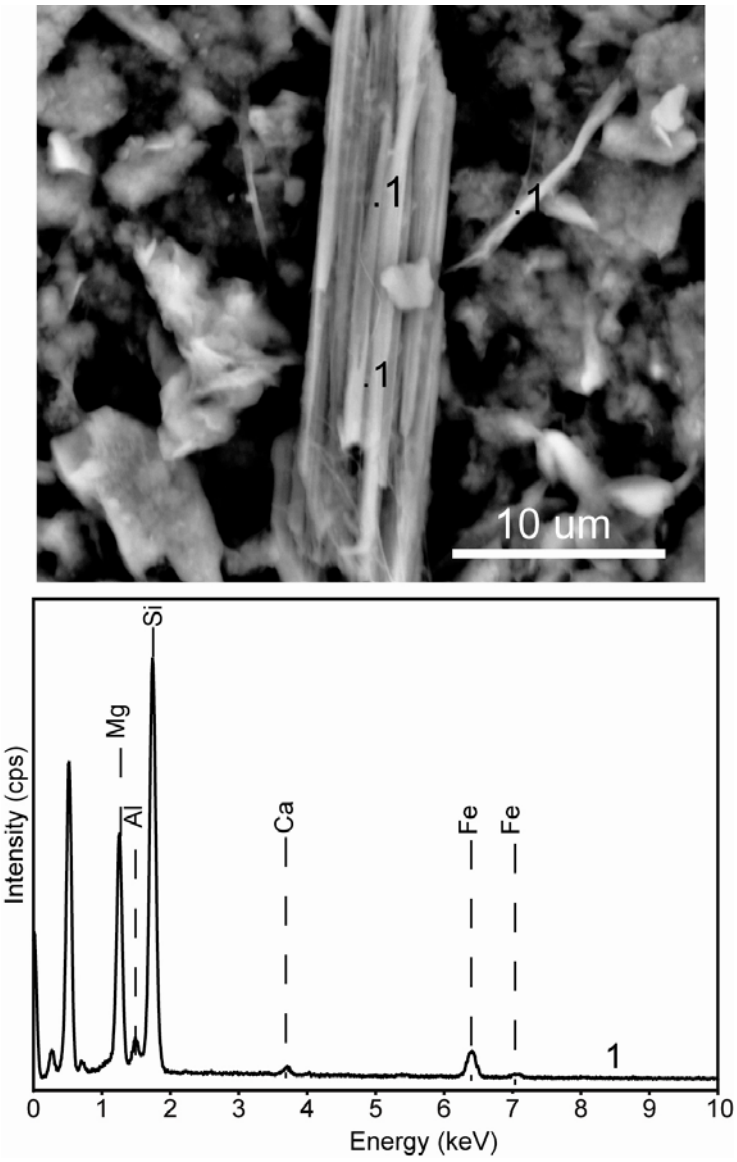

Fig. 4.10. SEM image (*top*) and EDS spectrum (*bottom*) of silt-sized particles in pediplain soils at Bannockburn showing fibrous morphology and chemical composition, respectively. Particles marked with the same numbers have identical chemical compositions.

In comparison with mineralogy in the sand fraction, all silt-sized particles in all soil pedons, irrespective of landscape position, contained enstatite, quartz, chlorite and talc in relatively greater amounts. Talc occurred in all the soil particle-size fractions, and its

content generally increased with soil depth, suggesting inheritance from the parent rocks and susceptibility to weathering. Some mineral occurrences were associated with soil pedons at particular landscape positions. For example, XRD patterns indicated that amphiboles occurred only in pedons in the pediplain. Carbonates were observed in all horizons of pedons at the toeslope and in subsoil horizons of pedons on the pediplain.

SUMMARY

Wide variations in mineralogical abundances and compositions, as well as soil chemical compositions, are apparent across the transect. The soils contain high concentrations of trace metal, higher levels of Mg than Ca and low levels of extractable K. All the soils at each landscape position contain negligible amounts of feldspars and lack micas in the clay fraction. Agriculture and soil quality are greatly impacted by the very low levels of extractable K, high Mg/Ca molar ratios and relatively high concentrations of potentially available heavy metals (Cr, Mn). The challenges are compounded by high contents of high-charge vermiculite and smectite that have greater propensity to fix K and further reduce the soil's ability to supply this essential plant nutrient. The concurrent occurrence of Cr and Mn in the easily-weatherable minerals is a potential concern to the environment and agriculture. The Mn oxides can oxidize the less toxic Cr(III) to the more toxic, mobile and carcinogenic Cr(VI) (Bartlett and James, 1979). Although no Cr (VI) was detectable, there is potential to form due to the presence of high Mn and Cr in the soil. Fibrous amphiboles in the silt fraction are a concern to human health because of the potential carcinogenic properties. The absence of feldspars and the presence of kaolinite in the soils demonstrate the importance of pyroxenes and amphiboles as alternative sources and pathway in the genesis of kaolinite.

CHAPTER V

MINERALOGY AND GEOCHEMISTRY OF ULTRAMAFIC-DERIVED SOILS FROM GILLESPIE COUNTY, TEXAS

INTRODUCTION

Ultramafic parent rocks intrinsically have high contents of Fe- and Mg-containing minerals that easily undergo weathering to form soil. These soils can have unique properties and diverse mineralogical and chemical compositions that have important implications to agriculture, ecology, human health and overall environmental quality (Brooks, 1987). Gillespie County, Texas, has soils developed from ultramafic parent materials. The main parent rock is serpentine and covers an estimated area of 8 km^2. Serpentine has been mined as an industrial mineral at this site for decades.

The abolition of the use and manufacture of asbestos in the United States of America (USA) has led to the cessation of mining operations at this site. Local and federal environmental legislation require the restoration of the mine site to its original condition (or better) prior to mining operations and a systematic monitoring of the environmental quality. The restoration of the mine sites usually involves the establishment of vegetation. Ultramafic (serpentine) soils have been known to support distinct, stunted and sparse vegetation with poorer plant-species diversity compared to that of non-serpentine soils (Roberts and Proctor, 1992). Although reasons for the specific vegetation in serpentine soils are not yet fully understood, soil properties are thought to be the major factor. Re-vegetation of the ultramafic-derived soil presents unique challenges to land management as well as to strategies to ensure environmental quality. A better understanding of the mineralogical and geochemical properties of these soils is central to the effective and sustainable management of these lands and the associated environments, as well as the assurance of environmental quality, food security and human health.

Previous research at the current study site has been limited to soil genesis and associated clay mineralogy. The dominant clay minerals found were chlorite, serpentine, talc, and montmorillonite (Maoui, 1966). However, little information is known about the geochemistry and overall mineralogy of the soils at the current study site. The objectives of the current study were to determine the geochemical properties and overall mineralogy of a soil developed from ultramafic parent materials from the Gillespie County, TX. This study is essential to understanding geochemical processes that impact agriculture and environmental quality.

MATERIALS AND METHODS

Study site

The study site is located in Gillespie County to the northeast of Fredericksburg (Fig. 5.1). A detailed description of the site is attached in Appendix C. The site is underlain by serpentine stretching 5.9 km in an east-west direction (Barnes et al., 1965). The width of serpentine deposit varies from 0.5 to 2.2 km. The Big Ranch gneiss lies adjacent to this serpentine at the southern and portions of the western side. Amphibole and mica schists form a contiguous border at the northern sides of the serpentine.

Sampling protocol

Soil samples were taken from the A1, A2, Bt and Cr horizons of a soil profile (Appendix C). Chemical analyses were performed on air-dried, gently crushed and sieved (< 2-mm sieve) soil. Soil pH was determined with a glass/calomel electrode in 1:2 soil:water (w/w) suspension. Soil organic carbon (OC) was determined by the Walkley-Black method (Nelson and Sommers, 1996) and particle size by the hydrometer method involving sedimentation after dispersion in pH 10, 10^{-3} M Na_2CO_3 (Gee and Bauder, 1986). Cation- exchange capacity was determined at pH 8.2 after saturation of the soil cation-exchange sites with Na^+ using 1M Na acetate, washing with 95% ethanol and displacement of the exchangeable Na with 1M ammonium acetate at pH 7.0 (Holmgren et al., 1977). Also extractable Ca, Mg, K, Na and Ni in soil were displaced by pH 7.0, 1

M ammonium acetate, and the concentrations were measured by atomic absorption (Ca, Mg, Ni) and flame emission (Na, K) spectrophotometry.

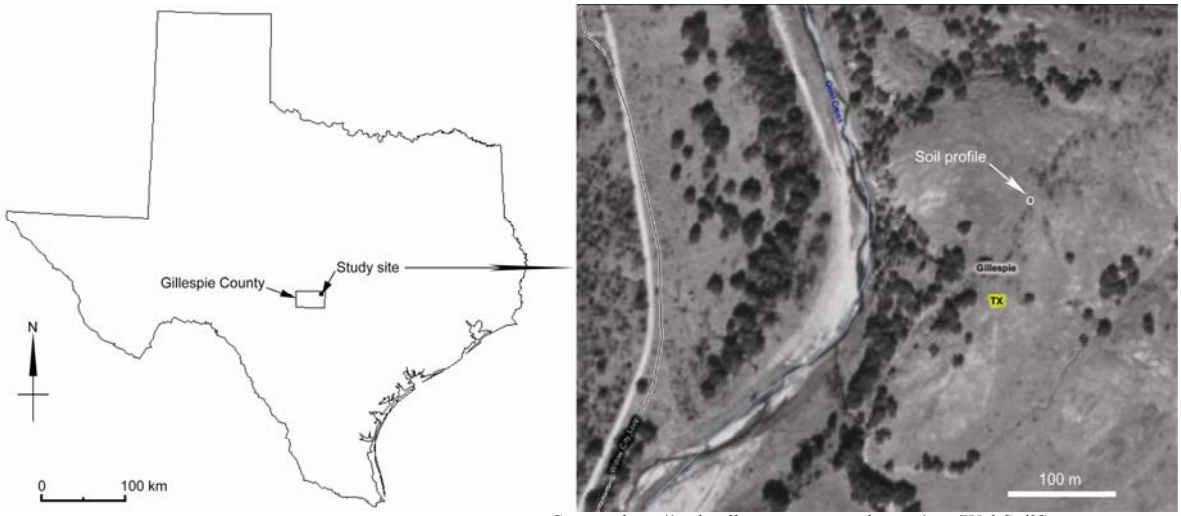

Source: http://websoilsurvey.nrcs.usda.gov/app/WebSoilSurvey.aspx

Fig. 5.1. Map of Texas (*left*) and an aerial photograph of the study site (*right*).

Chromium (VI (CrO_4^{2-}) in soil was extracted with 10 mM KH_2PO_4/K_2HPO_4 buffer solution at pH 7.2 by shaking for 1 hr (Bartlett and James, 1996). After filtration of the extract through a 0.2 μm cellulose-membrane filter, s-diphenylcarbazide solution was added to the filtrate from which the concentration of chromate was determined colorimetrically at 540 nm using a UV-visible spectrophotometer (Beckman Coulter, Brea, CA).

Total elemental analysis by neutron activation analysis

Total soil-elemental composition was determined by neutron-activation analysis (NAA) (Helmke, 1996). The air-dried soil samples were ground to pass a 0.10-mm sieve, and

about 55 mg of accurately weighed soil or standard rock sample, each in triplicate, were placed into plastic vials, which were then heat-sealed. The standard reference materials included NIST SRM-1633a coal fly ash, NIST SRM-688 basalt (National Institute for Standards and Technology, Washington, DC) and USGS standard rock AGV-1 (United States Geological Survey, Lakewood, CO). Samples were irradiated at the research nuclear reactor at Texas A&M University, College Station, TX, at a nominal neutron flux of 1×10^{13} $cm^{-2}s^{-1}$. Both short-time (30 s) and long-time (14 hr) radiations were performed for NAA. The short-radiated samples were counted for 500 s for the short-lived isotopes after a 20-min delay, and the long-radiated samples were counted for 2000 s for the intermediate-lived isotopes after a 7-day decay and for 3-hr for the long-lived isotopes after a 28-day decay. The counting system consisted of an Ortec (Ortec, Oak Ridge, TN) high purity Ge detector with a relative counting efficiency of 50% and a resolution of 1.74 keV. The spectra were acquired on a Canberra Genie-PC system (Canberra Industries, Meriden, CT) and transferred electronically to the VMS-based alpha processor at the campus laboratory. Spectra were processed using the Genie gamma evaluation software (Canberra Industries, Meriden, CT) and compared to calibrated standard data using Canberra's NAA software. The accuracy of the data was within 5-10%.

Selective dissolution of mineral phases

The association of heavy metals with total Fe oxides, poorly crystalline Fe oxides and Mn oxides were determined by extracting ground (< 0.1 mm) soil samples with dithionite-citrate (DC) (Holmgren, 1967), pH 3 ammonium oxalate (AO) in the dark (Loeppert and Inskeep, 1996), and hydroxylamine hydrochloride (HH) (Gambrell, 1996*)*, respectively. The concentrations of Fe, Cr, Mn, Ni, and Co in the extracts were determined with ICP-OES (Spectro, Mahwah, NJ).

Mineral analyses

To facilitate mineral identification and characterization, the soils were fractionated based on size, color, and magnetism. Sand (53–2000 μm), silt (2–53 μm), and clay (< 2 μm) fractions were separated by sieving and sedimentation (Gee and Bauder, 1986).

Magnetic minerals in the silt fractions were collected by a hand magnet, in which the silt:water (1:15 w/v) suspension was repeatedly sonicated to disperse the particles and a magnetic stir bar wrapped in a plastic bag was dipped into the suspension to attract the magnetic minerals. The magnetic minerals were transferred to a beaker by removing the magnet from the bag. Magnetic separation was repeated until no magnetic minerals could be attracted by the hand magnet. The mineralogy and chemical compositions of some minerals such as augite, maghemite/magnetite, and serpentine found in the soils were determined following hand-picking (under an optical microscope) some mineral specimens based on color, magnetism, and shape from the sand fractions of A2, Bt and Cr horizons under an optical microscope.

Mineral compositions were analyzed by X-ray diffraction (XRD), Fourier transform infrared (FTIR) spectroscopy, and scanning electron microscopy (SEM). The XRD analysis was performed on a Bruker D8 Advance (Bruker, Madison, WI) X-ray diffractometer with a CuKα source operated at 35 kV and 45 mA. A LynxEye (Bruker, Madison, WI) energy dispersive detector equipped with an anti-scatter slit extension was used to eliminate Fe fluorescence from the samples. Ground bulk, sand, and silt samples were mounted (front-end) as powder specimens for XRD analysis. Oriented K^+- or Mg^{2+}-saturated clays were air dried from aqueous suspensions on 25.4×1.6 mm round glass discs (Lakeside Brand, Hugh Courtright & Co., Monee, IL). The Mg^{2+}-saturated clay films were misted with 20% (v/v) glycerol/water solution and allowed to equilibrate in a closed petri dish for 4 hr. The K^+-saturated clays were heated to 330°C and then to 550°C for 1 hr, and following each heat treatment were cooled to about 100 °C and then immediately scanned by XRD. All XRD patterns were recorded with a dwell time of 2 s and a 0.017 °2θ step.

FTIR spectroscopy was used to verify the identity of clay minerals. Clay specimens were mixed with KBr (0.3% w:w) and pressed to pellets at a pressure of 20,000 psi for 5 min under vacuum suction and then oven dried at 140 °C for 24 hr prior to spectrum collection using a Spectrum 100 FTIR spectrometer (Perkin Elmer, Waltham, MA). The

spectra were recorded in transmission mode in the range of 4000-400 cm^{-1} at 4 cm^{-1} resolution.

SEM analyses were performed using a FEI- QUANTA 600 FE-SEM (FEI, Hillsboro, OR) microscope. The sand and silt specimens were mounted by pressing the particles on conductive C tabs (Ted Pella, Redding, CA). Clay particles were mounted by drying a diluted clay suspension on the C tab. All samples were coated under vacuum with about a 40-nm thickness of graphite C. Images and energy dispersive X-ray spectra were acquired at an accelerating voltage of 20 kV and a working distance of 10 mm.

RESULTS AND DISCUSSION

The soil pH is neutral in the A1, A2 and Bt horizons but is slightly alkaline in the *Cr* horizons, suggesting an increase in basic cations with increasing depth (Table 5.1). The A1 horizon contained the greatest concentration of organic C (OC) attributable to the decomposition of plant material. The extractable-Ca concentration was lower than that of extractable-Mg in each of the horizons. The highest concentration of Mg was in the Bt horizon, suggesting the translocation of Mg with clay. Although Na concentrations were similar in all of the horizons (0.1cmol(+) kg^{-1}), extractable-K concentration was seven times greater in the A1 horizon compared to the *Cr* horizon. Furthermore, extractable-Ca concentration in the *Cr* horizon was one-third that of the overlying horizons, indicating a possible change in parent material. As will be discussed in the mineralogy section, the A1, A2 and Bt horizons have different mineralogies from that of the *Cr* horizon. Soils developed from ultramafic parent materials have been reported to have very low concentrations of extractable-K (Alexander et al., 2007). The high concentration of extractable-K in the current study is attributable to the weathering of feldspars which might have been deposited by wind since they were only found in the A1, A2 and Bt horizons.

Table 5.1. Selected properties of a soil profile from the Gillespie County, TX.

Hori-zon	Depth (cm)	pH (H_2O)	Coarse fragments	Sand	Silt	Clay	O.C.†	Extractable bases				CEC	Mg/Ca
								Ca	Mg	K	Na		
			---------- % (w/w) ----------					--------- cmol(+) kg^{-1} ---------					
A1	0-13	6.7	33	29	40	31	2.62	7.1	22.3	0.7	0.1	41.4	3.1
A2	13-24	6.8	67	35	28	37	1.97	6.0	29.5	0.4	0.1	45.4	4.9
Bt	24-40	7.2	10	14	31	55	1.92	7.5	40.8	0.3	0.1	57.9	5.4
Cr	40-49	7.5		59	23	18	0.35	1.9	19.7	0.1	0.1	31.2	10.4

†O.C.- organic carbon.

These soils contain relatively high concentrations of total soil Cr, Fe, Ni and Ti. There were significant reductions in the concentrations of Ti and Fe at the 40-49 cm depth (*Cr*-horizon) compared to concentrations in the overlying horizons. However, Ni concentration in the *Cr*-horizon was nearly twice the concentrations in the A1, A2 and Bt horizons; the Mg concentrations in the *Cr*-horizon were more than twice the concentrations in the overlying horizons. The geochemistry of the soils in each horizon is attributable to the mineralogical composition of the soil (mineralogy section). Soil horizons with large amounts of serpentine, talc and magnetic Fe oxides (e.g., in the *Cr*-horizon) have high concentrations of Mg and Ni but very low concentrations of Al (Table 5.2). The concentrations of Mg were at least four-times higher than the concentrations of Ca in the A1, A2 and Bt horizons but dramatically increased to nearly 200-times higher in the *Cr* horizon. The concentrations of Al, Ca, K, and Na in the A1, A2 and Bt horizons were about eight-times higher than the concentrations in the *Cr* horizon. These trends suggest the presence of a lithological discontinuity or an abrupt change in the composition of the rocks from which the soils are derived (discussed in mineralogy section). Although previous research (Maoui, 1966) has shown a higher extractable-Mg concentration than that of Ca in each of the soil horizons at this site, K

and trace metal concentrations were not reported. In other studies of ultramafic soils, K concentrations have been found to be very low (Alexander et al., 2007). The current study has indicated unusually high total- and extractable-K concentrations in the A1, A2 and Bt horizons. As will be discussed later (mineralogy sections) the main K-source mineral is K-feldspars in the silt and sand fractions. No other sources of K have been detected in the clay fraction of this soil. The association of K-feldspars with ultramafic parent materials is unusual. It is likely that the K-feldspars have been deposited in the soil by wind. In similar studies, Rabenhorst et al., (1982), found high concentrations of K in the topsoil of a Maryland soil formed from ultramafic parent materials.

Cr speciation

In spite of the high concentrations of Cr and Mn in the soil, the toxic form of Cr, CrO_4^{2-}, was below the detection limit (5 μg L^{-1}). Previous studies have detected CrO_4^{2-} in ultramafic soils with high concentrations of Cr and Mn (Cooper, 2002; Fandeur et al., 2009). In the current study, the absence of CrO_4^{2-} was attributed to high concentrations of OC (2.6 %) in the A1, A2 and Bt horizons which resulted in the reduction of Cr(VI) to Cr(III) (Wittbrodt and Palmer, 1995). In the *Cr* horizon of the current study, despite low levels of organic C, no Cr(VI) was detected, suggesting the occurrence of Cr in the silicate and Fe-oxide structures. The oxidation of Cr(III) to Cr(VI) occurs readily in the presence of Mn(III,IV) and when the Cr(III) is in soluble form (Ross et al., 2001) . Such conditions would occur under acidic conditions. The soil pH reaction at the current site would be expected to lower the ability of Mn oxides to oxidize Cr(III) to Cr(VI).

Table 5.2. Total elemental composition of a soil profile from the Gillespie County, TX.

Horizon	Depth (cm)	Al	Ca	Mg‡	K	Na	Fe	Cr	Ni	Mn	Ti	Co	V	Zn
		---------- mg kg^{-1} ----------												
A1	0-13	41490	10920	44370	6560	3770	108230	7050	3490	1480	3350	160	130	90
A2	13-24	47390	9880	49410	4330	2470	119800	5480	3990	1850	2940	190	160	80
Bt	24-40	47490	6680	47620	1930	570	155200	5060	6630	1440	1500	240	140	100
Cr	40-49	5450	550	104750	260	210	76700	3760	6540	450	0	140	50	30

‡Determined by atomic absorption spectrophotometer in aqua-regia/HF.

Trace metals extracted by HH, AO and DC

Dithionite-citrate (DC) and acidified ammonium-oxalate (AO) (in the dark) extractions have been utilized extensively to obtain quantitative estimates of total and poorly crystalline Fe-oxide concentrations, respectively, in soil (Holmgren, 1967). Both of these extractions might also result in the partial dissolution of Fe-rich and trioctahedral silicate minerals (Arshad et al., 1972).

Fe

More than 30% of the total Fe was extractable by DC, suggesting that a substantial proportion of the Fe occurred in Fe oxides (Fig. 5.2a). The highest DC extractable-Fe proportion was in the Bt horizon implying a higher proportion of Fe as Fe oxide. The AO-extractable Fe represented less than 3% of the total Fe in the A and Bt horizons but significantly increased to about 10% in the *Cr* horizon. This result suggests an increase in poorly crystalline Fe oxide in the Cr horizon or the possible dissolution of Fe-containing minerals. X-ray diffraction patterns suggest the partial dissolution of serpentine and talc by pH 3.0 ammonium oxalate. Negligible amounts (<0.1%) of the total Fe was extractable by HH.

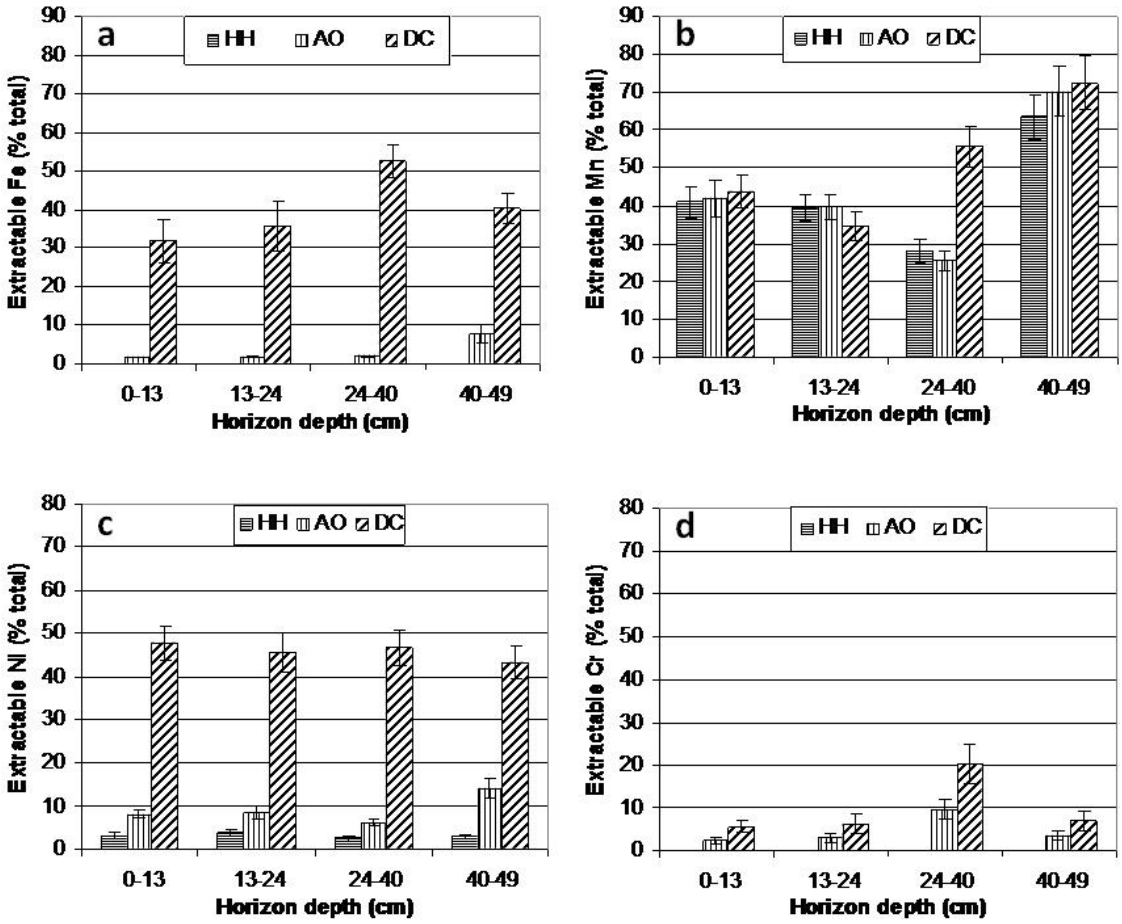

Fig. 5.2. Extractable Fe, Mn, Ni and Cr by hydroxylamine hydrochloride (HH), acidified ammonium oxalate in dark (AO) and dithionite-citrate (DC).

Mn

Almost identical proportions of the total Mn were extractable by HH, AO and DC in the A1 (~40 %), A2 (~40 %) and *Cr* (~70 %) horizons, though the extraction efficiencies were greater in the *Cr* horizon (Fig. 5.2b). In the Bt horizon, the DC-extractable Mn proportion was about twice the proportion of the total Mn extractable by HH and AO, suggesting a higher proportion of Mn oxides associated with the crystalline Fe oxides. Although total Mn concentrations were lowest in the *Cr* horizon, more than 60 % of the total Mn was extracted by each of the three reagents.

Ni

Nearly 50 % of the total Ni was extractable by DC from each of the horizons, suggesting the strong association with the Fe oxides (Fig. 5.2c). These results are consistent with the energy dispersive (EDS) spectra of the magnetic Fe oxides that show Ni peaks (Fig. 5.12). HH-extractable Ni represented less than 3% of the total Ni and was similar in all the horizons. AO-extractable Ni concentration was more than double the concentration of HH-extractable Ni, even though it represented less than 10% of the total Ni in the A1, A2 and Bt horizons. Also, this result supports the association of Ni with the poorly crystalline component. The concentration of Ni extracted by AO doubled in the *Cr* horizon, implying the dissolution of the Ni-containing minerals (e.g., serpentine).

Cr

The concentrations of Cr extractable by HH were below the detection limit in all the horizons (Fig. 5.2d). This observation seems to indicate that the poorly crystalline Fe oxides were not appreciably dissolved by the HH extraction. Both the AO- and DC-extractable Cr proportions were below 8% of the total Cr in the A1, A2 and *Cr* horizons but were 10% and 20% respectively in the Bt horizon. These trends indicate the greater proportion of Cr is associated with the insoluble minerals (e.g., Fe oxides, serpentine, chromite) and may not be bio-available in the short-term.

Mineralogy of the clay fraction

The XRD and FTIR analyses indicated that the clay fractions of the soils contained, smectite, talc, serpentine, chlorite and Fe oxides (including goethite and hematite).

Iron-rich smectite

Smectite was identified by the appearance of a 1.8-nm peak or the weakened intensity of the 1.45-nm peak in the XRD patterns after the glycerol solvation treatment (Fig. 5.3). The intense infrared-absorption bands at 3577, 876, 819, and 505 cm^{-1} are characteristic of Fe-rich smectite such as nontronite (Fig. 5.3). The infrared-absorption band at 3410 cm^{-1} common to the clay particle-size seperates of all soil horizons indicates large amounts of structural water associated with the clay minerals. The substitution of Fe for

Al in the octahedral sheet causes shifts of the stretching (3400-3600 cm^{-1}) and bending (700-920) vibrations of the OH groups to lower frequencies (Farmer, 1974). The 819 cm^{-1} band originates from the OH-bending vibrations at the Fe(III)Fe(III)-OH site, and its strong intensity suggests abundant Fe in the octahedral sheet of the smectite. The 505 cm^{-1} band represents the Fe^{3+}-O-Si bending and deformation vibration (Bishop et al., 2002).

Talc

Talc is evident by its 0.94 nm d(001) and higher order diffraction peaks on the XRD patterns. These XRD peaks were unaltered upon ion-exchange, solvation, and heat treatments (Fig. 5.3). Further evidence of talc was its characteristic infrared bands at 3677, 669, and 465 cm^{-1} (Fig. 5.4). The occurrence of the absorption band at 3661 cm^{-1}, which has been ascribed to the OH-stretching vibration at the MgMgFe(Ni)-OH site, suggests substitution of Fe, Ni, or both for Mg in the octahedral sheet of talc (Farmer, 1974; Wilkins and Ito, 1967). Energy dispersive spectroscopic (EDS) analysis indicated that Fe but not Ni was the substituting cation in the structures (discussed in the compositional and morphological variations of mineral particles section). Smaller amounts of Al substitution were also evident from the EDS analysis.

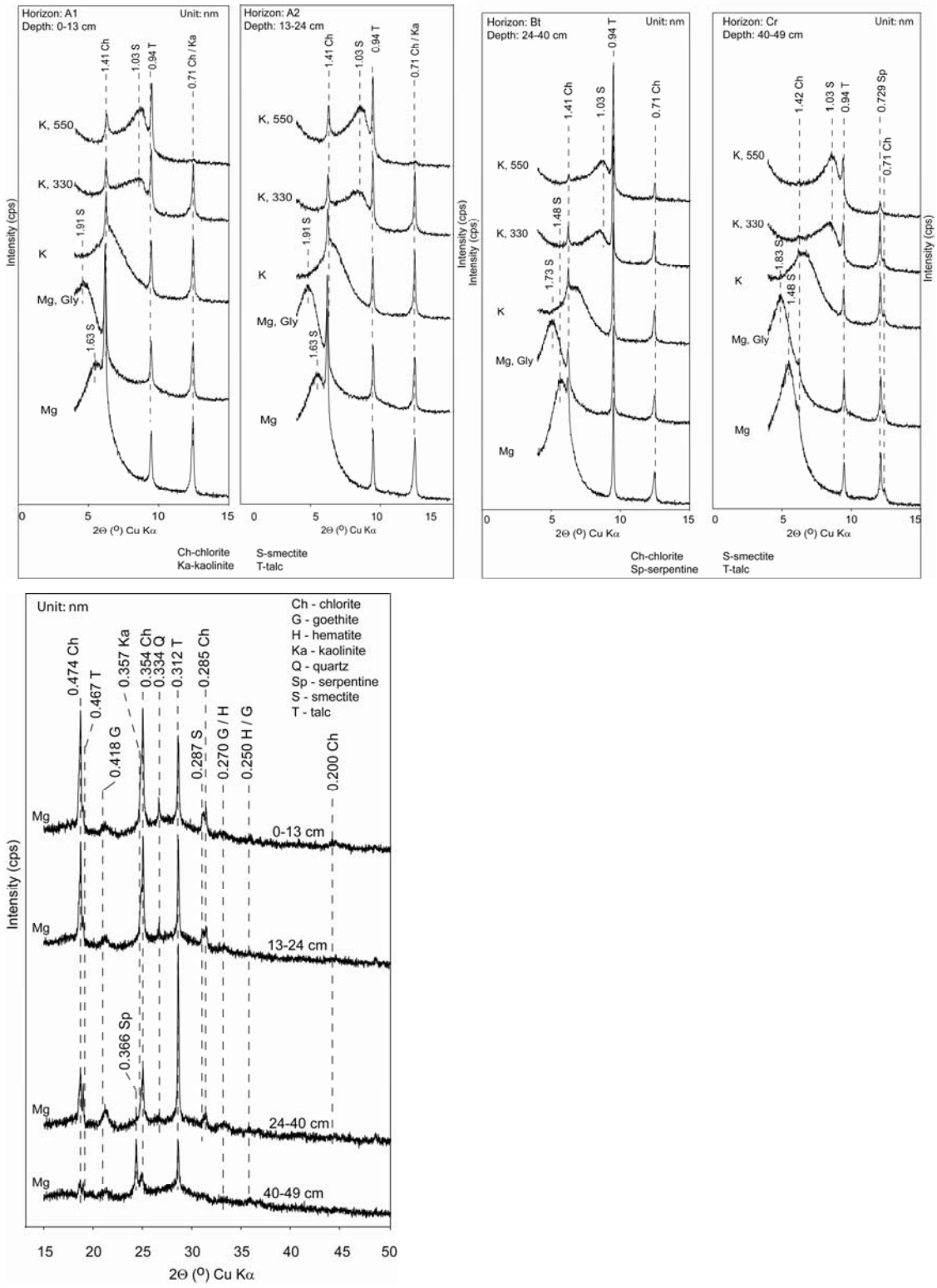

Fig. 5.3. X-ray diffraction patterns of the clay (< 2 μm) fraction from a soil profile.

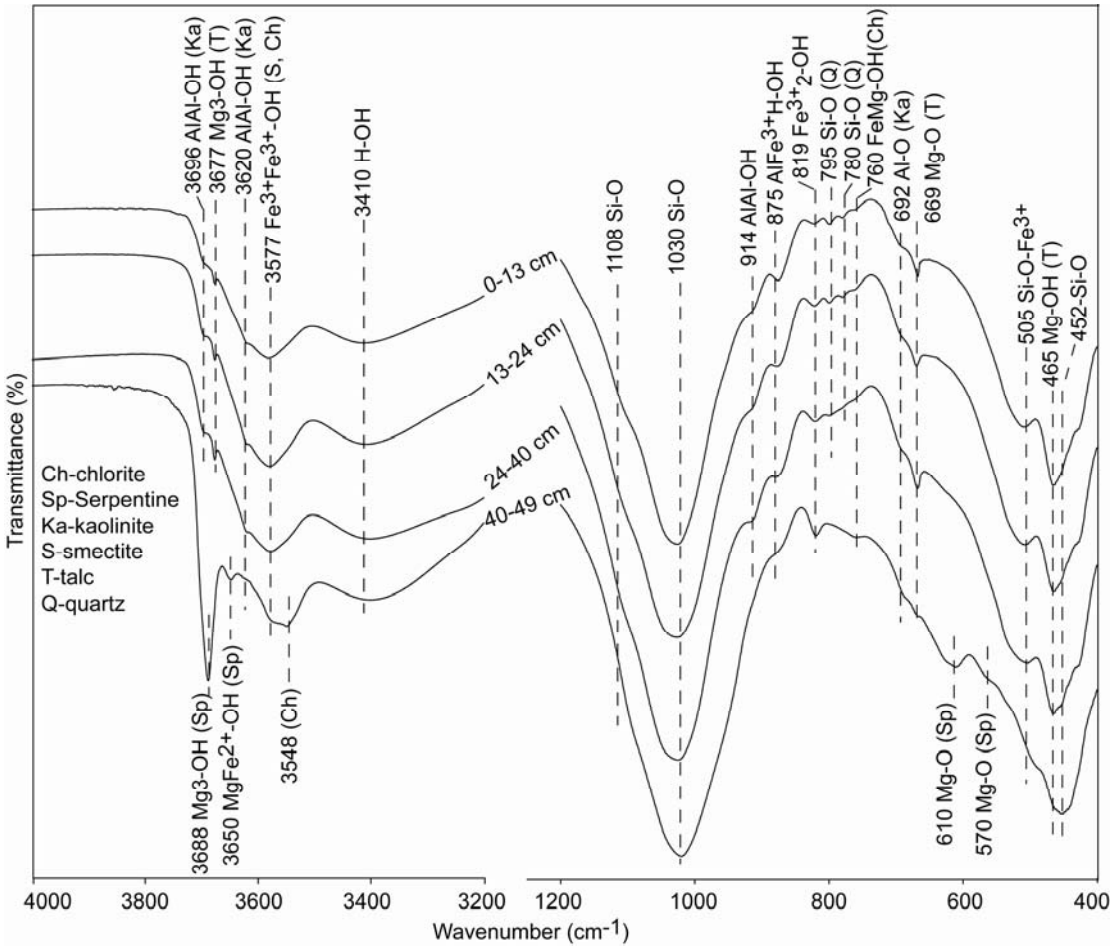

Fig. 5.4. Fourier transform infrared pattern of the oven-dry clay (< 2 μm) pressed pellets.

Serpentine and quartz

The clay fraction of the *Cr* horizon exhibited the characteristic XRD peaks of serpentine at 0.73 and 0.366 nm that were not affected by the ion-exchange reactions or heat treatment (Fig. 5.3). The 3688, 3650, 962, 610, and 571 cm^{-1} infrared absorption bands are also diagnostic for serpentine (Fig. 5.4). These bands were observed in the *Cr*-horizon only and corroborate XRD evidence of serpentine in this horizon.

Quartz was identified by the doublet infrared-absorption bands at 795 and 780 cm^{-1}. These bands have been assigned to Si-O bending and stretching vibrations (Farmer,

1974). The infrared absorption bands for quartz were present only in the clay fraction from the A and B horizons (Fig. 5.4).

Chlorite and kaolinite

The presence of chlorite in the clay samples is indicated by the sharp and strong 1.41 nm XRD peak for the Mg-treated samples and the persistence of this peak upon glycerol and K-treatment. The intensity of the 1.41 nm peak of K-treated samples was slightly reduced (Fig. 5.3). Heat treatment of the K-saturated clay to 550^{o}C resulted in broad peaks with a d-spacing of 1.03 nm. The failure of the d-spacing to completely collapse to 1.00 nm indicates the presence of hydroxyl-interlayered minerals.

The identification of kaolinite in the presence of chlorite using the d(001) and d(002) reflections was a challenge because of peak overlap. The poorly resolved XRD peak at 3.57 nm was used to identify kaolinite (Fig. 5.3). Kaolinite was further identified by its infrared absorption bands at 3696, 3622, and 914 cm^{-1} (Fig. 5.4). The absorption bands in the OH-stretching region (3697 and 3622 cm^{-1}) were very weak and broad, and the other two characteristic absorption bands of kaolinite at 3670 and 3650 cm^{-1} were too weak to be observed, suggesting a poorly crystalline and defective structure. These bands were evident in the clay seperates, except those from the *Cr*-horizon. Previous studies had not identified kaolinite in the clay fraction (Maoui, 1966). Few studies have reported the occurrence of kaolinite in ultramafic-derived soils (Yongue-Fouateu et al., 2009).

Iron oxides

Crystalline goethite and hematite in the clay fractions were identified by the XRD peaks at 0.418 and 0.269 nm for goethite and 0.250 nm and 0.269 nm for hematite (Fig. 5.3). Overall, the Fe oxide XRD peaks were weak and relatively broad, suggesting small crystallite sizes.

Mineralogy of sand, silt and rock fragments

Chlorite particles

X-ray diffraction patterns showed strong and sharp peaks of high intensity at 1.46 and 1.42 nm that were assigned to chlorite. These peaks were detected in the sand and silt fractions in each of the soil horizons (Fig. 5.5). However, only the 1.42 nm d spacing XRD peak was discernible in the clay fraction, suggesting weathering of the 1.46 nm d spacing chlorite. The 1.46 and 1.42 nm d-spacings might represent the different compositions and substitutions in chlorite. For example, Cr-containing clinochlore has a d(001) d-spacing at 1.45 nm while the Al-containing clinochlore has a d(001) at 1.42 nm (Bayliss et al., 1980). With the A1 horizon, the peaks were identical in intensity and sharpness; however, in the Bt- and *Cr*-horizons (Fig. 5.5), the intensities of the 1.42 nm peak of the sand fractions were significantly greater than those of the 1.46 nm peak, suggesting greater amounts of Al-chlorite with depth. The d(060) peak of random powder samples of nearly pure chlorites exhibit a stronger intensity of the peak at 1.54 nm but a negligible or non-detectable peak at 1.49 nm (Appendix C, Fig. C.1), suggesting the trioctahedral character of the chlorites. A fractured rock fragment composed of almost pure chlorite exhibited an intense red color (2.5 YR 3/6) attributable to Fe-rich minerals deposited on its surface its surface (Appendix C, Fig. C.2). These Fe-rich coatings are products of chlorite weathering, suggesting the substitution of Fe^{2+} for Mg in the chlorite structure. As will be discussed (compositional and morphological variations section), chlorite in this study contains structural Fe and Cr.

Almost pure chlorite was present in relatively large amounts as rock fragments in the A1, A2 and Bt horizons, implying that chlorite was a major parent mineral from which the soils were derived.

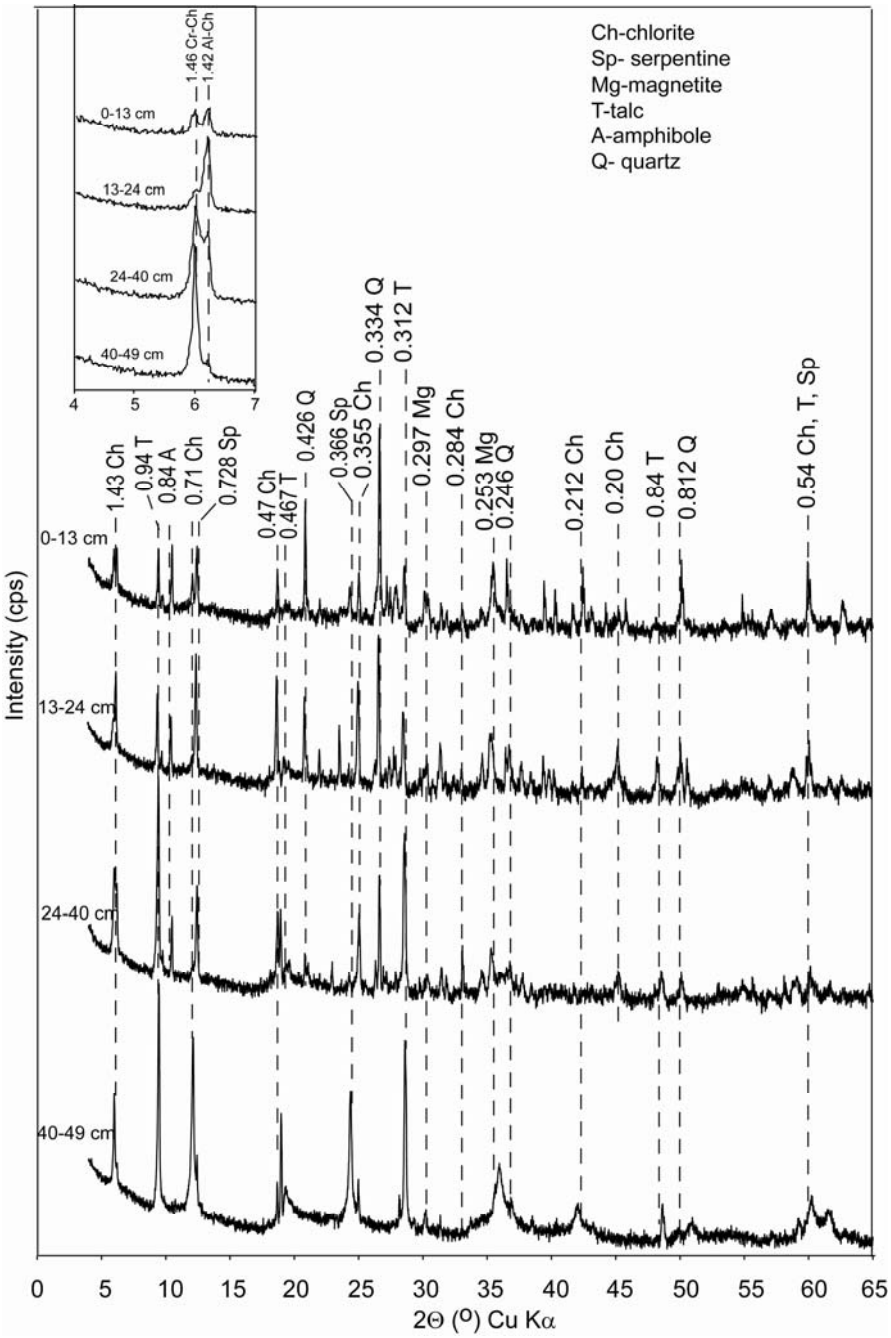

Fig. 5.5. Powder x-ray diffraction patterns of the sand fraction. The mineralogy is similar to the silt fraction (not shown).

Talc particles

Talc occurred in all soil horizons but was much more abundant in the *Cr*-horizon. XRD diffraction patterns showed no evidence of talc in the rock fragments suggesting rapid disintegration to smaller particle sizes. Talc is the softest known mineral in the Moh's scale (hardness =1).

Serpentine

The largest concentrations of serpentine were in the *Cr*-horizon; negligible amounts were present in the A1 and Bt horizons (Fig. 5.5). Serpentine was not detected in the rock fragments of the A1, A2 and A3 horizons. These results suggest a rapid weathering of serpentine in these soils.

Quartz and feldspars

Quartz and feldspars occurred in the sand and silt particle-size fractions of the A1, A2 and Bt horizons but not in the *Cr*-horizon or in rock fragments (Fig. 5.5). The occurrence of feldspars only in the sand and silt fractions of the A1, A2 and Bt horizons suggests transportation by wind. It is possible that with increasing weathering, quartz could form in the soil. Powder XRD patterns of hand-picked sand grains identified based on color and shape with the aid of a microscope indicated the presence of pure feldspars (Appendix C, Fig. C.3).

Amphibole and pyroxene particles

Amphibole (e.g., tremolite) was identified by the intense XRD peak at 0.842 nm and a weaker peak at 0.90 nm (Fig. 5.6). The amphiboles occurred in the sand, silt and rock fragments of the A1, A2 and Bt horizons but not the *Cr*-horizon. The intensity of XRD peaks suggests that larger amounts of amphiboles are present in the silt fraction than the sand fraction. Pyroxenes (e.g., augite) were identified from their 0.295 nm, 0.289 nm and 0.299 nm XRD peaks and were found in the A1, A2 and Bt horizons. The amphiboles and pyroxenes contained high but variable concentrations of Ca.

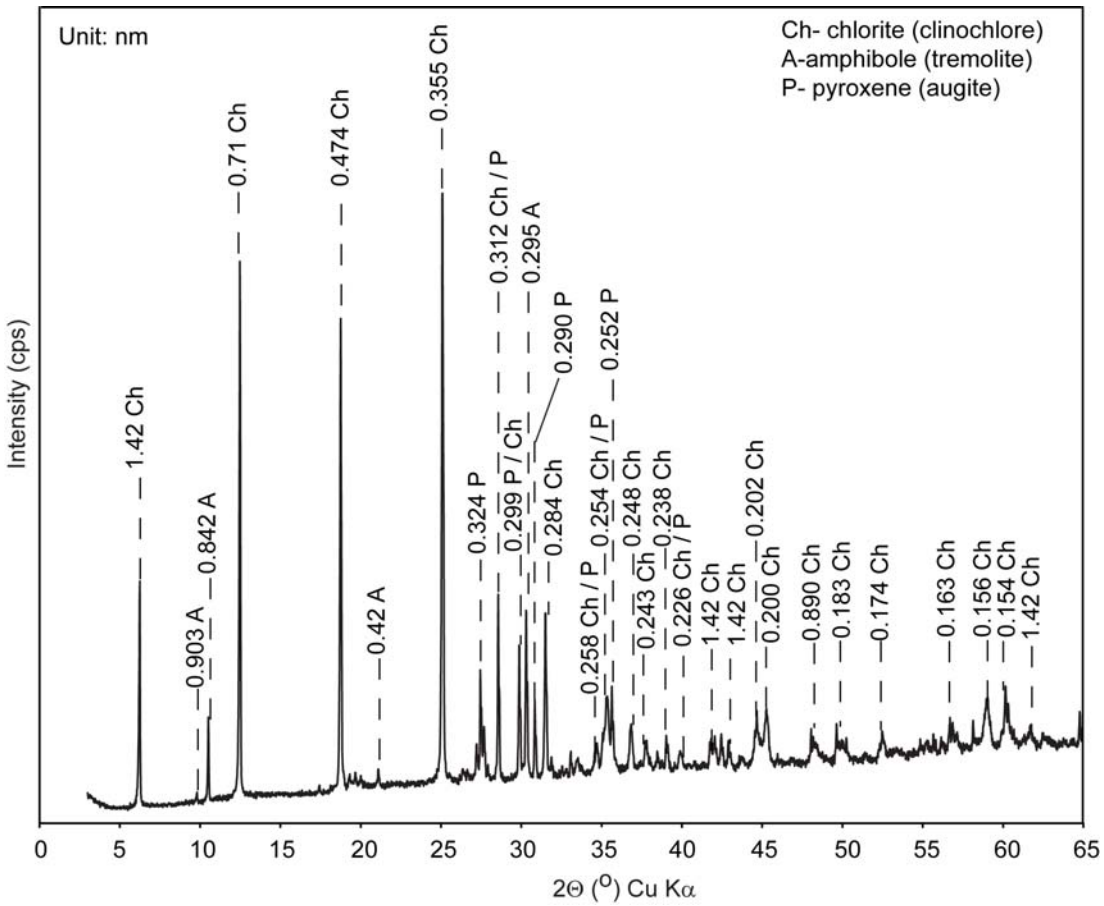

Fig. 5.6. Powder x-ray diffraction patterns of the coarse fragments (>2 mm) from the A and Bt horizons.

Magnetic mineral particles

Although the individual magnetic (Fe oxide) minerals could not be identified by XRD because of the overlap in peak position, the presence of twin XRD peaks at d-spacings of 0.160-0.161 nm and 0.147- 0.148 nm indicates the presence of both magnetite and maghemite (Fig. 5.7). The greater amount of the magnetic minerals was black, implying the predominance of magnetite. The magnetic minerals, which were mostly found in the silt fraction and comprised of about 15% (w/w) of the total silt fraction, were largely black, implying the predominance of magnetite (Schwertmann and Taylor, 1989).

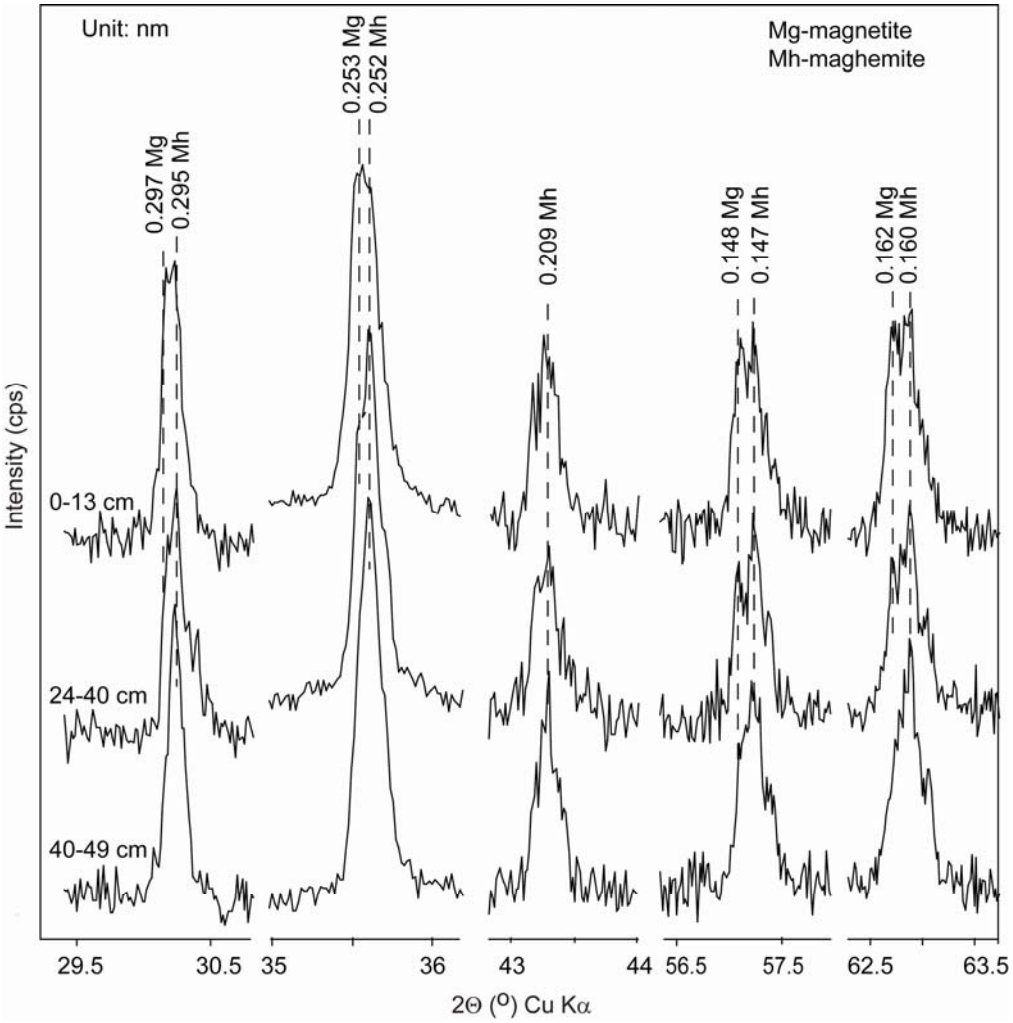

Fig. 5.7. Powder x-ray diffraction patterns of magnetic silt (2-50 μm) from the A1, Bt and *Cr* horizons.

Non-magnetic Fe oxide

The crystalline and non-magnetic Fe oxides detected were goethite (d-spacings of 0.418, 0.269 and 0.246 nm) and hematite (d-spacings of 0.250, 0.368 and 0.269 nm). They were present predominantly in the silt fractions of the A1, A2 and Bt horizons. The non-

magnetic Fe oxides occurred as reddish brown (2.5 YR 3/4) and yellowish-brown (10YR 5/6) coatings on silt-sized particles of minerals (e.g., chlorite). The former and latter colors of the Fe oxides suggest the predominance of hematite and goethite, respectively (Schwertmann and Taylor, 1989). The XRD peaks of these minerals were sharp but of low relative intensity, indicating a relatively high crystallinity (Appendix C, Fig. C.4).

Compositional and morphological variations of mineral particles

Particles of almost pure minerals were hand-picked with the aid of an optical microscope from the sand fraction and the coarse fragments (>2 mm), based on color, morphology and magnetism. The coarse fragments were ground to powder prior to XRD and FTIR analyses to identify particle mineralogy. Chemical compositions of the particles were determined by SEM equipped with an energy dispersive detector (EDS).

Chlorite

Two types of chlorites were distinguished: (1) light green particles and (2) grey, shiny particles with perfect cleavage. Previous XRD patterns of the sand fraction indicated seperate peaks at 1.46 nm and 1.42 nm (Fig. 5.5). The coarse fragments were almost pure phases of chlorite with a d(001) spacing at 1.42 nm. The SEM/EDS analysis of the light green chlorite indicated higher and variable contents of Al but relatively low concentrations of Fe (Fig. 5.8, image c). The green color of these chlorites suggests Fe^{2+} substitution for Mg in the octahedral layer. The grey shiny chlorite particles contained Cr in addition to Al and Fe (Fig. 5.8, image a). A semi-quantitative analysis (by EDS) of these chlorite particles indicated contents of about 2.1 and 1.4% (w/w) of Fe and Cr, respectively. The XRD peaks at 1.46 nm and 1.42 nm were therefore attributed to variations in Al, Cr and Fe concentrations in the chlorites. Substitution of Fe^{2+} (0.074 nm ionic radius) for Mg^{2+} (0.066 nm ionic radius) increase the size of the octahedral sheet. Furthermore, increased Al^{3+} (0.051 nm ionic radius) for Si^{4+} (0.042 nm ionic radius) substitution in the tetrahedral layer, as well as Al^{3+} substitution for Mg^{2+} in the brucite layer resulted in a reduced the d(001) spacing in chlorite (Brindley, 1961).

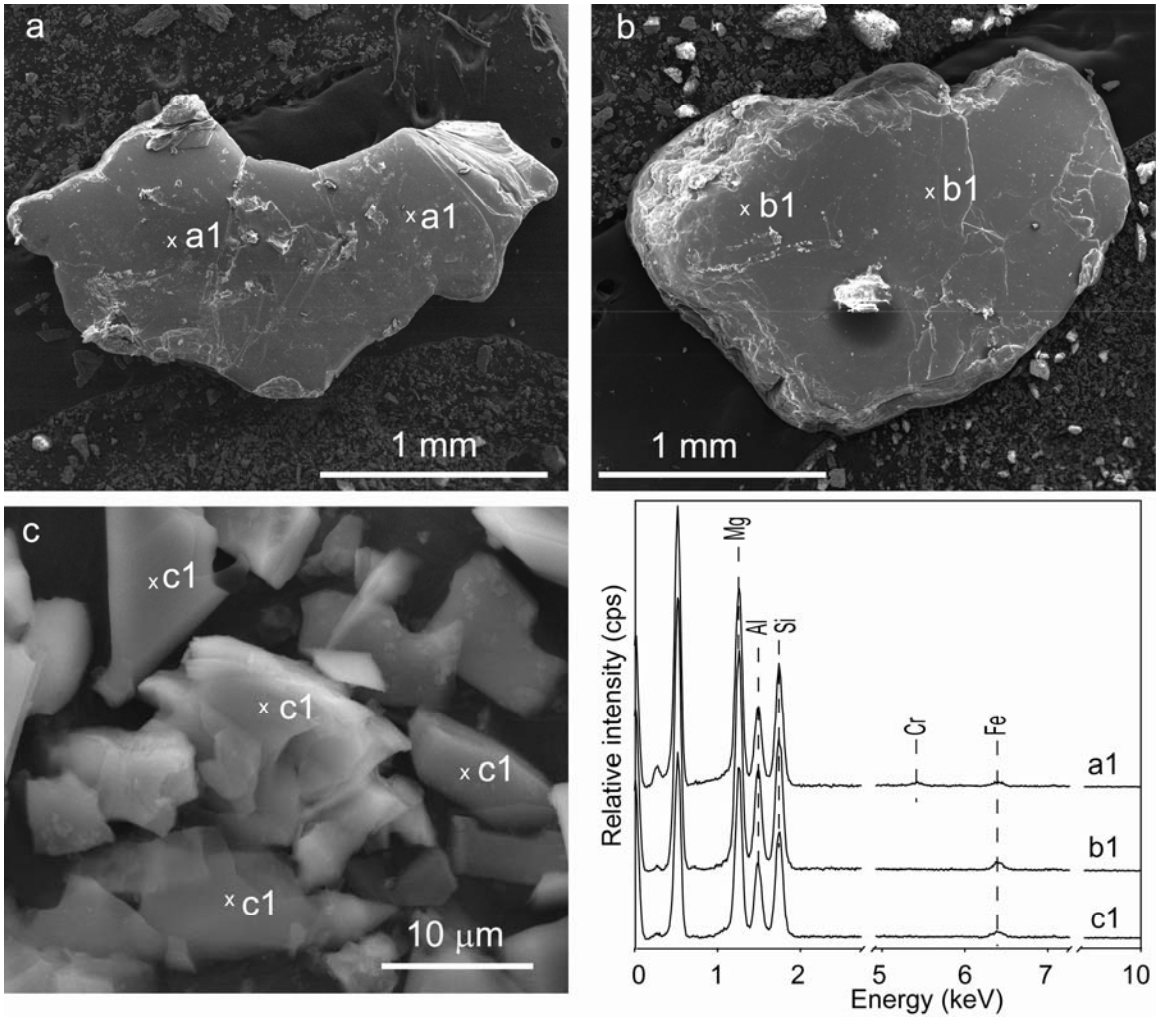

Fig. 5.8. SEM images of pure chlorite in the sand fraction of the A1 horizon (a and b), and coarse fragments from the Bt horizon. Energy dispersive spectra (EDS) of the marked particles are shown in the graph (*bottom right*). Particles marked with the same letters or symbols have identical compositions.

Serpentine and talc

Serpentine was distinguished from talc by the relative ratio of the Mg:Si peak heights from the EDS analysis (Fig.5.9). Energy dispersive spectra of an ideal serpentine

$[Mg_3Si_2O_5(OH)_4]$ and talc $[Mg_3Si_4O_{10}(OH)_2]$ have Mg:Si ratios of 3:2 and 3:4, respectively. Identification of these minerals was further corroborated by their morphologies when observed under SEM. Electron diffraction spectroscopy (EDS) indicates minor amounts of Fe and Ni substitution in serpentine (Fig. 5.10). Serpentine minerals showed both rod-shaped (or fibrous) and platy morphologies, suggesting the occurrence of chrysotile and lizardite polymorphs (Fig. 5.9, image f). EDS analyses indicated minor amounts of Fe and Ni substitution in serpentine (Fig. 5.10, spectrum e1). The substitution of Fe or Ni in serpentine was corroborated by the 3650 cm^{-1} absorption band in the FTIR OH-stretching region (earlier discussed in mineralogy of the clay fraction section), attributed to the MgFe,Ni –[OH]. Similarly to serpentine, talc contained minor amounts of Fe (Fig. 5.10, spectrum f1); Ni was not detected in the talc particles from this site.

Amphiboles/pyroxenes

The amphibole and pyroxene particles were rod-shaped and contained relatively high concentrations of Ca but little Al and Fe (Fig. 5.10, spectrum d2). Trace metals were not detectable in these particles.

Magnetic minerals

Although most of the Fe oxides were crystalline and had smooth surfaces, a greater proportion showed irregular surfaces and grooves that suggest crystallization at the interface with other minerals or melting and re-crystallization onto the surfaces of the existing larger bigger articles (Fig. 5.11, image j and k). The EDS peaks of the magnetic minerals show that they contain substantial amounts of Cr and smaller amounts of Ni and Co (Fig. 5.12, spectra h4, i5, j4 and k6). Semi-quantitative analyses of the magnetic particles indicate that Cr concentrations ranged from 2 to 18 % (w/w). The magnetic particles also contain varying amounts of Mg and/or Al (Fig. 5.12, spectra h4 and i5).

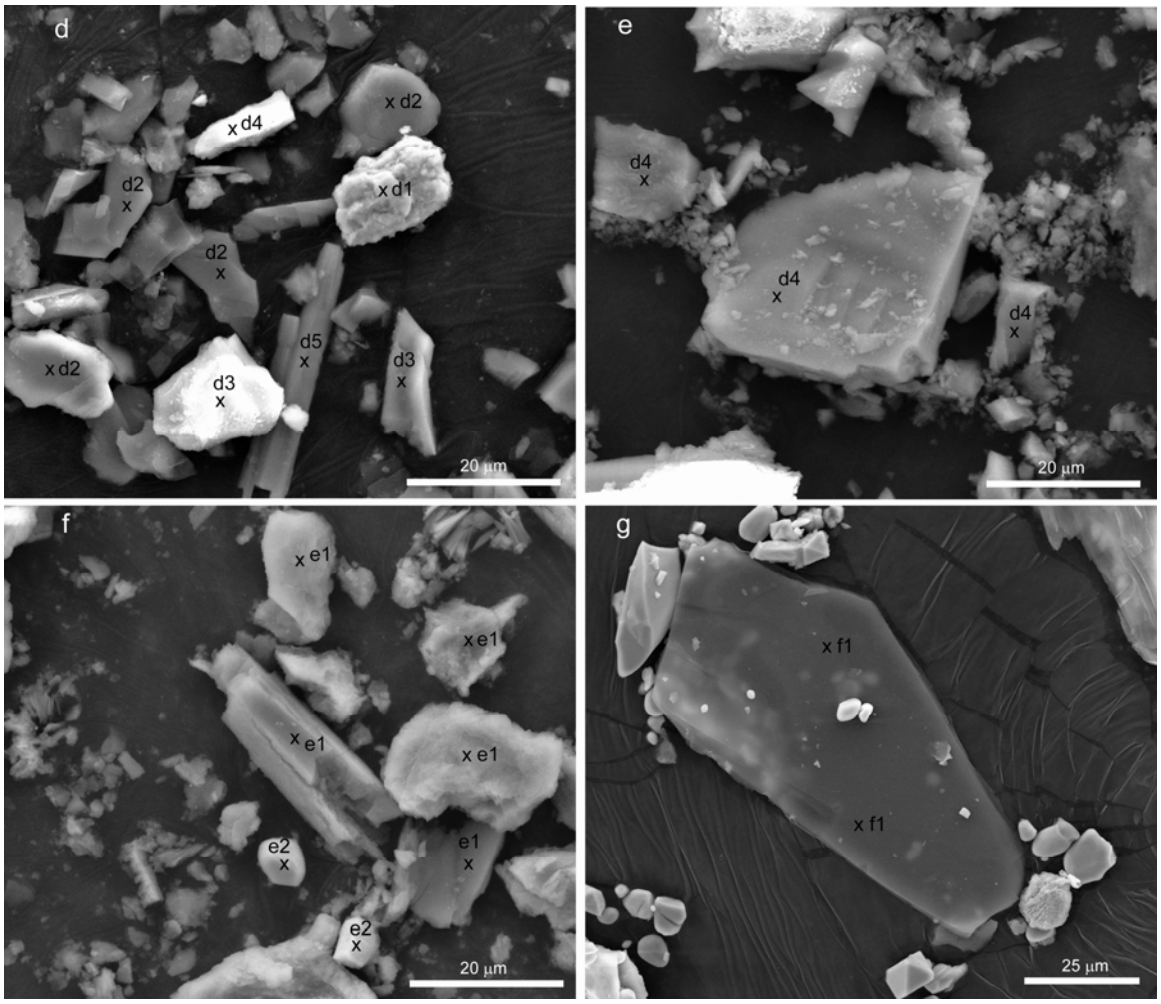

Fig. 5.9. SEM images of the non-magnetic minerals in the silt fraction of the Bt (d and e) and *Cr* horizons (f and g). The composition of the marked particles is shown in Fig. 5.10.

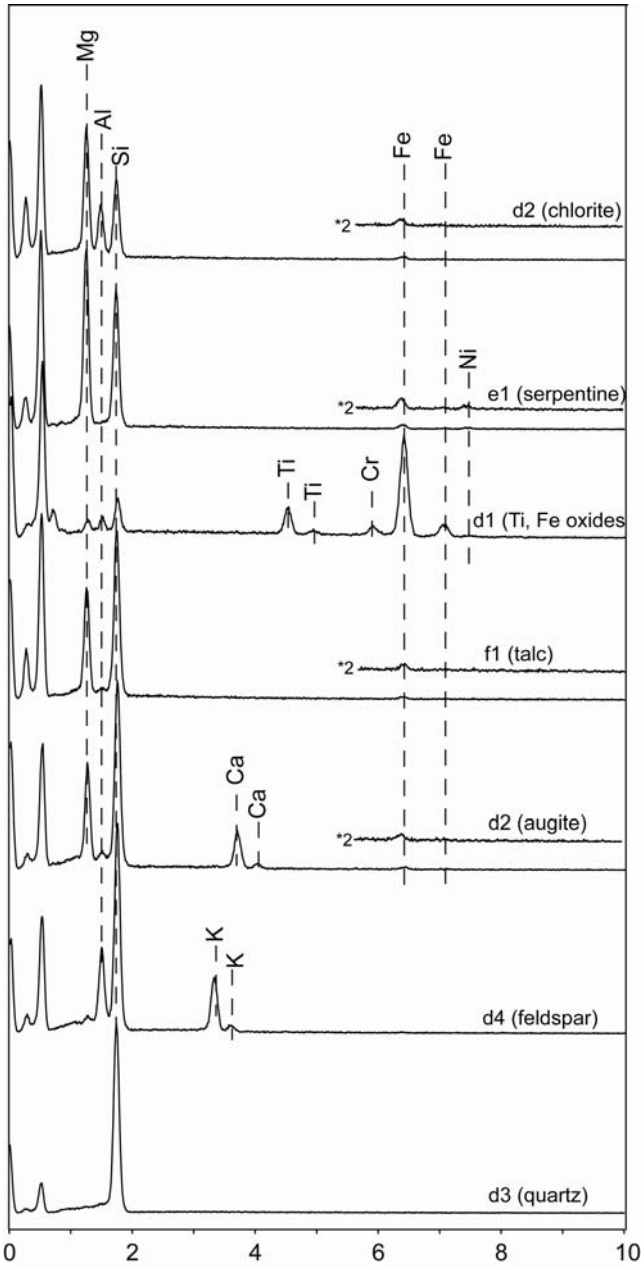

Fig. 5.10. EDS spectra of mineral particles shown in Fig. 5.9 showing their chemical compositions.

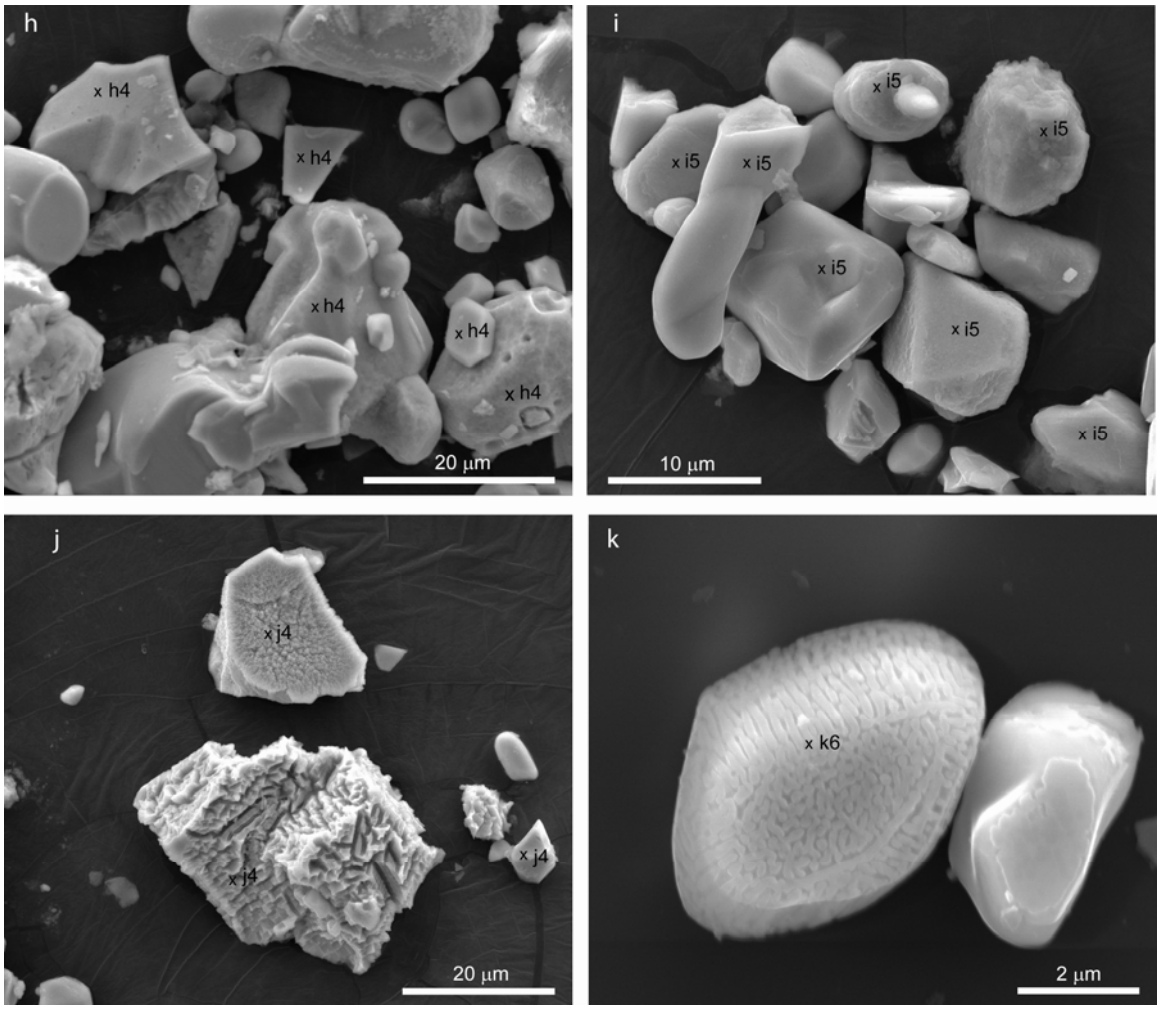

Fig. 5.11. SEM images of the magnetic minerals (magnetite/maghemite) from the silt fraction of the Bt (h and k) and *Cr* horizons (i and j). The composition of the marked particles is shown in Fig. 5.12. Particles marked with the same letters or symbols have identical compositions.

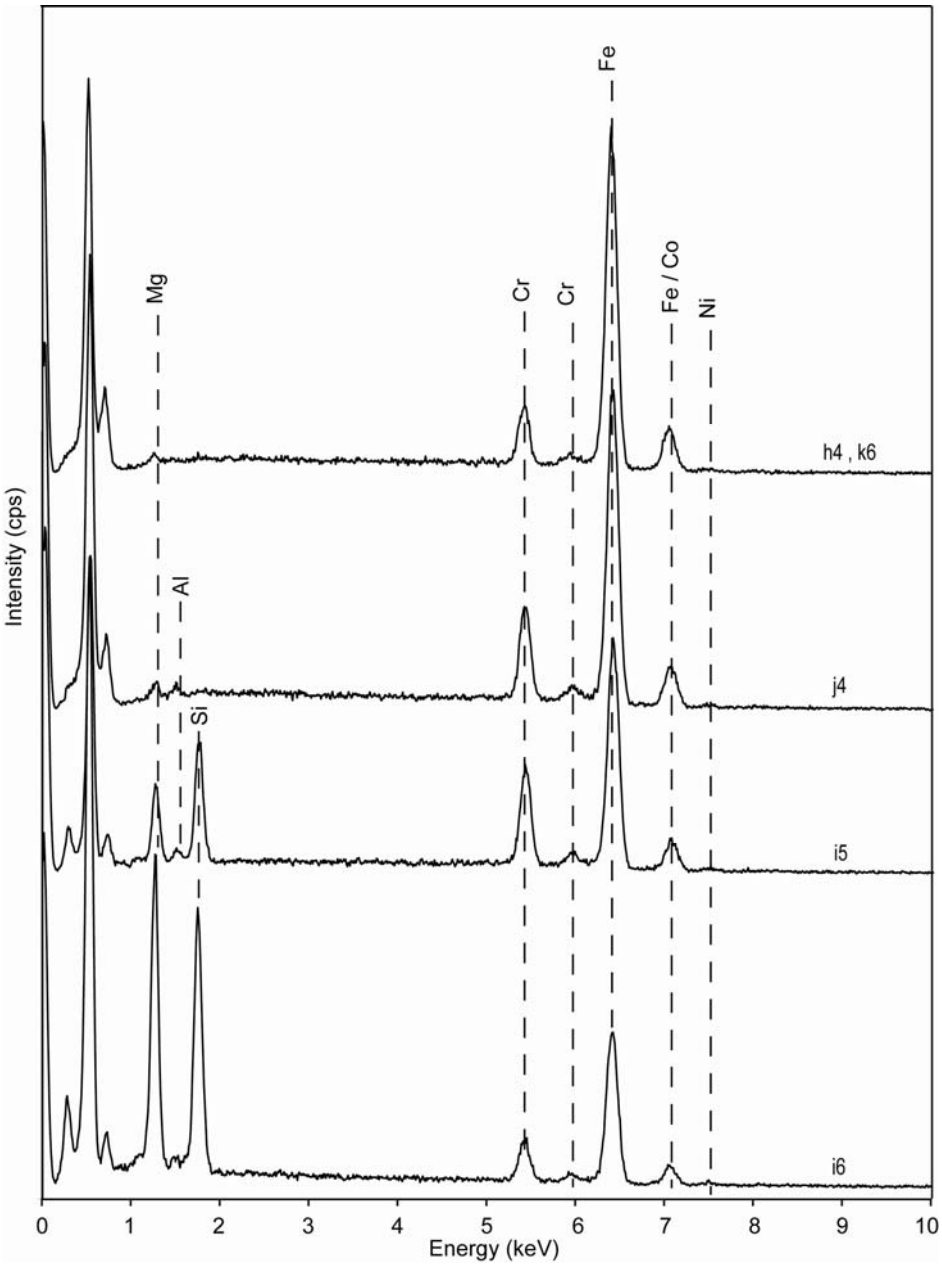

Fig. 5.12. EDS images of the magnetic mineral particles shown in Fig. 5.11. Talc (spectrum i5) and serpentine (spectrum i6) were coated with magnetic Fe oxides.

CONCLUSIONS

The minerals at this site are uncommon in most agricultural soils and are mostly inherited from the parent materials. The secondary minerals are rich in Fe but lack K-bearing minerals in the clay fraction. Geochemical data have provided evidence of foreign mineral input in horizons overlying the *Cr* horizon. High concentrations of Fe, Cr, Mn, Ni and the presence of serpentine minerals can potentially impact agricultural productivity, human health and overall environmental quality. The low concentrations of extractable Ca compared to Mg, and the high contents of Mg-containing minerals compared to Ca-containing minerals could impact ecosystem function.

CHAPTER VI

SUMMARY

The objectives of the current study were to assess and compare the mineralogical and bio-geochemical characteristics of several diverse soils from the Great Dyke, Zimbabwe and Gillespie County, Texas that were both developed from ultramafic parent materials. In the case of the Great Dyke, transects were evaluated at both the northern (Mpinga) and southern (Bannockburn) regions. The mineralogical and chemical information is essential to address changing land use patterns and the inherent challenges to agriculture, environmental quality, and health. There were both similarities and wide variations in chemical composition and mineralogy at each specific site and between sites. The soils at both the Zimbabwean and Gillespie sites contained relatively high concentrations of Cr, Mn, Ni, Fe, Mg and organic C but low levels of Ca compared to the most agricultural soils. The concentrations of Mg are higher than those of Ca. Unlike the Great Dyke soils that contained negligible concentrations of K, the Gillespie County ultramafic soil had considerably higher concentrations of this element. The concentrations of Cr in soils of the Great Dyke were higher than the representative ultramafic soil from Gillespie County, with Cr(VI), which is phytotoxic and mutagenic, being detected at the Mpinga site. Other metals (e.g., V, Co) were in relatively higher concentrations in the soils of the Great Dyke compared to the Gillespie County soil.

The characteristic minerals of the clay particle-size fractions in each of the study sites were talc, serpentine, chlorite, Fe-rich smectite and Fe oxides. The silt-size fractions contained relatively high concentrations of magnetic minerals (e.g., maghemite/magnetite). Except for the Fe-rich and Fe-oxide minerals that can form in soil, the major minerals in these soils are derived from the parent materials. The same lithologic minerals were also found in relatively high concentrations in both the silt- and sand-size fractions. The minerals sometimes occurred in specific landscape positions and soil horizons, and their occurrence was largely influenced by parent material, drainage and climate. Common minerals in agricultural soils (e.g., kaolinite, feldspars) were

absent or in negligible concentration. A characteristic feature of these soils is the absence of mica in the clay-size fraction. Unique to the Zimbabwean soils was the predominance of chromite, pyroxenes and amphiboles in the silt and sand-sized fractions. In ultramafic soils from the Gillespie County, chlorite was more abundant than in the Zimbabwean ultramafic soils.

The two sites on the Great Dyke differed in mineral and chemical composition as well. The Mpinga site contained higher concentrations of Ni, serpentine, and Fe oxide (including the magnetic minerals). Bannockburn, however, contained lower concentrations of Ni, and neither magnetic minerals nor serpentine were detected. Palygorskite was unique to the Bannockburn site, and its occurrence was likely influenced by the climate.

The microbial community structure of the whole-soil at Mpinga indicates the presence of both bacteria and fungi (including arbuscular mycorrhizal fungi) at each of the landscape positions; Gram-positive bacteria were relatively more abundant than Gram-negative ones. Biomarkers for actinomycetes were not detected. It is likely that the geochemical properties of these soils and the specific vegetation associated with them might have considerable impact on the whole-soil microbial community structure.

In the Great Dyke soils, the low concentration or absence of K-containing minerals (e.g., micas) and the relatively low concentrations of Ca-containing minerals (e.g., anorthite) and exchange Ca^{2+}, which is essential for normal plant growth, would have a considerable impact on agricultural productivity. These problems are further compounded by the presence of relatively high concentrations of vermiculite and high-charge smectite that can fix K. Also, the relatively high concentrations of heavy metals (e.g., Ni, Cr) can be toxic to plants. In order to increase the concentrations of Ca and as well as to reduce the bio-availability of the toxic heavy metals, it might be essential that a Ca source, e.g., calcite or gypsum, be considered in the development of agricultural management systems.

Although there is potential for increasing agricultural productivity when appropriate plant nutrients are added by way of inorganic fertilizers, there is the potential risk for heavy metal uptake by the plants grown in these soils. Consumption of contaminated food by way of the food chain could pose potential health hazards to humans. The occurrence of carcinogenic minerals (e.g., serpentine, amphiboles) in the easily-inhaled particle-size fractions (e.g., clay and silt) is also a potential health hazard. Management strategies that reduce wind erosion (e.g., good vegetative cover) should be considered. Furthermore, the more toxic and carcinogenic Cr(VI) present in some of the ultramafic soils in Zimbabwe, as well as its potential to form in similar soil environments, is of potential concern to human health. Further research is needed to determine the safety of food grown in these soils as well as the safety of drinking water. The soil environmental conditions in which Cr(VI) can form in these soils deserves further research.

REFERENCES

Alexander, E.B., C.C. Ellis, and R. Burke. 2007. A Chronosequence of soils and vegetation on serpentine terraces in the Klamath Mountains, USA. Soil Sci. 172:565 - 576.

Amir, H., and R. Pineau. 1998a. Influence of plants and cropping on microbiological characteristics of some New Caledonian ultramafic soils. Aust. J. Soil Res. 36:457 - 472.

Amir, H., and R. Pineau. 1998b. Effects of metals on the germination and growth of fungal isolates from New Caledonian ultramafic soils. Soil Biol. Biochem. 30:2043 - 2054.

Amir, H., D.A. Jasper, and L.K. Abbott. 2008. Tolerance and induction of tolerance to Ni of arbuscular mycorrhizal fungi from New Caledonian ultramafic soils. Mycorrhiza 19:1- 6.

Anderson, S. 1975. Addition to the checklist of the minerals of Rhodesia. Ann. Rhodesia Geol. Survey 1:62 - 64.

Arshad, M.A., R. Arnaud, and P.M. Huang. 1972. Dissolution of trioctahedral layer silicates by ammonium oxalate, sodium dithionite-citrate-bicarbonate, and potassium pyrophosphate. Can. J. Soil Sci. 52:19 - 26.

Baath, E., M. Diaz-Ravina, A. Frostegard, and C.D. Campbell. 1998. Effect of metal-rich sludge amendments on the soil microbial community. Appl. Environ. Microbiol. 64:238 - 245.

Barnes, V.E., D.A. Shock, and W.A. Cunningham. 1965. Utilization of Texas serpentine. University of Texas Publication No.5020.

Barshad, I., and F.M. Kishik. 1970. Factors affecting potassium fixation and cation exchange capacities of soil vermiculite clays. Clays Clay Miner. 18:127 - 137.

Bartlett, R., and B.R. James. 1979. Behavior of chromium in soils: III. Oxidation. J Environ. Qual. 8:31 - 35.

Bartlett, R.J., and B.R. James. 1996. Chromium. p. 683 - 701, *In* D. L. Sparks (ed.) Methods of soil analysis, Vol. 3. Soil Science Society of America, Inc., American Society of Agronomy, Inc., Madison, WI.

Batten, K.M., K.M. Scow, K.F. Davies, and S.P. Harrison. 2006. Two invasive plants alter soil microbial community composition in serpentine grasslands. Biol. Invasions 8:217-230.

Bayliss, P., L.G. Berry, M.E. Mrose, and D.K. Smith. 1980. Mineral powder diffraction search manual. JCPDS International Centre for Diffraction Data, Swarthmore, PA.

Berner, R.A., and J. Schott. 1982. Mechanism of pyroxene and amphibole weathering; II: Observations of soil grains. Am. J. Sci. 282:1214 - 1231.

Becquer, T., C. Quantin, M. Sicot, and J.P. Boudot. 2003. Chromium availability in ultramafic soils from New Caledonia. Sci. Total Environ. 301:251 - 261.

Bigham, J.M., W.F. Jaynes, and B.L. Allen. 1980. Pedogenic degradation of sepiolite and palygorskite on the Texas High Plains. Soil. Sci. Soc. Am. J. 44:159 - 167.

Bishop, J., E. Murad, and M.D. Dyar. 2002a. The influence of octahedral and tetrahedral cation substitution on the structure of smectites and serpentines as observed through infrared spectroscopy. Clay Miner. 37:617 - 628.

Bishop, J., J. Madejova, P. Komadel, and H. Froschl. 2002b. The influence of structural Fe, Al and Mg on the infrared OH bands in spectra of dioctahedral smectites. Clay Miner. 37:607 - 616.

Bonifacio, E., E. Zanini, V. Boero, and M. Franchini-Angela. 1997. Pedogenesis in a soil catena on serpentinite in north-western Italy. Geoderma 75:33 - 51.

Bossio, D.A., K.M. Scow, N. Gunapala, and K.J. Graham. 1998. Determinants of soil microbial communities: Effects of agricultural management, season, and soil type on phospholipid fatty acid profiles. Microb. Ecol. 36:1-12.

Brindley, G.W. 1961. The chlorite minerals. p. 242-291. *In* G. Brown (ed.) X-ray identification and structure of clay minerals. Mineralogical Society, London.

Brooks, R.R., and X. Yang. 1984. Elemental levels and relationships in the endemic serpentine flora of the Great Dyke, Zimbabwe and their significance as controlling factors for the flora. Taxon 33:392 - 399.

Brooks, R.R., (ed.) 1987. Serpentine and its vegetation: A multi-disciplinary approach. Dioscorides Press, Portland, OR.

Brookes, P.C., S.P. McGrath, and C. Heijnen. 1986. Metal residues in soils previously treated with sewage-sludge and their effects on growth and nitrogen fixation by blue-green algae. Soil Biol. Biochem. 18:345 - 353.

Bulmer, C.E., and L.M. Lavkulich. 1994. Pedogenic and geochemical processes of ultramafic soils along a climatic gradient in southwestern British Columbia Can. J. Soil Sci.74:165 -177.

Burford, E.P., M. Fomina, and G.M. Gadd. 2003. Fungal involvement in bioweathering and biotransformation of rocks and minerals. Mineral Mag. 67:1127-1155.

Caillaud, J., D. Proust, S. Philippe, C. Fontaine, and M. Fialin. 2009. Trace metals distribution from a serpentinite weathering at the scales of the weathering profile and its related weathering microsystems and clay minerals. Geoderma 149:199 - 208.

Callen, R.A. 1984. Clays of the palygorskite-sepiolite group: Depositional environment, age and distribution. p. 1-37. *In* A. Singer and E. Galan (ed.) Develop. Sediment., Vol. 37. Elsevier, Amsterdam, The Netherlands.

Chao, T.T. 1972. Selective dissolution of manganese oxides from soils and sediments with acidified hydroxylamine hydrochloride. Soil Sci. Soc. Am. J. 36:764 - 768.

Chao, T.T., and P.K. Theobald. 1983. The significance of iron and manganese oxides in geochemical exploration. Econ. Geol. 71:1560 - 1569.

Chardot, V., G. Echevarria, M. Gury, S. Massoura, and J. Morel. 2007. Nickel bioavailability in an ultramafic toposequence in the Vosges Mountains (France). Plant Soil 293:7 - 21.

Cooper, G.R.C. 2002. Oxidation and toxicity of chromium in ultramafic soils in Zimbabwe. Appl. Geochem. 17:981 - 986.

Cornell, R.M., and U. Schwertmann. 1979. Influence of organic anions on the crystallization of ferrihydrite. Clays Clay Miner. 27:401 - 410.

Cornell, R.M., and U. Schwertmann, U. 2003. The iron oxides: Structure, properties, reactions, occurrences, and uses. p. 39-57. Wiley-VCH Verlag GmbH & Co., KGaA, Weinheim.

DeGrood, S.H., V.P. Claassen, and K.M. Scow. 2005. Microbial community composition on native and drastically disturbed serpentine soils. Soil Biol. Biochem. 37:1427 - 1435.

Department of Meteorological Services.1978. Climate handbook supplement: Climatological summaries. Zimbabwe Rhodesia Government, Salisbury.

Ebinger, M.H., and D.G. Schulze. 1989. Mn-substituted goethite and Fe-substituted groutite synthesized at acid pH. Clays Clay Miner. 37:151 - 156.

Fandeur, D., F. Juillot, G. Morin, L. Olivi, A. Cognigni, S.I.M. Webb, J.-P. Ambrosi, E. Fritsch, F. Guyot, and J.G.E. Brown. 2009. XANES Evidence for oxidation of Cr(III) to Cr(VI) by Mn-oxides in a lateritic regolith developed on serpentinized ultramafic rocks of New Caledonia. Environ. Sci. Technol. 43:7384 - 7390.

Farmer, V.C. (ed.) 1974. The infrared spectra of minerals. Mineralogical Society, London.

Fendorf, S., M.J. Eick, P. Grossl, and D.L. Sparks. 1997. Arsenate and chromate retention mechanisms on goethite. 1. Surface structure. Environ. Sci. Technol. 31:315 - 320.

Foord, E., H. Starkey, J. Taggart Jr, and D. Shawe. 1987. Reassessment of the volkonskoite-chromian smectite nomenclature problem. Clays Clay Miner. 35:139-149.

Frost, R.L., O.B. Locos, H. Ruan, and J.T. Kloprogge. 2001. Near-infrared and mid-infrared spectroscopic study of sepiolites and palygorskites. Vibr. Spectrosc 27:1 - 13.

Gambrell, R.P. 1996. Manganese. p. 665 - 682. *In* D. L. Sparks (ed.) Methods of soil analysis, Vol. 3. Soil Science Society of America, Inc., American Society of Agronomy, Inc., Madison, WI.

Garnier, J., C. Quantin, E. Guimarães, V.K. Garg, E.S. Martins, and T. Becquer. 2009. Understanding the genesis of ultramafic soils and catena dynamics in Niquelândia, Brazil. Geoderma 151:204 - 214.

Gaskin, A.J., P.J. Darragh, and F.C. Loughnan. 1979. Australian kaolins. p. 591-599. *In* M.M. Mortland and V.C. Farmer (ed.) Proc. Int. Clay Conf. 1978. Elservier North Holland, Inc., New York.

Gates, W.P., (ed.) 2005. Infrared spectroscopy and the chemistry of dioctahedral smectites . *In* T. Kloprogge (ed.) Vibrational spectroscopy of layer silicates and hydroxides. CMS Workshop Lectures, Vol 13. p.125-168. The Clay Minerals Society, Aurora, CO.

Gaudin, A., S. Petit, J. Rose, F. Martin, A. Decarreau, Y. Noack, and D. Borschneck. 2004. The accurate crystal chemistry of ferric smectites from the lateritic nickel ore of Murrin Murrin (Western Australia): II. Spectroscopic (IR and EXAFS) approaches. Clay Miner. 39:453 - 467.

Gaudin, A., A. Decarreau, Y. Noack, and O. Grauby. 2005. Clay mineralogy of the nickel laterite ore developed from serpentinised peridotites at Murrin Murrin, Western Australia. Aust. J. Earth Sci. 52:231 - 241.

Garnier, J., C. Quantin, E. Guimarães, V.K. Garg, E.S. Martins, and T. Becquer. 2009. Understanding the genesis of ultramafic soils and catena dynamics in Niquelândia, Brazil. Geoderma 151:204 - 214.

Graham, R.C., and S.W. Buol. 1990. Soil-geomorphic relations on the Blue Ridge Front: II. Soil characteristics and pedogenesis. Soil Sci. Soc. Am. J. 54:1367 - 1377.

Gee, G.W., and J.W. Bauder. 1986. Particle size analysis. p. 383 - 411. *In* A. Klute (ed.) Methods of soil analysis. Part 1: Physical and mineralogical methods. Agronomy Society of America, Soil Science Society of America Inc, Madison, WI.

Grayston, S.J., C.D. Campbell, R.D. Bardgett, J.L. Mawdsley, C.D. Clegg, K. Ritz, B.S. Griffiths, J.S. Rodwell, S.J. Edwards, W.J. Davies, D.J. Elston, and P. Millard. 2004. Assessing shifts in microbial community structure across a range of grasslands of differing management intensity using CLPP, PLFA and community DNA techniques. Appl. Soil Ecol. 25:63-84.

Gregorich, E.G., M.R. Carter, J.W. Doran, C.E. Pankhurst, and L.M. Dwyer. 1997. Biological attributes of soil quality. p. 81-113. *In* E. G. Gregorich and M. R. Carter (ed.) Develop. Soil Sci. Vol. 25. Elsevier, Amsterdam, The Netherlands.

Harris, W.G., L.W. Zelazny, and J.C. Baker. 1984. Depth and particle size distribution of talc in a Virginia Piedmont Ultisol. Clays Clay Miner. 32:227 - 230.

Harwood, J.L., and N.J. Russel (ed.) 1984. Lipids in plants and microbes. George Allen & Unwin, London.

Haselwandter, K., O. Bobleter, and D.J. Read. 1990. Degradation of ^{14}C-labelled lignin and dehydropolymer of coniferyl alcohol by ericoid and ectomycorrhizal fungi Arch. Microbiol. 153:352-354.

Helmke, P.A. 1996. Neutron activation analysis. p. 141-159. *In* D. L. Sparks (ed.) Methods of soil analysis, Vol. 3. Soil Science Society of America, Agronomy Society of America, Inc, Madison, WI.

Högberg, M.N., and P. Högberg. 2002. Extramatrical ectomycorrhizal mycelium contributes one-third of microbial biomass and produces, together with associated roots, half the dissolved organic carbon in a forest soil. New Phytol. 154:791-795.

Holmgren, G.G.S. 1967. A Rapid citrate-dithionite extractable iron procedure. Soil Sci. Soc. Am. J. 31:210 - 211.

Holmgren, G.G.S., R.L. Juve, and R.C. Geschwender. 1977. A mechanically controlled variable rate leaching device. Soil Sci. Soc. Am. J. 41:1207 -1208.

Hopkins, N.A. 1987. Mycorrhizae in a California serpentine grassland community. Can. J. Bot. 65:484-487.

Hossner, L.R. 1996. Dissolution for total elemental analysis. p. 49-64. *In* D. L. Sparks (ed.) Methods of soil analysis, Vol. 5. Soil Science Society of America Inc., American Society of Agronomy, Inc., Madison, WI.

Hseu, Z.Y. 2007. Weathering sequences of clay minerals in soils along a serpentinitic toposequence. Clays Clay Miner. 55:389-401.

Hungwe, A.P. 1988. A pedological study of the Siabuwa Valley, Zimbabwe and preliminary investigations into the water relations of some Madumabisa mudstone-derived soils, University of Zimbabwe, Harare, Zimbabwe.

Innes, L., P.J. Hobbs, and R.D. Bardgett. 2004. The impacts of individual plant species on rhizosphere microbial communities in soils of different fertility. Biol. Fertil. Soils 40:7-13.

Istok, J.D., and M.E. Harward. 1982. Influence of soil moisture on smectite formation in soils derived from serpentinite. Soil Sci. Soc. Am. J. 46:1106 - 1108.

Jones, B.F., and E. Galan (ed.) 1988. Palygorskite-sepiolite Vol.18. pp. 1-44. Mineralogical Society of America.

Kadir, S., and M. Eren. 2008. The occurrence and genesis of clay minerals associated with quaternary caliches in the Mersin area, Southern Turkey. Clays Clay Miner. 56:244 - 258.

Kennedy, A.C. 1994. Carbon utilization and fatty acid profiles for characterization of bacteria. p. 543-556. *In* R. W. Weaver (ed.) Methods of soil analysis Part 2. SSSA Book Series No. 5. Soil Science Society of America, Inc., Madison, WI.

Ketterings, Q.M., J.M. Bigham, and V. Laperche. 2000. Changes in soil mineralogy and texture caused by slash-and-burn fires in Sumatra, Indonesia. Soil Sci. Soc. Am. J. 64:1108 - 1117.

Kim, J.G., J.B. Dixon, C.C. Chusuei, and Y. Deng. 2002. Oxidation of chromium(III) to (VI) by manganese oxides. Soil Sci. Soc. Am. J. 66:306 - 315.

Kodama, H., and M. Schnitzer. 1977. Effect of fulvic acid on the crystallization of Fe(III) oxides. Geoderma 19:279 - 291.

Kunze, G.W., and J.B. Dixon. 1986. Pretreatment for mineralogical analysis. p. 91-100. *In* A. Klute (ed.) Methods of soil analysis. Part 1: Physical and mineralogical methods. Agronomy Society of America, Soil Science Society of America Inc., Madison, WI.

Lee, B.D., S.K. Sears, R.C. Graham, C. Amrhein, and H. Vali. 2003. Secondary mineral genesis from chlorite and serpentine in an ultramafic soil toposequence. Soil Sci. Soc. Am. J. 67:1309 - 1317.

Loeppert, R.H., and W.P. Inskeep. 1996. Iron. p. 639-664. *In* D. L. Sparks (ed.) Methods of soil analysis, Vol. 3. Soil Science Society of America, Agronomy Society of America, Inc., Madison, WI.

Manceau, A., L. Charlet, M.C. Boisset, B. Didier, and L. Spadini. 1992. Sorption and speciation of heavy metals on hydrous Fe and Mn oxides. From microscopic to macroscopic. Appl. Clay Sci. 7:201 - 223.

Manning, C.B., V. Vallyathan, and B.T. Mossman. 2002. Diseases caused by asbestos: Mechanisms of injury and disease development. Int. Immunopharmacol. 2:191 - 200.

Maoui, H. 1966. A mineralogy and genetic study of serpentine derived soils from Gillespie County, Texas., Texas Tech University, Lubbock.

McBride, M.B. 1994. Oxidation-reduction reactions. p. 242-249. *In* M.B. McBride (ed.) Environmental chemistry of soils. Oxford University Press, New York.

McGahan, D.G., R.J. Southard, and V.P. Claassen. 2008. Tectonic inclusions in serpentinite landscapes contribute plant nutrient calcium. Soil Sci. Soc. Am. J. 72:838 - 847.

Meharg, A.A. 2003. The mechanistic basis of interactions between mycorrhizal associations and toxic metal cations. Mycol. Res. 107:1253-1265.

Mengoni, A., R. Barzanti, C. Gonnelli, R. Gabbrielli, and M. Bazzicalupo. 2001. Characterization of nickel-resistant bacteria isolated from serpentine soil. Environ. Microbiol. 3:691 - 698.

Mertens, J., D. Springael, I. De Troyer, K. Cheyns, P. Wattiau, and E. Smolders. 2006. Long-term exposure to elevated zinc concentrations induced structural changes and zinc tolerance of the nitrifying community in soil. Environ. Microbiol. 8:2170 - 2178.

Mossman, B.T., and J.B.L. Gee. 1989. Asbestos-related diseases. New England J. Med. 320:1721-1730.

Munjonji, L., A. Manyanga, A. Manyevere, and E. Chikwari. 2006. Soils of the proposed Bannockburn irrigation project. Chem. Soil Res. Inst., Zimbabwe. Soil Report No. A684.

Nelson, D., and L. Sommers. 1996. Total carbon, organic carbon and organic matter. p. 961-1010. *In* D. L. Sparks (ed.) Methods of soil analysis, Vol. 3. Soil Science Society of America, Inc., Agronomy Society of America, Inc, Madison, WI.

Noble, A.D., and J.C. Hughes. 1991. Sequential fractionation of chromium and nickel from some serpentinite-derived soils from the eastern Transvaal. Commun. Soil Sci. Plant Anal. 22:1963 -1973.

Nyamapfene, K.W. 1984. Transmission electron microscopy and electron diffraction studies on the clay fraction of three Zimbabwean vertisols derived from basalt. Zimbabwe J. Agric. Res. 23:111 -117.

Nyamapfene, K.W., and T. Yin. 1986. Mineralogy of a fersiallitic soil derived from an ultramafic rock. Zimbabwe J. Agric. Res. 24:65 - 76.

Oline, D.K. 2006. Phylogenetic comparisons of bacterial communities from serpentine and nonserpentine soils. Appl. Environ. Microbiol. 72:6965-6971.

Olsson, P., E. Baath, and I. Jakobsen. 1997. Phosphorus effects on the mycelium and storage structures of an arbuscular mycorrhizal fungus as studied in the soil and roots by analysis of fatty acid signatures. Appl. Environ. Microbiol. 63:3531-3538.

Oze, C., S. Fendorf, D.K. Bird, and R.G. Coleman. 2004. Chromium geochemistry in serpentinized ultramafic rocks and serpentine soils from the Franciscan complex of California. Am. J. Sci. 304:67 -101.

Pal, A., S. Dutta, P.K. Mukherjee, and A.K. Paul. 2005. Occurrence of heavy metal-resistance in microflora from serpentine soil of Andaman. J. Basic Microbiol. 45:207-218.

Paquet, H., and G. Millot. 1973. Geochemical evolution of clay minerals in the weathered products in soils of Mediterranean climate. p. 199-206. *In* J.M. Serratosa (ed.) Proc. Int. Clay Conf. Madrid, Spain. 1972. The Clay Minerals Society, Bloomington, IN.

Prendergast, M.D. 1990. The Wedza-Mimosa platinum deposit, Great Dyke, Zimbabwe: Layering and stratiform PGE mineralization in a narrow mafic magma chamber. Geol. Mag. 128:235-249.

Petitt, S., J. Caillaud, J. Righi, J.Madejova, F. Elsass, and H.M. Koster. 2002. Characterization and crystal chemistry of an Fe-rich montmorillonite from Ölberg, Germany. Clay Miner. 37:283-297.

Proctor, J. 1999. Toxins, nutrient shortages and droughts: The serpentine challenge. Trends Ecol. Evol. 14: 334-335.

Proctor, J., J. Burrow, and G.C. Craig. 1980. Plant and soil analayses from a range of Zimbabwean serpentine sites. Kirkia 12:127-139.

Proust, D., J. Caillaud, and C. Fontaine. 2006. Clay minerals in early amphibole weathering : Tri- to dioctahedral sequence as a function of crystallization sites in the amphibole. Clays Clay Miner. 54:351-362.

Quantin, C., V. Ettler, J. Garnier, and O. Sebek. 2008. Sources and extractibility of chromium and nickel in soil profiles developed on Czech serpentinites. Comp. Rendus Geosci. 340:872-882.

Rabenhorst, M.C., J.E. Foss, and D.S. Fanning. 1982. Genesis of Maryland soils formed from serpentinite. Soil Sci. Soc. Am. J. 46:607-616.

Roberts, B.A. 1980. Some chemical and physical properties of serpentine soils from western Newfoundland. Can. J. Soil Sci. 60:231-240.

Roberts, B.A., and J. Proctor (ed.) 1992. The ecology of areas with serpentinized rocks-A world view. p. 1-429. Kluwer Academic Publishers, Dordrecht, The Netherlands.

Robertson, A.I., and M.E.R. Meakin. 1980. The effect of Ni on cell division and growth of Brachystegia spiciformis seedlings. J. Bot. Zimbabwe 12:115-125.

Ross, D.S., H.C. Hales, G.C. Shea-McCarthy, and A. Lanzirotti. 2001. Sensitivity of soil manganese oxides: Drying and storage cause reduction. Soil Sci. Soc. Am. J. 65:736-743.

Schwertmann, U., and R. Taylor. 1989. Iron oxides. p. 379-438. *In* J.B. Dixon and S. Weed (ed.) Minerals in soil environments, 2nd Edition. Soil Science Society of America, Inc., Madison, WI.

Senkayi, A.L. 1977. Clay mineralogy of poorly drained soils developed from serpentinite rocks. University of California, Davis.

Shen, S., S.-I. Tu, and W.D. Kemper. 1997. Equilibrium and kinetic study of ammonium adsorption and fixation in sodium-treated vermiculite. Soil Sci. Soc. Am. J. 61:1611-1618.

Singer, A. 2003. Palygorskite and sepiolite. p. 555-583. *In* J.B. Dixon and D.G. Schulze (ed.) Soil mineralogy with environmental applications. Soil Science Society of America, Inc., Madison, WI.

Singh, B., and R.J. Gilkes. 1992. Properties and distribution of iron oxides and their association with minor elements in the soils of south-western Australia. Eur. J. Soil Sci. 43:77-98.

Singh, B., D.M. Sherman, R.J. Gilkes, M.A. Wells, and J.F.W. Mosselmans. 2002. Incorporation of Cr, Mn and Ni into goethite ({alpha}-FeOOH): Mechanism from extended X-ray absorption fine structure spectroscopy. Clay Miner. 37:639-649.

Soane, B.D., and D.H. Saunder. 1959. Nickel and chromium toxicity of serpentine soils in Southern Rhodesia. Soil Sci. 88:322-330.

Sprent, J.I., and R. Parsons. 2000. Nitrogen fixation in legume and non-legume trees Field Crops Res. 65:183–196.

Sterflinger, K. 2000. Fungi as geologic agents. Geomicrobiol. J. 17:97 - 124.

Stucki, J.W., Golden, D.C. and Roth, D.C. 1984. Effects of reduction and re-oxidation of structural iron on the surface charge and dissolution of dioctahedral smectites. Clays Clay Miner. 32:350-356.

Suárez, M., and E. García-Romero. 2006. FTIR spectroscopic study of palygorskite: Influence of the composition of the octahedral sheet. Appl. Clay Sci. 31:154-163.

Traore, D., A. Beauvais, F. Chabaux, C. Peiffert, J.-C. Parisot, J.-P. Ambrosi, and F. Colin. 2008. Chemical and physical transfers in an ultramafic rock weathering profile: Part 1. Supergene dissolution of Pt-bearing chromite. Am. Mineral. 93:22-30.

Trivedi, P., L. Axe, and T.A. Tyson. 2001. XAS studies of Ni and Zn sorbed to hydrous manganese oxide. Environ. Sci. Technol. 35:4515-4521.

Trolard, F., G. Bourrie, E. Jeanroy, A.J. Herbillon, and H. Martin. 1995. Trace metals in natural iron oxides from laterites: A study using selective kinetic extraction. Geochim. Cosmochim. Acta 59:1285-1297.

van Cromphaut, C., E. van Ranst, V.G. de Resende, R.E. Vandenberghe, E. de Grave, and G. Lambiv Dzemua. 2008. Characterization by Mossbauer spectroscopy of Fe phases in highly weathered serpentinitic soil from southern Cameroon. Clay Miner. 43:117-128.

Vempati, R.K., and R.H. Loeppert. 1989. Influence of structural and adsorbed Si on the transformation of synthetic ferrihydrite. Clays Clay Miner. 37:273-279.

Wang, M.K., P.C. Tseng, S.S. Chang, D.T. Ray, Y.H. Shau, Y.W. Shen, R.C. Chen, and P.N. Chiang. 2009. Origin and mineralogy of sepiolite and palygorskite from the Tuluanshan Formation, Eastern Taiwan. Clays Clay Miner. 57:521-530.

Weaver, C.E., and K.C. Beck. 1977. Miocene of the S.E. United States: a model for chemical sedimentation in a peri-marine environment. Sediment. Geol. 17:1-234.

White, G.N., and J.B. Dixon. 1996. Iron and manganese distribution in nodules from a young Texas vertisol. Soil Sci. Soc. Am. J. 60:1254 -1262.

Wilkins, R.W.T., and J. Ito. 1967. Infrared spectra of some synthetic talcs. Am. Miner. 52:1649-1661.

Wilson, A.H. 1982. The geology of the Great 'Dyke', Zimbabwe: The ultramafic rocks. J. Petrol. 23:240-292.

Wilson, A.H. 1992. The Geology of the Great Dyke, Zimbabwe: Crystallization, layering, and cumulate formation in the P1 Pyroxenite of Cyclic Unit 1 of the Darwendale Subchamber. J. Petrol. 33:611-663.

Wilson, A.H., and M.D. Prendergast. 1989. The Great Dyke of Zimbabwe: Tectonic setting, stratigraphy, petrology, structure, emplacement and crystallization. p. 1-20. *In* M.D. Prendergast and M.J. Jones (ed.) Magmatic sulphides - The Zimbabwe Volume, London.

Wilson, A.H., and M.D. Prendergast. 2001. Platinum-group element mineralisation in the Great Dyke, Zimbabwe, and its relationship to magma evolution and magma chamber structure. South Afr. J. Geol. 104:319-342.

Wilson, A.H., A.J. Naldrett, and M. Tredoux. 1989. Distribution and controls of platinum group element and base metal mineralization in the Darwendale subchamber of the Great Dyke, Zimbabwe. Geology 17:649-652.

Wilson, A.H., C.Z. Murahwi, and B.M. Coghill. 2000. The geochemistry of the PGE Subzone in the Selukwe Subchamber, Great Dyke: An intraformational layer model for Platinum Group element enrichment in layered intrusions. Miner. Petrol. 68:115-140.

Wittbrodt, P.R., and C.D. Palmer. 1995. Reduction of Cr(VI) in the presence of excess soil fulvic acid. Environ. Sci. Technol. 29:255-263.

Worst, B.G. 1960. The Great Dyke of Southern Rhodesia. South. Rhodesia Geol. Surv. Bull. 47: 1-234.

Wright, J. 2007. Local adaptation to serpentine soils in Pinus ponderosa. Plant Soil 293:209-219.

Yongue-Fouateu, R., M. Yemefack, A.S.L. Wouatong, P.D. Ndjigui, and P. Bilong. 2009. Contrasted mineralogical composition of the laterite cover on serpentinites of Nkamouna-Kongo, southeast Cameroon. Clay Miner. 44:221-237.

Zelles, L. 1999. Fatty acid patterns of phospholipids and lipopolysaccharides in the characterisation of microbial communities in soil: A review. Biol. Fertil. Soils 29:111-129.

APPENDIX A

SOIL PROFILE AT THE PEDIPLAIN AT MPINGA

Photo by C. Bangira, 2006.

Picture of stunted maize (*Zea mays*) in newly-opened fields located at the pediplain at Mpinga. Firing at the tip of the leaves is typical for K and Ca deficiencies (photo by C. Bangira, 2006).

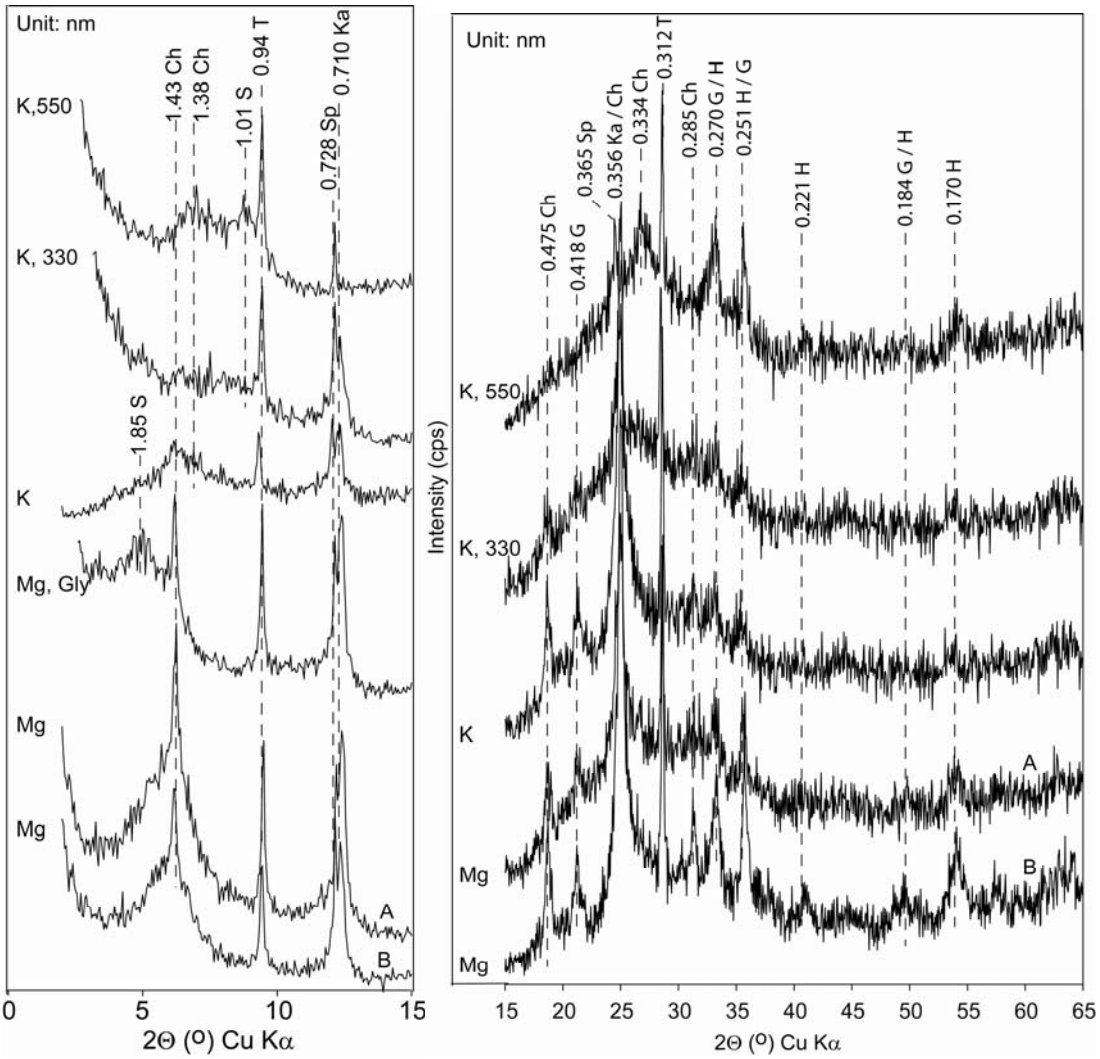

Fig. A.1. X-ray diffraction pattern of clay from cultivated soil at Mpinga site. S-smectite; Ch-chlorite; T-talc; Sp-serpentine; Ka-kaolinite; G-goethite; H-hematite. The soil were sampled from A (0-20 cm) and B (20-40 cm) depth.

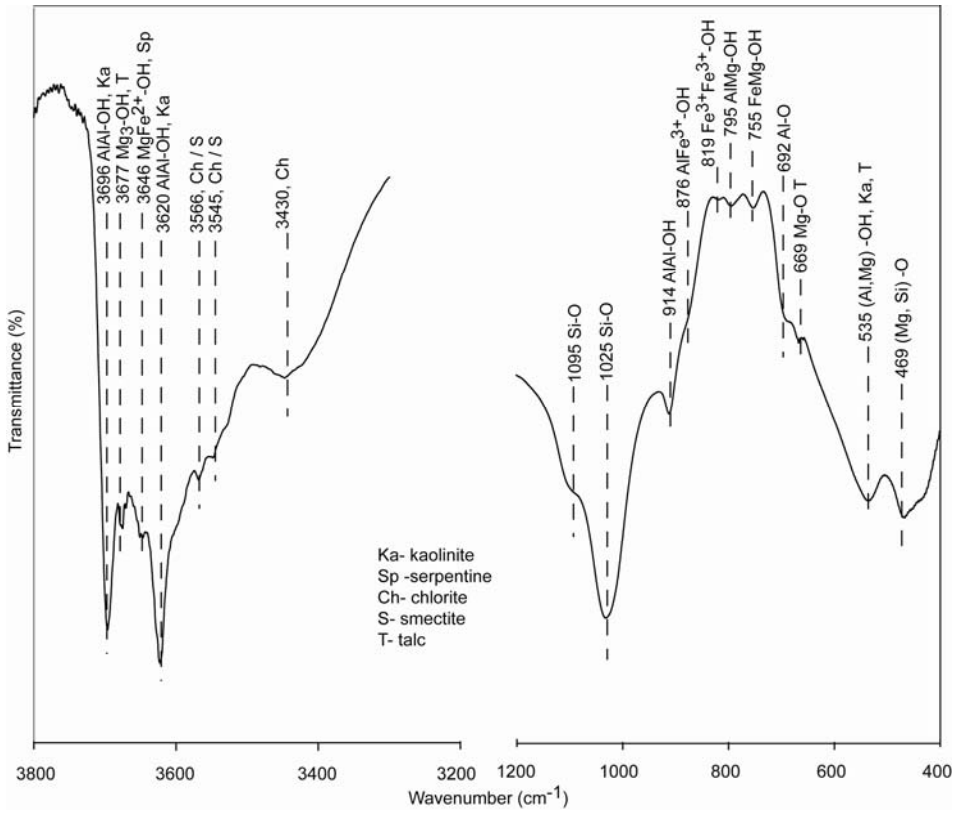

Fig. A.2. FTIR pattern of clay from the cultivated field at Mpinga site.

Table A.1. Elemental composition (by NAA) of cultivated soil at Mpinga site.

Depth (cm)	Al	Ca	Mg	K	Na	Fe	Cr	Ni	Mn	Ti	Co	V	Zn
	----------mg kg^{-1}----------												
0-20	43101	3450	34293	3737	1267	194963	78316	3258	2680	6850	356	339	356
20-40	45439	2587	37334	3071	1067	211364	88729	3565	2680	6590	380	385	398

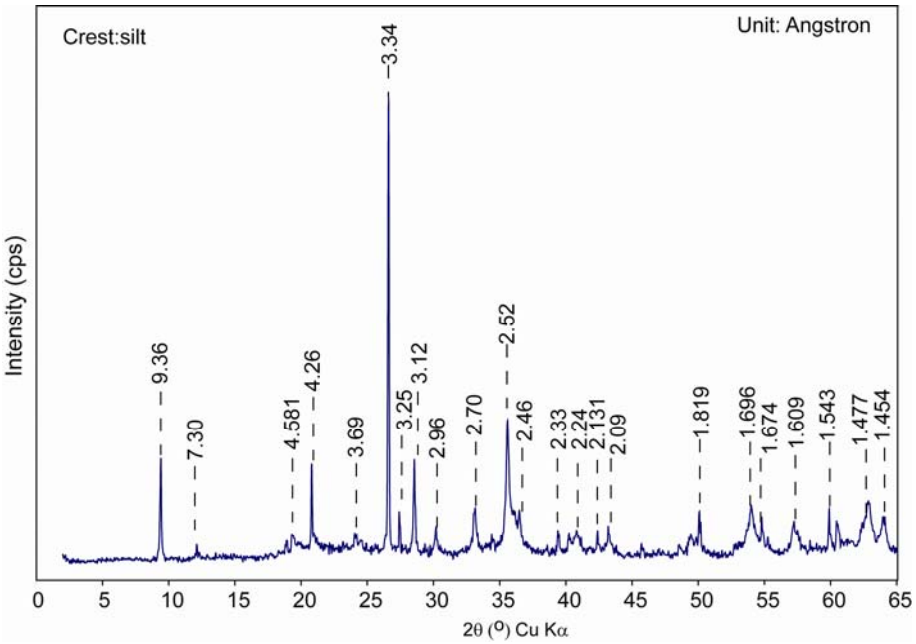

Fig. A.3. Powder XRD pattern of crest silt fraction at Mpinga.

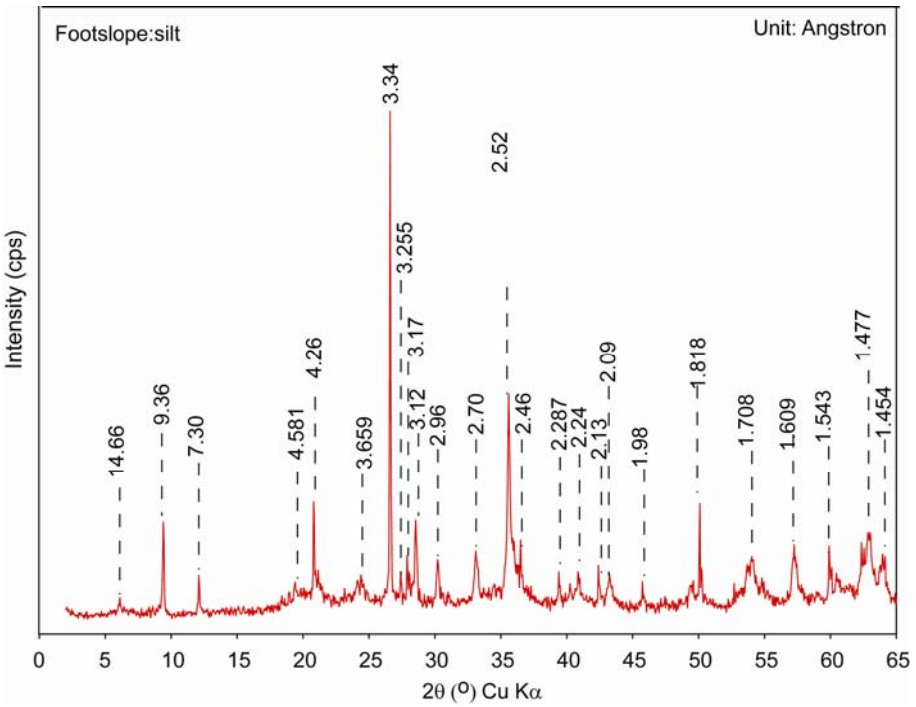

Fig. A.4. Powder XRD pattern of footslope silt fraction at Mpinga.

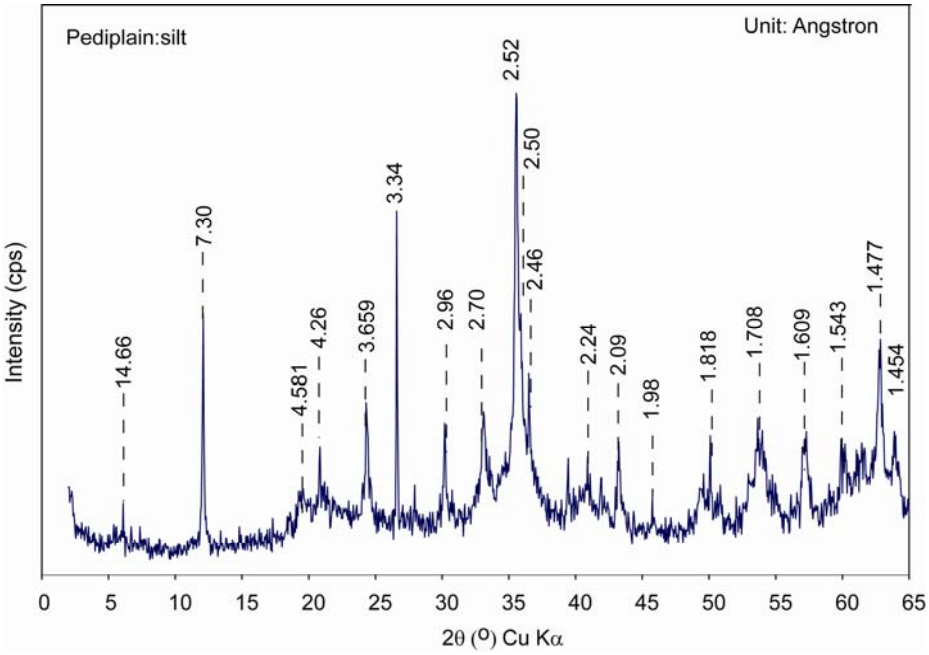

Fig. A.5. Powder XRD pattern of pediplain silt fraction at Mpinga.

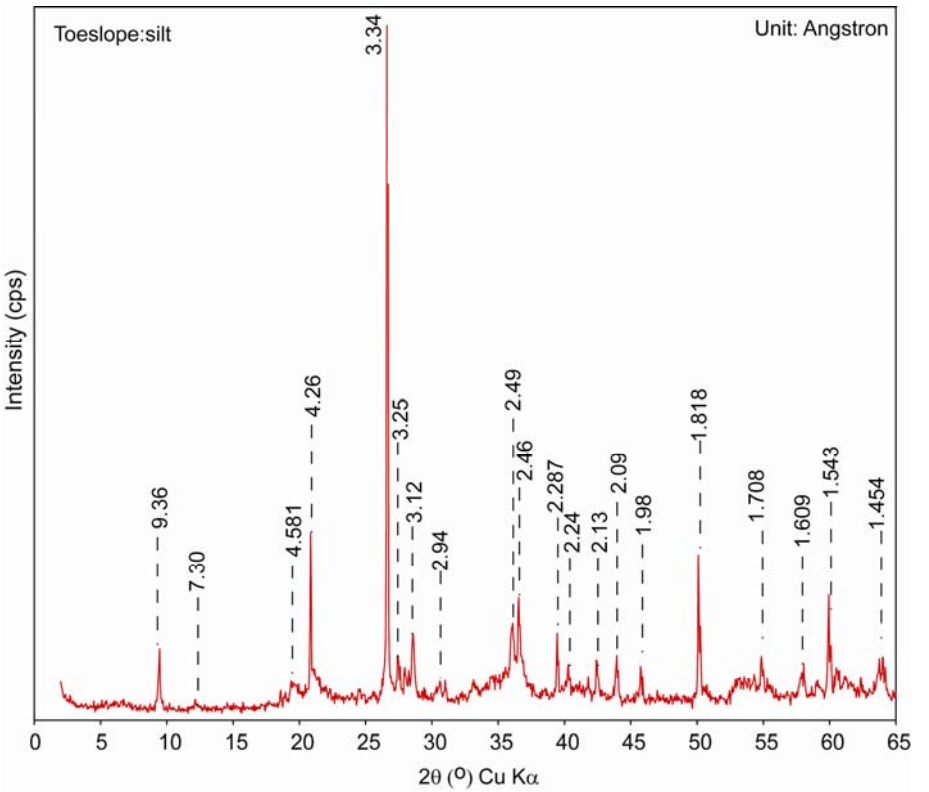

Fig. A.6. Powder XRD pattern of toeslope silt fraction at Mpinga.

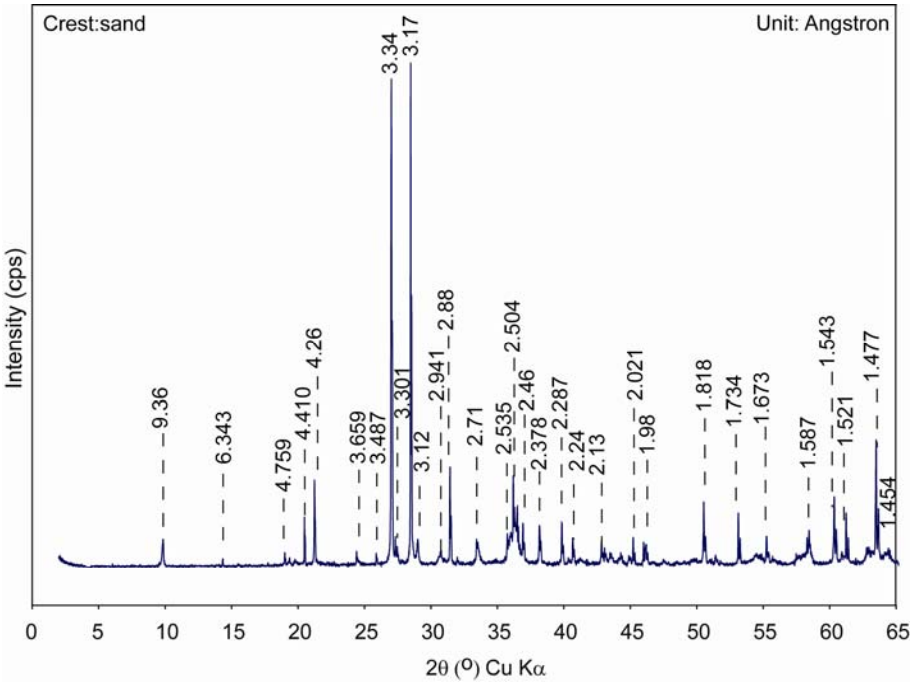

Fig. A.7. Powder XRD pattern of crest sand fraction at Mpinga.

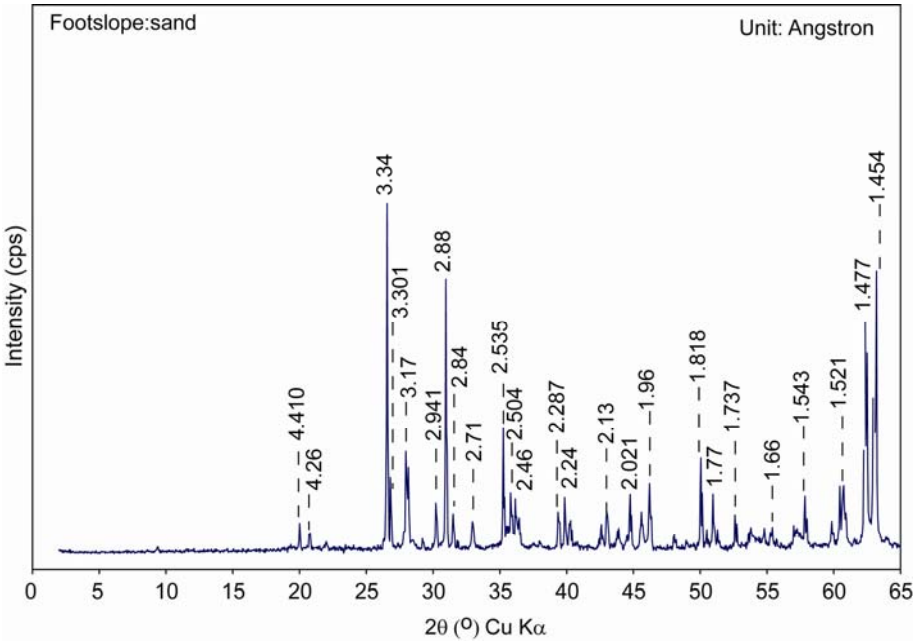

Fig. A.8. Powder XRD pattern of footslope sand fraction at Mpinga.

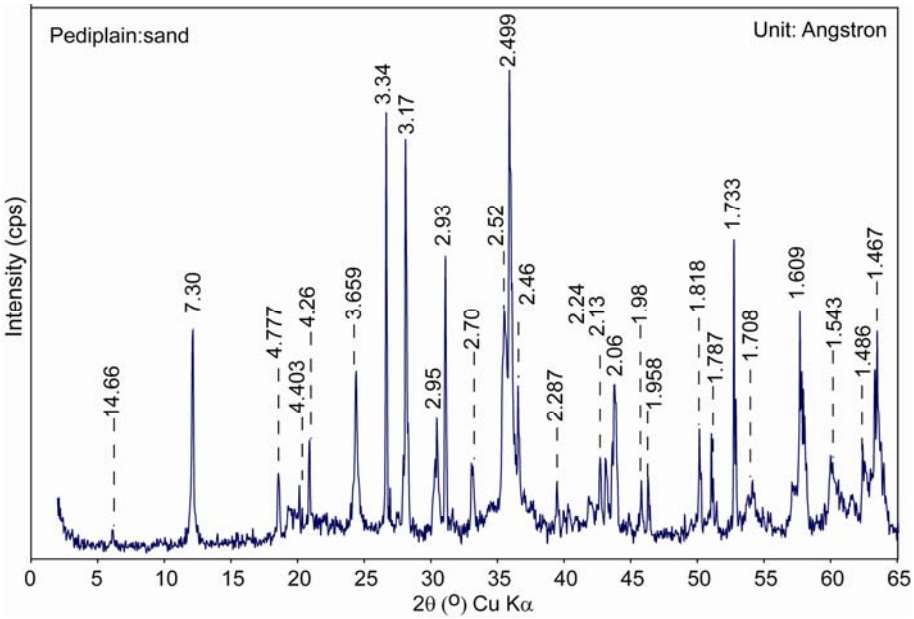

Fig. A.9. Powder XRD pattern of pediplain sand fraction at Mpinga.

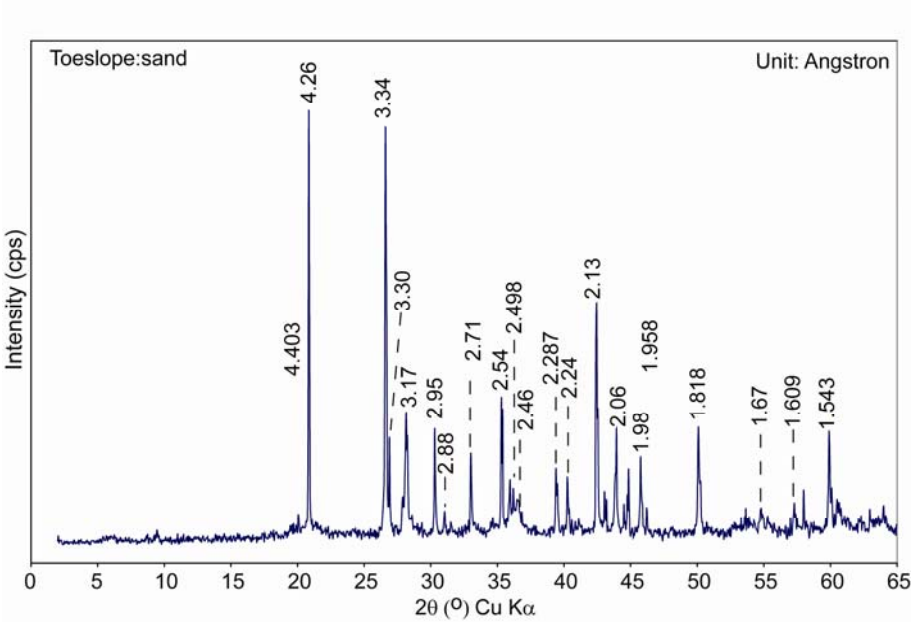

Fig. A.10. Powder XRD pattern of toeslope sand fraction at Mpinga.

APPENDIX B

Table B.1. Selected physical and chemical properties of soil at Mpinga site.

Depth	Color	pH	O.C.	Clay	Silt	Sand	Exchangeable Cations Ca	Mg	K	Na	Ni	CEC	Mg/Ca	Great Group
(cm)	(moist)		------Weight % -----				---------cmol(+) kg^{-1}---------							
							Crest:							
0-15	2.5YR3/3	5.1	2.4	27	27	46	0.8	7.5	0.2	0.1	0.37	11.5	9.4	Haplustolls
							Footslope:							
0-15	2.5YR3/3	5.2	2.7	22	17	61	1.5	7.5	0.1	0.1	0.44	12.0	5.0	Haplustolls
							Pediplain:							
0-15	2.5YR3/3	6.2	2.9	28	22	50	0.6	7.6	0.1	0.1	0.74	12.5	12.7	Haplustolls
							Toeslope:							
0-20	2.5Y 3/1	7.5	4.8	61	22	17	3.9	74.3	0.2	0.1	0.22	72.8	19.1	Haplusterts

Table B.2. Total elemental concentrations (% w/w) in soil at Mpinga site[†].

Depth (cm)	Fe_2O_3	Al_2O_3	Cr_2O_3	MgO[‡]	CaO[‡]	Na_2O	MnO	NiO	ZnO	CoO
				Crest:						
0-15	30.9	5.5	3.5	8.4	0.04	0.11	0.42	0.28	0.02	0.05
				Footslope:						
0-15	30.6	5.8	3.7	7.9	0.16	0.10	0.47	0.21	0.02	0.05
				Pediplain:						
0-15	33.7	5.3	6.4	7.7	0.09	0.12	0.39	0.44	0.03	0.06
				Toeslope:						
0-20	14.9	7.0	2.1	8.2	0.09	0.17	0.34	0.24	0.03	0.04

[†]K concentration < limit of quantitation (< 0.06%(w/w).
[‡]Ca determined by atomic absorption spectrophotometer following soil dissolution in aqua-regia/HF.

Table B.3. Percentages of total Fe, Mn, Cr, and Ni dissolved by hydroxylamine hydrochloride (HH), ammonium oxalate (AO) and dithionite-citrate (DC) methods.

Depth (cm)	Fe			Mn			Cr			Ni		
	HH	AO	DC	HH	AO	DC	HH	AO	DC	HH	AO	DC
Crest:												
0-15	0.1	1.2	40.5	40.3	34.7	8.3	<0.01	0.2	7.8	11.3	12.1	39.3
Footslope:												
0-15	0.2	1.3	49.8	36.2	31.9	9.1	<0.01	0.2	9.1	18.4	20.3	78.3
Pediplain:												
0-15	0.2	2.1	51.5	30.6	31.0	25.3	<0.01	0.1	2.2	16.2	21.9	61.5
Toeslope:												
0-20	0.8	12.6	54.2	40.2	36.3	41.2	0.03	0.3	6.6	23.9	47.5	62.7

APPENDIX C

SOIL PROFILE AND SITE DESCRIPTION

Figure 3: PEDON DESCRIPTION for S09TX171003
Site Record ID: 18 **Pedon Record ID:** 18
Pedon ID: S09TX171003 **Site ID:** S09TX171003
Transect:T09TX1711000; **Stop#:** N/A; **Interval:** N/A; **Authors:** JAM,BMJ,ALB; **Kind:** random point
Description Date: 7/9/2009 9:38:08 AM **Print Date:** 7/26/2009
Soil Name As Described/Sampled: Renick **Soil Name As Correlated:** ReD
Describer: TH,AB,CB,BJ **Site Notes: Text:** ridge on dissected plateau
Pedon Notes: Text: stunted mesquite, 3awn, prickly pear, buffalograss **Text:** 10% ROC on surface

Classification: Clayey-skeletal, mixed, active, thermic Lithic Argiustolls
Non-MLRA Soil Survey Area: TX319 - Mason County, Texas
MLRA: 82A - Texas Central Basin **County or Parish:** TX171 - Gillespie
State or Territory: TX - Texas **7.5' Quad:** 30098-D6 - Willow City, Texas
Lat/Long: 30°28'32.724" north, 98°37'40.434" west
UTM: 535716.05E, 3371563.78N -- Datum NAD83, Zone 14
Landform: low hill
Geomorphic Component: Side Slope
Profile Pos: Shoulder
Slope: 5 percent
Elevation: 369 meters (1210.6 feet)
Aspect: 180°
Drainage: Well drained
Primary Earth Cover: Grass/herbaceous cover; **Secondary Earth Cover:** Other grass/herbaceous cover
Parent Materials: residuum weathered from serpentinite
Bedrock: Very weakly cemented serpentinite, 10 to < 45 cm between fractures at 40 centimeters (15.7 inches)
Particle Size Control Section: 24 to 40 centimeters (9.4 to 15.7 inches)
Diagnostic Features: Mollic epipedon: 0 to 40 centimeters (0 to 15.7 inches), Argillic horizon: 24 to 40 centimeters (9.4 to 15.7 inches), Paralithic materials: 40 to 49 centimeters (15.7 to 19.3 inches) (Restrictive layer) and Lithic contact: 49 centimeters (19.3 inches) (Restrictive layer)
Restrictions: Paralithic bedrock: 40 to 49 centimeters (15.7 to 19.3 inches) and Lithic bedrock: 49 centimeters (19.3 inches)

Slope	Elevation	Aspect	MAAT	MSAT	MWAT	MAP	Frost-Free Days	Drainage Class	Slope Length	Upslope Length
5 percent	369 meters (1210.6 feet)	180°						well		

A1 --- 0 to 13 centimeters (0 to 5.1 inches); dark reddish brown (5YR 3/2) dry, cobbly clay loam; dark reddish brown (5YR 3/2) moist; null percent sand; null percent silt; 38 percent clay; strong medium subangular blocky and strong fine subangular blocky structure; firm, hard, moderately sticky, moderately plastic; 30 percent 75 to 250 millimeters (3 to 10 inches) serpentinite fragments; noneffervescent; clear smooth boundary.

A2 --- 13 to 24 centimeters (5.1 to 9.4 inches); dark reddish brown (5YR 3/2) dry, very cobbly clay loam; dark reddish brown (5YR 3/2) moist; null percent sand; null percent silt; 38 percent clay; strong fine subangular blocky structure; firm, hard, moderately sticky, moderately plastic; 30 percent (common) continuous faint clay films on all faces of peds; 55 percent angular 76 to 250 millimeters (3 to 10 inches) serpentinite fragments; noneffervescent; clear wavy boundary.

Bt --- 24 to 40 centimeters (9.4 to 15.7 inches); dark reddish brown (2.5YR 3/3) dry, gravelly clay; dark reddish brown (2.5YR 3/3) moist; null percent sand; null percent silt; 48 percent clay; moderate medium prismatic parting to strong medium angular blocky structure; very firm, extremely hard, very sticky, very plastic; 40 percent (common) continuous distinct clay films on all faces of peds; 15 percent 2 to 75 millimeters (0.1 to 3 inches) serpentinite fragments; noneffervescent; discontinuous n places and border-line sic; very abrupt irregular boundary.

Cr --- 40 to 49 centimeters (15.7 to 19.3 inches); pale olive (5Y 6/3) dry, very weakly cemented serpentinite bedrock, fractured at intervals of 10 to < 45 cm between fractures; very weakly cemented; noneffervescent; abrupt wavy boundary.

R --- 49 centimeters (19.3 inches); light greenish gray (10GY 7/1) dry, bedrock; strongly cemented; noneffervescent; Coal creek serpentine.

Soil profile at the study site, Gillespie County.


A photograph of vegetation at the study site, Gillespie County.

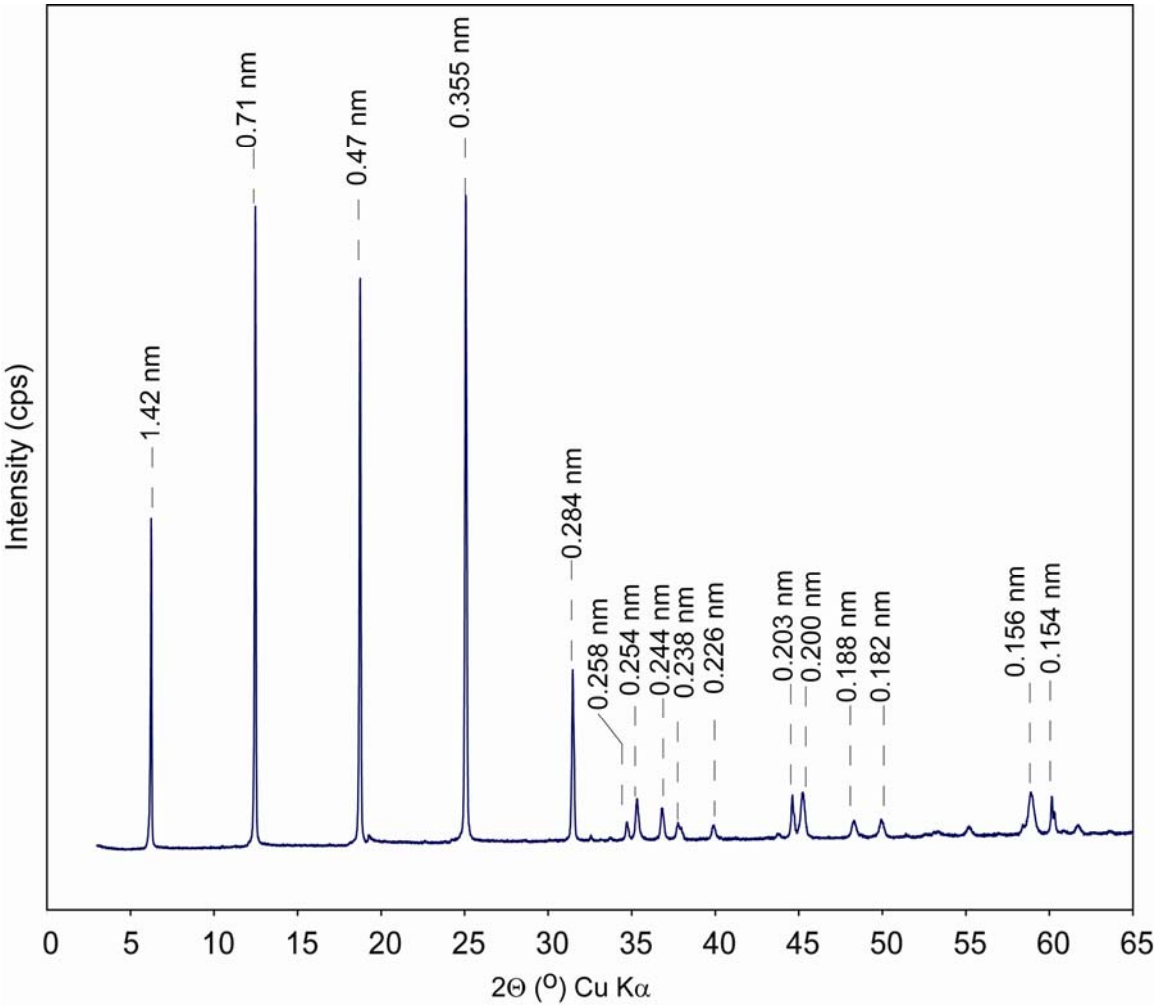

Fig. C.1. Powder XRD patterns of chlorite from the coarse fragments (>2 mm) taken from the Bt horizon of the Gillespie County pedon.

Fig. C.2. An image of chlorite particle taken from the Bt horizon of the Gillespie County pedon showing the formation of Fe-rich minerals (red in color) on its freshly exposed surface.

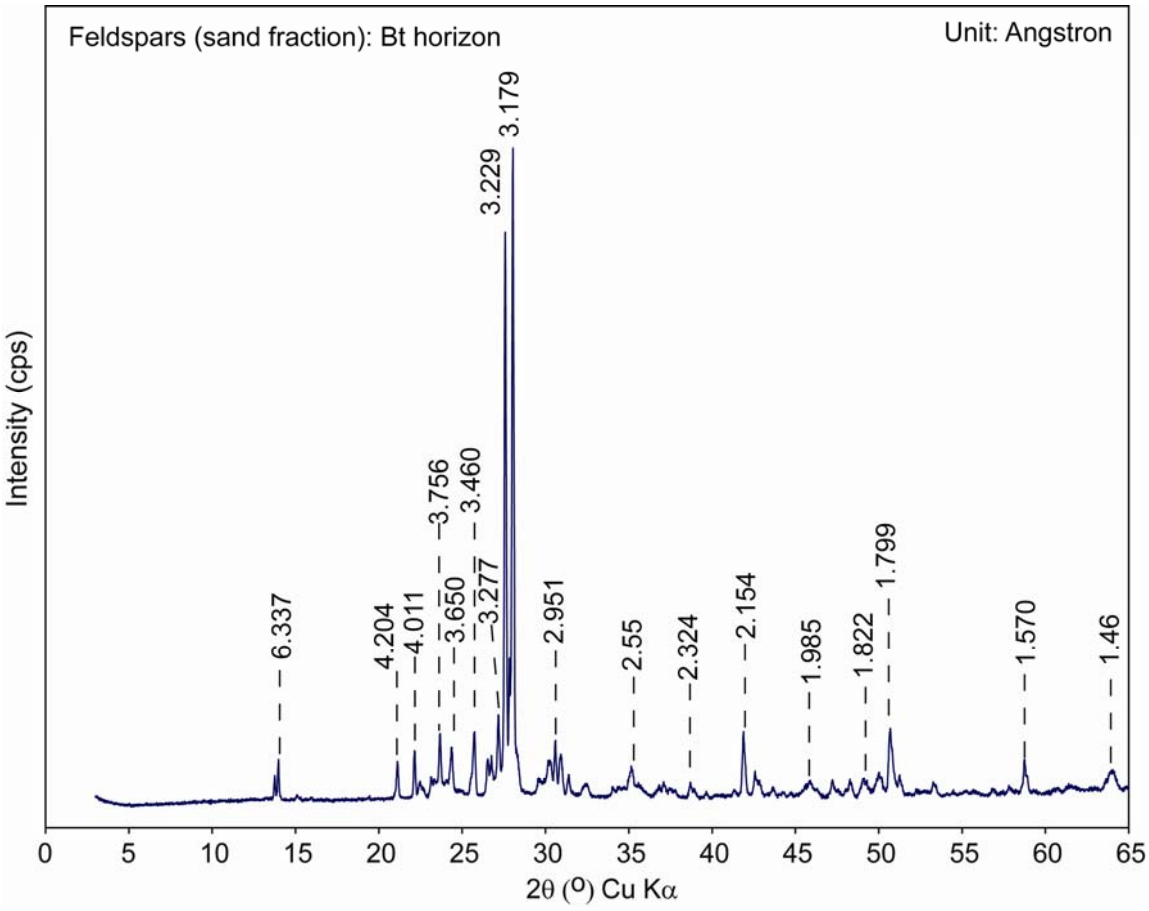

Fig. C.3. Powder XRD diffraction patterns of feldspars in the sand-sized fractions taken from the Bt horizon of the Gillespie County pedon.

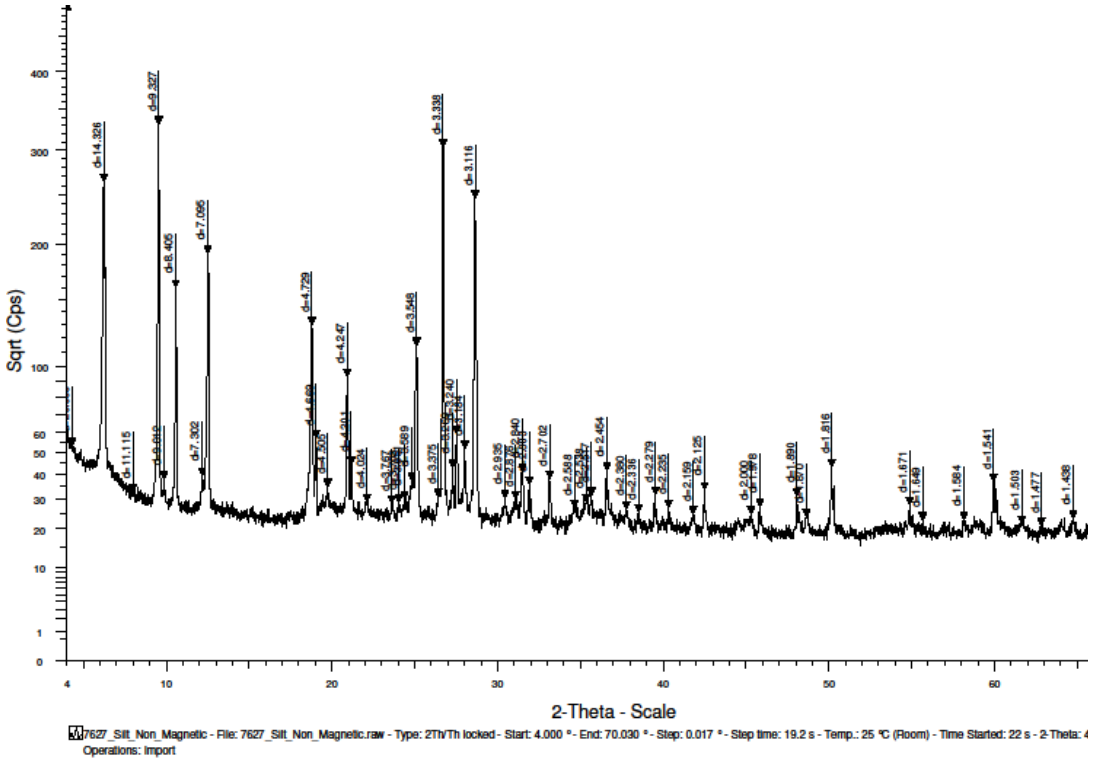

Fig. C.4. Powder XRD patterns of the silt-sized fractions taken from the A2 horizon of the Gillespie County pedon.

VITA

Name:	Courage Bangira
Address:	Department of Soil & Crop Sciences 370 Olsen Blvd 2474 TAMU College Station, TX 77843
Email Address:	kbangira@yahoo.co.uk
Education:	B.S., Agriculture, Honours, University of Zimbabwe, 1992 M.S., Soil Science, Gent University, Belgium, 1998 Ph.D., Soil Science, Texas A&M University, 2010